VANDERBILT UNIVERSITY

EVA GLOVE RESEARCH TEAM

ANNUAL REPORT

July, 1992

EVA Glove Research Team Members

Dept. of Mechanical Engineering, Vanderbilt University
Dr. Alvin M. Strauss, Professor and Chairman
Dr. Steven W. Peterson, Assistant Professor
John A. Main, Research Assistant
Reuben D. Dickenson, Research Assistant
Bobby L. Shields, Research Assistant

Dept. of Radiology and Radiological Sciences,
Vanderbilt University Medical Center
Christine H. Lorenz, Assistant Professor

Table of Contents

1. Introduction and Review of Project Goals

The current NASA EVA glove is an extremely complex fabric structure that must perform a number of critical functions to insure the success of any mission requiring EVA. The glove must provide environmental containment, thermal protection, radiation protection, and abrasion resistance, all requirements that necessitate a very durable and robust glove. However, the glove must also be sufficiently flexible to allow the crew member to move and grasp efficiently, so that tasks may be performed in a reasonably efficient manner. In general glove safety and durability considerations have been paramount, resulting in an EVA glove with less than ideal flexibility and dexterity characteristics. Glove stiffness has even been noted as one of the limiting factors in EVA productivity (O'Hara et al.,1990). It is the overall goal of this research program to develop a thorough understanding of the interaction between the hand and the EVA glove, and to develop technology for improving the flexibility and dexterity of the gloved hand without compromising any safety considerations.

The Vanderbilt University EVA Glove Research Program has to date been broken down into two broad areas: basic research and technical improvements. The general goal of the basic research initiatives is to improve understanding of the EVA glove structure, the kinematics of the hand, and the interaction between the two. A novel method of obtaining biomechanical data has been developed and utilizes the three dimensional imaging capabilities of magnetic resonance imaging. The true dimensions and positions of both the tissue and bones of the hand can be determined in a non-invasive and extremely accurate fashion by using this instrument (Dickenson et al., 1992a, 1992b). This method facilitates a greater understanding of the kinematics of the bones and tissue of the hand both through improved accuracy

of the data acquisition and the better visualization that the imaging capabilities of the MRI provide. This knowledge has the potential to lead directly to improvements in EVA glove design.

Another portion of the basic research initiative focuses on the understanding and modeling of the EVA glove itself. The EVA glove is an extremely complex structure that defies conventional structural modeling techniques. The principal goal of this portion of the research is simply to gain a greater understanding of the characteristics of the EVA glove. A general model for the EVA glove has been developed (Main et al., 1992a, 1992b) that has led to some novel methods of reducing the stiffness of the EVA glove metacarpophalangeal (MCP) joint.

In contrast to the basic research described above, the technical improvements initiative is intended to identify and develop specific technologies that may improve the dexterity, flexibility, or endurance of the gloved hand during EVA. The recently developed coil spring MCP joint is an example of one of these projects. This joint (Main et al., 1992b) resulted in 20% reduction in MCP joint stiffness when compared to a standard glove. An improved flexibility MCP joint that uses pneumatic actuators in place of the springs was designed, built, and tested and reduced MCP joint stiffness 40% when compared to the standard, but with the penalty of increased complexity and size.

Also under investigation are hand exoskeleton assemblies to add a power assist and force magnification capability to the EVA glove. The exoskeleton design is evolving and currently utilizes four-bar linkage joints and shape memory allow actuators.

2. Basic Research Achievements 1991-1992

As stated previously, the goal of the basic research portion of the program is to gain a greater understanding of the kinematics of the hand, the characteristics of the pressurized EVA glove, and the interaction of the two. Examination of the literature showed that there existed no acceptable, non-invasive method of obtaining accurate biomechanical data on the hand. For this reason a project was initiated to develop magnetic resonance imaging as a tool for biomechanical data acquisition and visualization. Literature reviews also revealed a lack of practical modeling methods for fabric structures, so a basic science research program was also initiated in this area.

2.1 Development of MRI as a Tool for Obtaining Biomechanical Data

Magnetic Resonance Imaging is currently evolving into an imaging modality which promises to provide information on the function as well as the anatomy of tissue structures (Le Bihan, 1990; Moseley et al., 1990; Pickens et al., 1991; Price et al., 1990). It is an important tool which has been used by the Department of Mechanical Engineering in its glove research activities and holds great potential for future studies of the hand enclosed by a pressurized glove. MRI is an extremely helpful tool for this type of study because it images both the hard and soft tissue of the body, so data can be obtained not only about relative bone positions, but also about tendon, ligament, and muscle position and condition. Our studies using MRI have focused on two areas during the period to date: fatigue characteristics and hand kinematics. The past year has seen successful completion of feasibility studies investigating the capabilities of the MRI to acquire data both on hand fatigue and kinematics. This has led to the current applications oriented program.

1. Fatigue Studies. The first area explored using MRI was that of fatigue of the hand during various forms of exercise (Niemann et al., 1991; Lorenz et al., 1990). The hand was imaged in both the rest state and various states of fatigue following strenuous exercise. The imaging done focused on the differences in blood perfusion in the hand, which is a measure of fatigue. The resulting data provided valuable information on the areas of the hand most affected during certain exercises during specified workloads. A method of determining the regions of the hand that are fatigued during specific tasks has great potential for testing, in a completely objective fashion, future EVA glove design enhancements.

This research was presented by Dr. Steve Peterson during the 1991 International Conference on Environmental Systems, held in San Francisco, CA.

2. Kinematics Studies. The second area of MRI research involved generating 3-D data sets and using this volume data to determine the exact nature of the rotations and translations of the bones of the hand during various motions and tasks (Dickenson et al., 1992a, 1992b). This was an as yet unexplored area of research, since past kinematic and biomechanic studies of the hand have used other methods, such as computed tomography, goniometric linkages, or cadaver testing. The first step was to determine the ability of MRI to produce images with sufficient resolution, reproduce acceptable volumes on the 3-D workstation, and finally to manipulate the resulting data and determine the validity of the results. The research conducted during the past year has shown MRI to be more accurate and reliable than other methods. Initial tests were conducted on the metacarpophalangeal (MCP) joint of the index finger, and the current focus is on expanding the kinematic analysis to the entire hand. Once this is complete, calculations concerning work, energy, and stress in the bones, muscles, and tendons of the hand can be determined.

A summary of the research was presented by Reuben Dickenson at the 1992 International Conference on Environmental Systems in Seattle, WA and the newer results will be presented at the 1992 World Space Conference in Washington, D.C.

2.2 Static Modeling of Fabric Structures in Bending

The results of our research to date show that the bending behavior of the EVA glove MCP joint is analogous to that of a pressurized tube. Although dependent upon the geometry of the palm bar and the tightness of fit, the cross-section of the glove at this point can be represented by a pressurized fabric tube with a circular cross section. The bending behavior of this idealized MCP joint (Main et al., 1992a, 1992b) may be expressed in the following fashion.

$$\frac{1}{\rho} = \frac{M(x)}{EI}$$

E = fabric modulus (N / m)

I = moment of inertia (m^3)

M = applied moment (Nm)

$\frac{1}{\rho}$ = joint curvature (m^{-1})

Tests were undertaken at Vanderbilt University to determine the validity and accuracy of the model for the inflated cylinder. A number of inflated cylindrical structures were constructed and tested with encouraging results. The results of one of these tests are plotted against the computer generated model curve in Figure 1. The cylinder tested in this case was a 5 cm diameter 30 cm long cantilever with the load applied to the tip. Bending tests were run until buckling at both the 5 PSI and 10 PSI pressurization levels. As the figure shows, the model

accurately predicts both the load path and ultimate bending moment of the inflated cylinder.

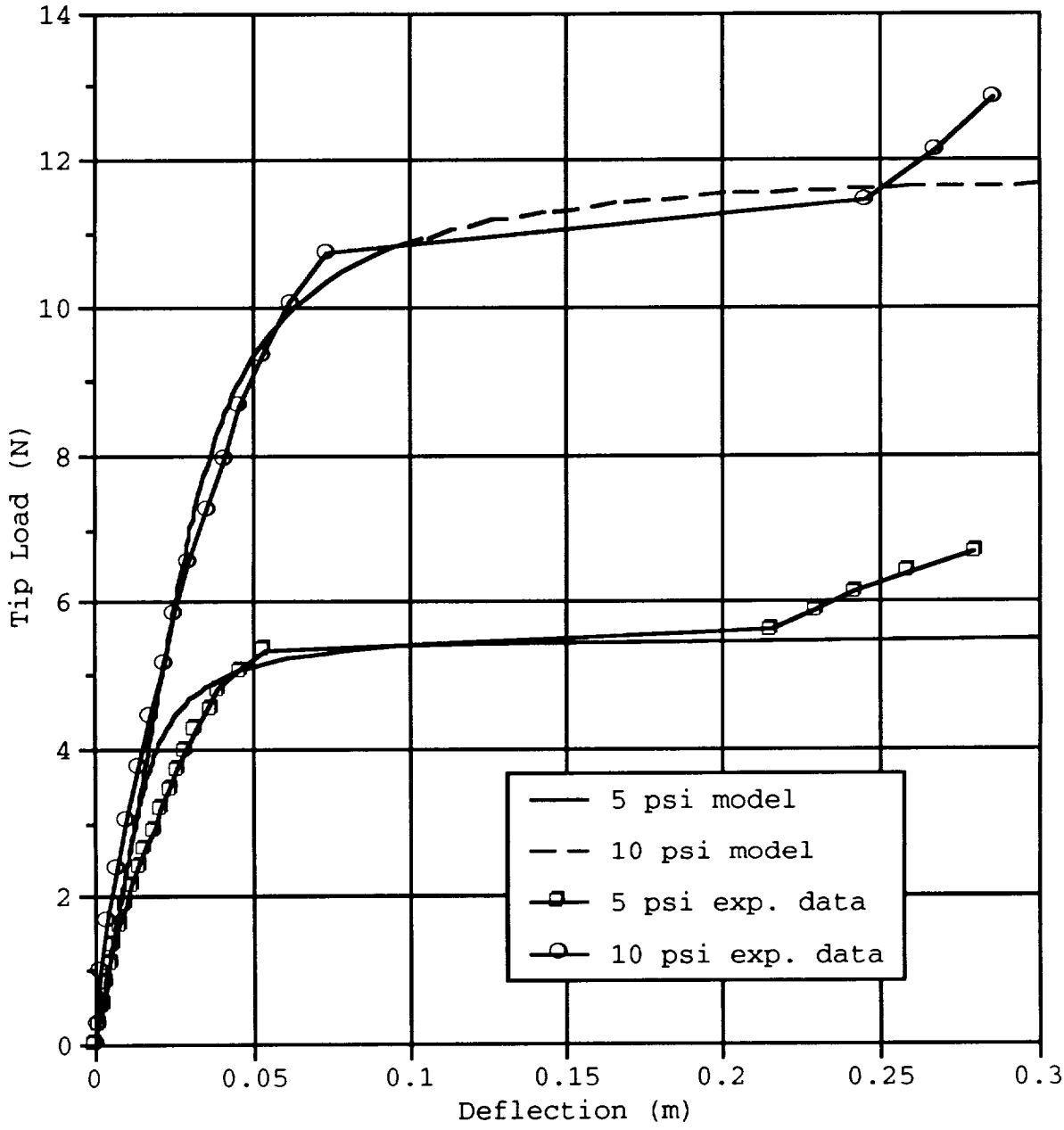

Figure 1. The load deflection curve compared to the model prediction for a 5 cm diameter, 30 cm long inflated cantilever with the load applied to the tip.

With the validity of the model established, conclusions can be drawn about the design of EVA gloves, or indeed any

pressurized fabric structure (Main et al., 1992b). In terms of the model embodied in the equation above, the goal of the EVA glove designer is to achieve a given joint curvature ($1/\rho$) while minimizing the necessary moment (M) that must be supplied by the hand. One way to accomplish this (Main et al., 1991a) is to supply a moment from exterior actuators to reduce the contribution necessary from the hand. The model also supports the efforts of Kosmo et al., 1988, and Spampinato et al., 1990, to design and construct closer fitting gloves since, for a given glove curvature, the required applied moment from the hand can be reduced by lowering the moment of inertia (I) of the glove cross section. The lowest moment of inertia would be the closest fitting glove possible. Further examination of the model leads to another technique for reducing the applied moment necessary to bend the MCP joint. This is accomplished by reducing the elasticity (E), or spring constant, of the glove material on the back of the hand. One of the advantages of increasing joint mobility in this fashion is that the only hardware additions necessary are on the back of the hand, so hand/tool coupling is not compromised by any hardware additions to the palm.

This research was presented by John Main at the 22nd International Conference on Environmental Systems in Seattle, WA. The fabric structure modeling aspects were presented at the 1992 European Systems Design and Analysis Conference in Istanbul, Turkey.

2.3 Dynamic Modeling of Fabric Structures

Not only are the static characteristics of the EVA glove important, but the dynamics must also be examined when considering finger dexterity and rate of motion. Virtually no work is evident in the literature on the subject of dynamics of pressurized fabric structures, although some analogies can be drawn to the work done on automobile tires. Some preliminary work done during this research program

indicates that the dynamic behavior of an inflated cylinder, the primitive shape used to develop the model for the MCP joint, is similar to that of an elastic beam (Main et al., 1992a). The relationship that was tested is

$$\omega_n = a_n \sqrt{\frac{EI}{\mu l^4}}$$

This equation is the expression for the natural frequency of a cantilever beam. It was used, with some modifications to make it more applicable to fabric structures, to accurately determine the small deflection natural frequency of a number of inflated fabric cantilevers. This encouraging result may lead to other important analogies that will lead to a more in depth understanding of the dynamics of inflated fabric structures. Developing this understanding of the dynamic behavior of the EVA glove is at least as important as the static modeling initiative if increased levels of endurance and productivity, and thus higher rates of hand and finger motion, are desired from the EVA crew.

3. Technical Achievements 1991-1992

The technical achievements of the research program are distinct from the basic research achievements previously listed in that they are attempts to develop technology that can be directly accommodated in the development of the EVA glove. Early research focused on developing tools that we deemed necessary for the subsequent research, such as the low profile pressure sensor for evaluating hand/glove interaction. Some of the research completed in this portion of the program is a direct outgrowth of results of the basic research program, such as the coil spring MCP joint. Other research, such as the hand exoskeleton program, is using a more independent and intuitive approach.

The low profile sensor, coil spring MCP joint and the active actuator MCP joint research results were presented by John Main at the 22nd International Conference on Environmental Systems in Seattle, WA.

3.1 Low Profile Pressure Sensor for Evaluating Hand/Glove Interaction and Glove Stiffness

Early in this research program it became evident that one major problem with evaluating pressurized EVA gloves was the lack of any objective, repeatable test that could be used to evaluate the gloves. This problem led us to the development (Main et al., 1992b) of an extremely thin (approx. 0.5 mm) pressure sensor that can be placed at any desired position on the hand and used to monitor the pressure between the hand and the glove at that point. This sensor can be used to monitor hot spots, joint torque, and overall glove fit. Numerous tests demonstrated that the sensor is a valuable tool, but unfortunately not particularly durable. The sensors are, however, very inexpensive, so the relatively short lifetime is not an issue in the laboratory environment. A photo of the sensor is included as Figure 2.

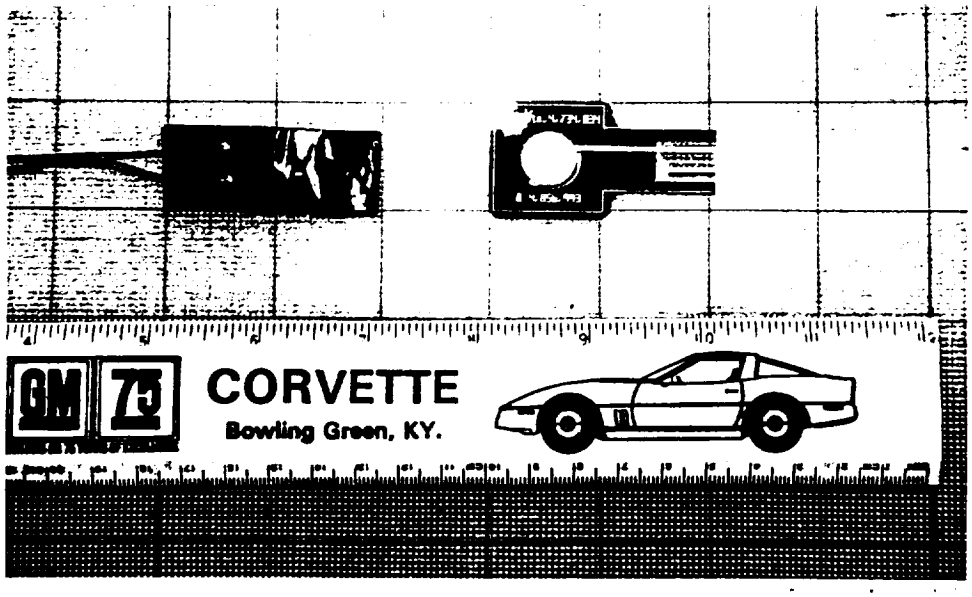

Figure 2. Photo of Tekscan, Inc., pressure sensor. Stock version (right) and after lead attachment (left).

3.2 Low Stiffness Coil Spring EVA Glove MCP Joint

The results of the fabric structure static modeling indicated that a more flexible EVA glove MCP joint could be fashioned by replacing the portion of the back of the EVA glove that is in tension with an assembly that has a lower modulus (or spring rate). An EVA glove mockup with a coil spring dorsal assembly at the MCP joint was constructed with this in mind (see Figure 3). The springs chosen for this assembly (SPEC Model E0360-039-2000, k=0.508 N/mm, free length=50.8 mm, diameter=9.14 mm) have a spring constant significantly less than the fabric used in the standard EVA glove.

The effects of this coil spring dorsal assembly on MCP joint flexibility were evaluated by placing the previously described pressure sensor between the hand and the glove at the base of the middle finger of the right hand. The pressure between the hand and the glove at this point is a measure of the amount of torque required to bend the glove at the MCP joint. A plot of the pressure between the middle finger and the glove during a 90 degree MCP joint flexion task is shown in Figure 5. The coil spring MCP joint resulted in a 20% drop in the pressure between the hand and the glove as compared to a glove with a simple fabric back.

3.3 Low Stiffness Active Actuator EVA Glove MCP Joint

An EVA glove mockup was also constructed that takes advantage of an active actuation system to significantly reduce the stiffness of the MCP joint (Main et al., 1992b). A photo of this mockup is included as Figure 4. The actuators respond to signals from a control system that used the sensors described in Section 3.1 for input. As the fingers bend toward the palm the pressure on the sensors at

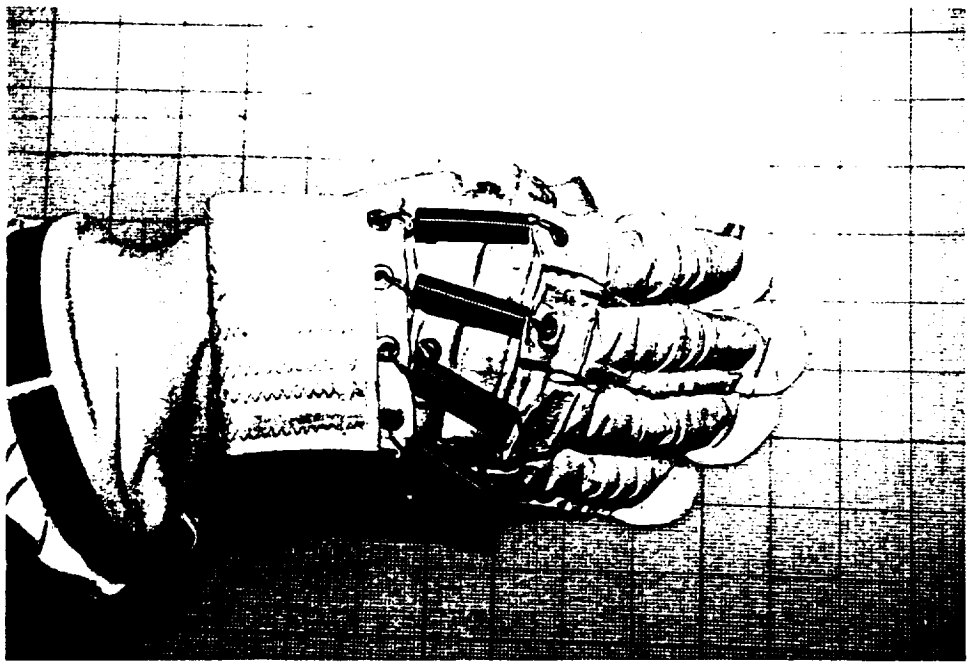

Figure 3. Photo of the EVA glove mockup with the coil spring dorsal assembly.

the base of each finger increases. The control system responds to this increasing signal by opening a valve that allows pressurized nitrogen into the actuators mounted on the back of the glove. The actuators are designed to lengthen when pressurized, so that the back of the glove lengthens and the glove bends at the MCP joint. Compared to the standard glove, this scheme for improving the flexibility of the MCP joint resulted in a 40% drop in the pressure detected by the sensor between the hand and the glove at the base of the middle finger. This indicates a corresponding drop in the torque necessary to bend the joint. A sample of the data taken during the 90 degree MCP joint flexion task showing the pressure between the hand and the glove for the different glove versions is included as Figure 5.

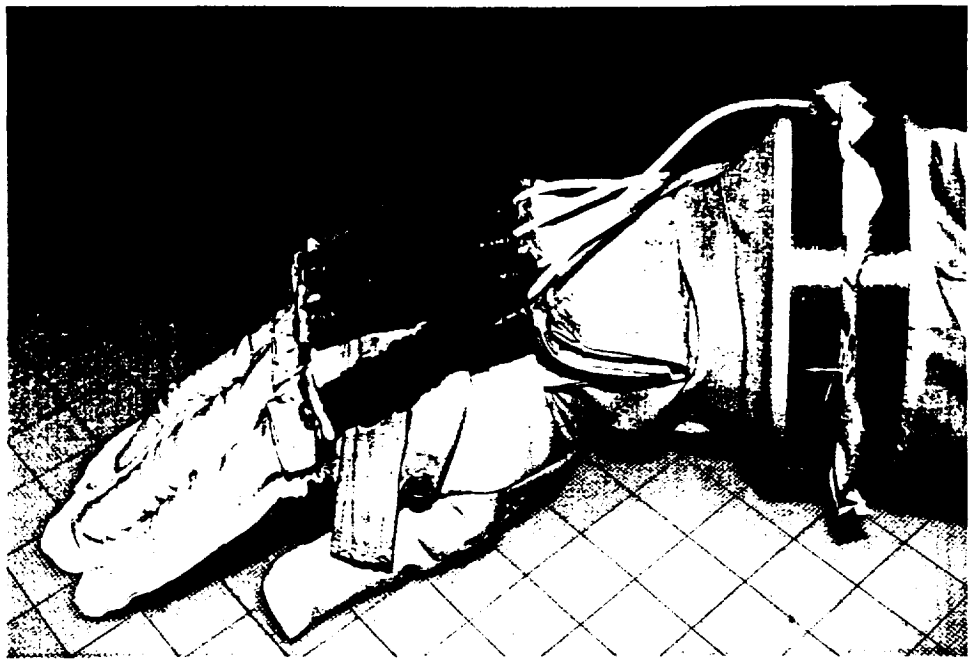

Figure 4. Photo of the EVA glove mockup with the active pneumatic actuators.

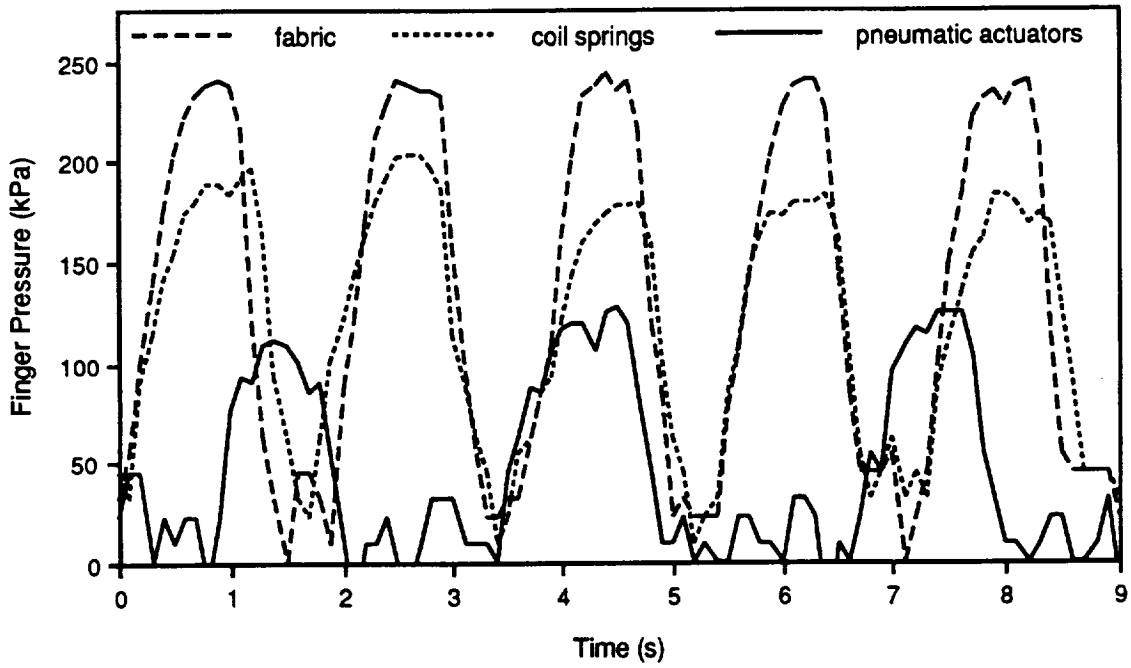

Figure 5. Plot of the pressure sensor output when placed between the hand and the pressurized glove at the base of the middle finger. The coil spring MCP joint and the active actuator MCP joint compared to a plain fabric glove mockup during a 90 degree MCP joint finger flexion task.

3.4 First Generation Hand Exoskeleton

The development of a powered hand exoskeleton represents an effort to develop not only novel technologies that may find application in overcoming the inherent stiffness of the EVA glove, but to perhaps supply strength augmentation as well. The first generation exoskeleton design featured an exoskeleton structure that fit over the back of the hand and a simple hinge joint at the MCP joint (See Figure 6). The force was supplied to bend the exoskeleton at the MCP joint by inclusion of a strand of nickel-titanium alloy wire, a shape memory alloy. Heating and cooling this wire changes the phase of the material and causes it to lengthen and contract, thus providing a force to move the exoskeleton. This early prototype showed great promise, bending the finger over 45 degrees and supplying a joint torque of over 1.1 Nm.

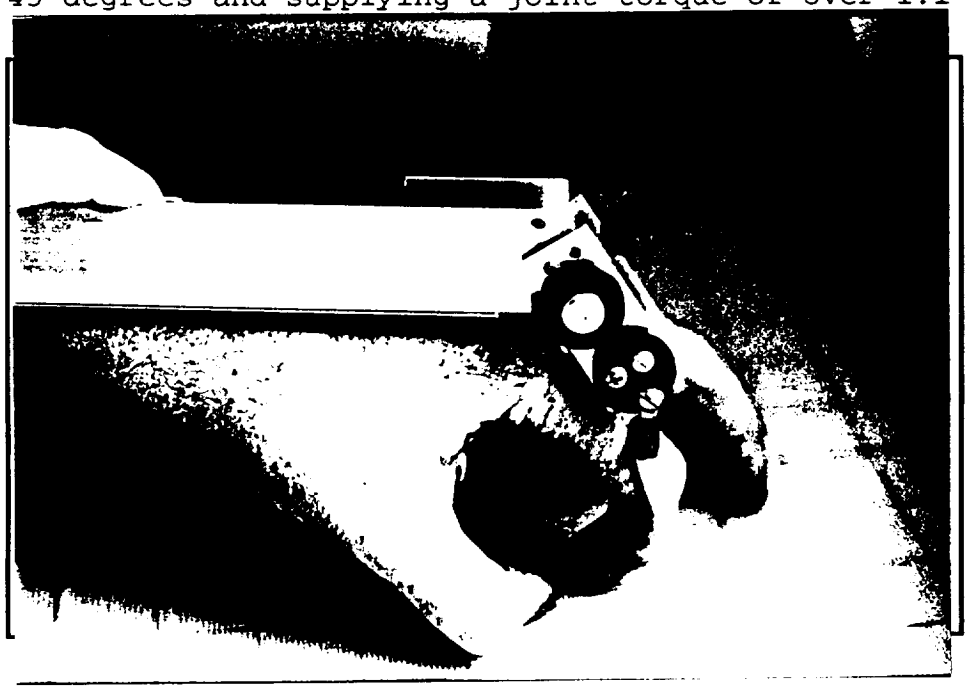

Figure 6. Photo of the first generation hand exoskeleton.

3.5 Second Generation Hand Exoskeleton

Since the completion of the first generation exoskeleton, research has focused on development of a more anthropomorphic exoskeleton design. Problems were

encountered with the hinge joint of the early model. The first change made was the design of a linkage mechanism to better mimic the kinematics of the MCP joint. The problem with the simple hinge joint used in the previous hand exoskeleton is that a finger undergoes not only rotation during motion, but also translation due to the extension of tendons. Therefore, a more realistic exoskeleton joint must have the same center of rotation as that of an actual finger. The motion of the linkage mechanism built for the second generation hand exoskeleton (see Figure 7) corresponds well to the motion of the human finger.

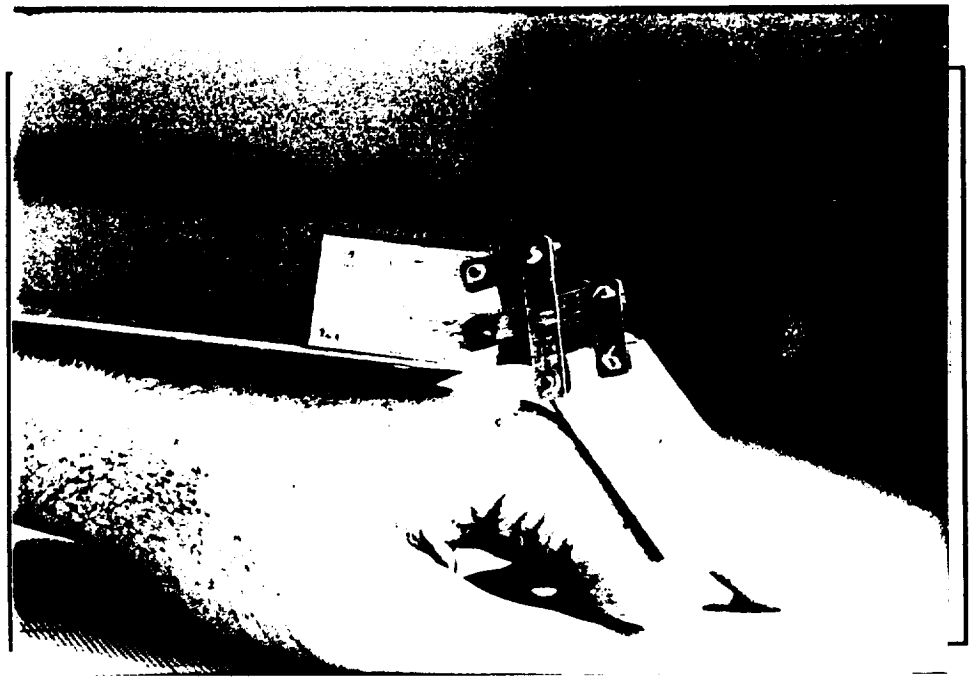

Figure 7. Photo of the second generation hand exoskeleton MCP joint linkage.

4. Bibliography of Related Work

The following examples of publications on space suit glove technology comprise a representative collection of the current directions in this field and include the complete citations of the publications of the Vanderbilt University EVA Glove Research Team.

Balinskas, R., McBarron, J., and Spampinato, P., "Shuttle Extravehicular Mobility Unit (EMU) Operational Enhancements", Presented at the 20th Intersociety Conference on Environmental Systems in Williamsburg, VA, July 9-12, 1990, SAE Paper #901317.

Brown, M. and Schentrup, S., "Requirements for Extravehicular Activities on the Lunar and Martian Surfaces", Presented at the 20th Intersociety Conference on Environmental Systems in Williamsburg, VA, July 9-12, 1990, SAE Paper #901427.

Chodack, J., and Spampinato, P., "Spacesuit Glove Thermal Micrometeoroid Garment Protection Versus Human Factors Design Parameters", proceedings of the 21st International Conference on Environmental Systems in San Francisco, CA, July 15-18, 1991, SAE Paper #911383.

Clapp, M., "Design and Testing of an Advanced Spacesuit Glove", Proceedings of the AIAA 22nd Aerospace Sciences Meeting in Reno, NV, January 9-12, 1984, AIAA Paper #84-0067.

Dickenson, R., Lorenz, C., Peterson, S., Strauss, A., and Main, J., "A Feasibility Study of Hand Kinematics for EVA Analysis Using Magnetic Resonance Imaging", Presented at the 22nd International Conference on Environmental Systems, Seattle, WA, July 13-16, 1992, SAE Paper #921253.

Dickenson, R., Lorenz, C., Peterson, S., Strauss, A., and Main, J., "Magnetic Resonance Imaging as a Tool for Extravehicular Activity Analysis", Presented at the 43rd Congress of the International Astronautical Federation, August 28 - September 5, 1992, Washington, DC, AIAA Paper #IAF/IAA-92-0254.

Fisher, W. and Price, C., "Space Station Freedom External Maintenance Task Team, Final Report", NASA, Johnson Space Center, Houston, TX, July 1990.

Jacobs, G., "A Methodology for Choosing Candidate Materials for the Fabrication of Planetary Space Suit Structures", Presented at the 20th Intersociety Conference on Environmental Systems in Williamsburg, VA, July 9-12, 1990, SAE Paper #901429.

Kosmo, J. J., Bassick, J. and Porter, K., "Development of Higher Operating Pressure Extravehicular Space-Suit Assemblies," proceedings of the 18th Intersociety Conference on Environmental Systems in San Francisco, CA, July 11-13, 1988, SAE Paper #881102.

Kosmo, J., "Design Considerations for Future Planetary Space Suits", Presented at the 20th Intersociety Conference on Environmental Systems in Williamsburg, VA, July 9-12, 1990, SAE Paper #901428.

Le Bihan, D., "Magnetic Resonance Imaging of Perfusion", Magn Reson Med 1990;14:283-292.

Lorenz, C., Powers, T., Holburn, G., and Price, R., Quantitative Analysis of MR Perfusion/Diffusion Images in a Dog Model of Renal Artery Stenosis with Microsphere Correlation", Radiology 1990; 177(P):284.

Main, J. A., Peterson, S. W., and Strauss, A. M., "A Prototype Power Assist EVA Glove," proceedings of the 21st Intersociety Conference on Environmental Systems in San Francisco, CA, July 15-18, 1991, SAE Paper #911384.

Main, J. A., Peterson, S. W., and Strauss, A. M., "Design of Space-Based Inflatable Tubular Frame Structures," in Proceedings of the International Design for Extreme Environments Assembly in Houston, TX, November 1991.

Main, J. A., Peterson, S. W., and Strauss, A. M., "Preliminary Structural Analysis of Space-Based Inflatable Tubular Frame Structures," paper presented at the European Joint Conference on Engineering Systems Design and Analysis, June 29-July 4, 1992, in Istanbul, Turkey.

Main, J. A., Peterson, S. W., and Strauss, A. M., "Power Assist EVA Glove Development," Presented at the 22nd Intersociety Conference on Environmental Systems in Seattle, WA, July 13-15, 1992.

Moseley, M., Cohen, Y., Mintorovitch, J., Chileuitt, L., Shimizu, H., Kucharczyk, J., Wendland, M., and Weinstein, P., "Early Detection of Regional Cerebral Ischemia in Cats: Comparison of Diffusion- and T2-Weighted MRI and Spectroscopy", Magn Reson Med 1990;15:330-346.

Niemann, T., Lorenz, C., Peterson, S., and Strauss, A., "MR Imaging of Hand Microcirculation as a Potential Tool for Space Glove Testing and Design", paper presented at the 21st International Conference on Environmental Systems in San Francisco, CA, July 15-18, 1991, SAE Paper #911382.

Ockels, W., "Combinaison pressurisee pour astronaute equipee de gants a pression variable a dexterite amelioree", ESA Patent 88-05609.

O'Hara, J., Cleland, J. and Winfield, D., "The Development of a Test Methodology for the Evaluation of EVA Gloves", Presented at the 18th Intersociety Conference on Environmental Systems in San Francisco, CA, July 11-13, 1988, SAE Paper #881103.

O'Hara, J., Briganti, M., Cleland, J., and Winfield, D.,"Extravehicular Activities Limitations Study Volume II: Establishment of Physiological and Performance Criteria for EVA Gloves," NASA Contractor Report AS-EVAL-FR-8701, NTIS N89-17393.

Ollivier, Y. and Diener, M., "Development of the Suit Enclosure of the European EVA Spacesuit", Presented at the 20th Intersociety Conference on Environmental Systems in Williamsburg, VA, July 9-12, 1990, SAE Paper #901244.

Pickens, D., Dawson, R., Holburn, G., Lorenz, C., and Price, R., "Quantitative Perfusion/Diffusion-Weighted Imaging of Normal Brain and Induced Stroke in an Animal Model with Microsphere Correlation", 10th Annual Society of Magnetic Resonance in Medicine Abstract Book, 1168, 1991.

Price R., Pickens, D., Lorenz, C., "Gd-DTPA Kinetics in an Excised Kidney Model with Use of Snapshot FLASH MR Imaging", Radiology 1990; 177(P):110.

Shepherd, C., and Lednicky, C., "EVA Gloves: History, Status, and Recommendations for Future NASA Research", April 1990, JSC-23733.

Spampinato, P., Cadogan, D., McKee, T., and Kosmo, J., "Advanced Technology Application in the Production of Spacesuit Gloves," proceedings of the 20th Intersociety Conference on Environmental Systems in Williamsburg, VA, July 9-12, 1990, SAE Paper #901322.

5. Eva Glove Research Team Publications 1991-1992

SAE TECHNICAL
PAPER SERIES

921253

A Feasibility Study of Hand Kinematics for EVA Analysis Using Magnetic Resonance Imaging

Reuben D. Dickenson
Vanderbilt Univ.

Christine H. Lorenz
Vanderbilt Medical Center

Steven W. Peterson, Alvin M. Strauss, and John A. Main
Vanderbilt Univ.

SAE 75 YEARS AEROSPACE

22nd International Conference
on Environmental Systems
Seattle, Washington
July 13-16, 1992

SAE The Engineering Society For Advancing Mobility Land Sea Air and Space®
INTERNATIONAL

400 COMMONWEALTH DRIVE, WARRENDALE, PA 15096-0001 U.S.A.

All SAE papers, standards, and selected books are abstracted and indexed in the SAE Global Mobility Database.

ISSN 0148-7191

Printed in USA

A Feasibility Study of Hand Kinematics for EVA Analysis Using Magnetic Resonance Imaging

Reuben D. Dickenson
Vanderbilt Univ.

Christine H. Lorenz
Vanderbilt Medical Center

Steven W. Peterson, Alvin M. Strauss, and John A. Main
Vanderbilt Univ.

ABSTRACT

A new method of analyzing the kinematics of joint motion is developed in this study. Magnetic Resonance Imaging (MRI) offers several distinct advantages. Past methods of studying anatomic joint motion have usually centered on four approaches. These methods are x-ray projection, goniometric linkage analysis, sonic digitization, and landmark measurement of photogrammetry. Of these four, only x-ray is applicable for in vivo studies. The remaining three methods utilize other types of projections of inter-joint measurements, which can cause various types of error. MRI offers accuracy in measurement due to its tomographic nature (as opposed to projection) without the problems associated with x-ray dosage.

Once the data acquisition of MR images was complete, the images for this study were processed using a 3-D volume rendering workstation. In this study, the metacarpalphalangeal (MCP) joint of the left index finger was selected and reconstructed into a three-dimensional graphic display. From the reconstructed volumetric images, measurements of the angles of movement of the applicable bones were obtained and processed by analyzing the screw motion of the MCP joint. Landmark positions were chosen at distinctive locations of the joint at fixed image threshold intensity levels to ensure repeatability. The primarily two-dimensional planar motion of this joint was then studied using a method of constructing coordinate systems using three (or more) points. A transformation matrix based on a world coordinate system described the location and orientation of a local target coordinate system.

This study will lead to future research involving volume rendering of MRI data focusing on the internal kinematics of the hand's individual ligaments, cartilage, tendons, etc. Its findings will show the applicability of MRI to joint kinematics for gaining further knowledge of the hand-glove (power-assisted) design for EVA.

INTRODUCTION

The purpose of this research is to determine the feasibility of using Magnetic Resonance Imaging (MRI) as a tool for the study of hand kinematics. This project was funded by the NASA Office of Aeronautics and Space Exploration and the NASA National Space Grant College and Fellowship Program. Various methods of determining the internal motion of the hand's internal bone structures exist, but MRI offers several advantages which will be discussed in detail later in this article.

DATA ACQUISITION METHODS

The data for this study came from the images of the left hand of a 29 year old male. The entire hand was imaged, but for the purposes of this study, only the index finger was analyzed. The study focused on the rotation and translation characteristics of the proximal phalanx and its relation to the MCP joint, so that only the portions of the images pertaining to these areas were used. A restraint device was constructed to ensure that both random hand motion and vibratory noise were minimized during imaging. Although random hand motion can vary from one individual to the next, the magnitude of this motion is very small. Over the image acquisition period, this type of motion results in negligible position error. The device was designed to ensure that the index finger was separated from the other fingers in a fixed position. Six preset angles of rotation were possible using this device, of which three were used for this study. Since MR images' signal intensity is based on density of certain atoms (hydrogen in this case), markers containing water were placed on the restraint. Two of the markers were attached to the bottom of the device, while the third was attached to the hinged portion, just past the tip of the index finger (Fig 2) The markers appear as circles in Figure 2, with A denoting the marker beneath the hinge, B showing the marker affixed to the tip of the base, and C showing the marker at the fingertip. These markers allowed calibration of the procedure and a means for determining the accuracy of the group's results.

MRI is used widely for its tomographic capabilities, high spatial resolution, and ability to produce high contrast between different tissue types. The physics of MRI are among the most complicated of all the current imaging modalities [2,3,7]. Briefly, the basic MR process is to place a subject into a strong uniform magnetic field in the bore of a large magnet, which typically has a field strength on the order of 1.0-1.5 Tesla. This field aligns the net magnetic spin of the individual atoms. In order to produce a usable signal, these aligned magnetic spins must be perturbed. A radiofrequency (RF) pulse is applied at the resonant frequency of the atomic spin of interest (hydrogen is usually chosen due to its abundance). The spins are moved away from their preferred axis of rotation by the energy imparted by the RF pulse. The spins will try to realign with their original axis of rotation (along the bore of the magnet), and as they realign, they emit a RF signal. This signal can be decomposed into its frequency and phase components which are related to the location in the subject from which the signal was measured. The magnitude of the signal is proportional to the signal intensity generated by the various structures in the image. This magnitude is, in turn, related to the density of hydrogen atoms in the tissue and the realignment (relaxation) parameters of the tissue studied. These parameters are called T1, the longitudinal relaxation time, and T2, the transverse relaxation time. The density of the hydrogen atoms determines the material present in a give 3-D volume of space. This information is then projected onto a 2-D display for viewing (Figure 1). The image data can be manipulated to reorient the slices in different orientations for further analysis.

The programs used to control the MR scanner to create images are called pulse sequences. Each type of pulse sequence provides different contrast between various tissue types or has different spatial resolution or signal-to-noise properties. The most traditional (and slowest) type of pulse sequence is the spin echo pulse sequence. There are also many pulse sequences designed to provide essentially the same tissue contrast or signal-to-noise ratio as spin echo sequences,

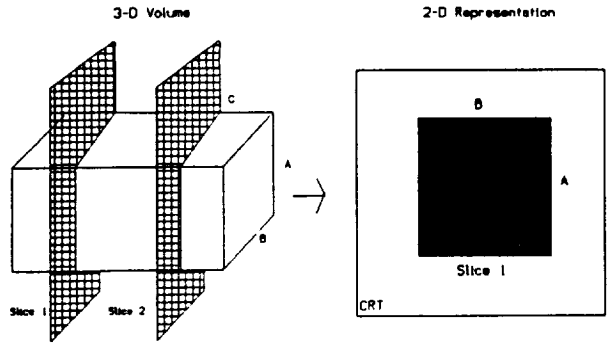

Figure 1 - Diagram showing the 3-D slices of a volume depicted on a 2-D CRT display.

but in a fraction of the time. Since our goal was to optimize speed, image quality, resolution, and tissue contrast, we used a variation of a fast pulse sequence called TurboFLASH. The scanner used was a 1.5T clinical unit (Siemens Magnetom SP, Iselin, NJ). In order to obtain approximately isotropic image volume elements (voxels), we used a volumetric acquisition version of TurboFLASH known as MPRAGE (Magnetization Prepared Rapid Acquisition Gradient Echo). With this sequence, we obtained acceptable spatial resolution (1-2 mm) images through the entire hand with good differentiation between tissue types, and an acceptable signal-to-noise ratio in approximately 7 minutes. The pulse sequence parameters used were TR = 6 msec, flip angle = 10 degrees, acquisition matrix = 130 x 256 x 128, and a field of view = 250 mm.

Figure 1 demonstrates the tomographic capability of MRI. Since a volume of image data of up to 30 cm^3 can be acquired using the particular radiofrequency coil chosen for this study, imaging the hand in an EVA glove will be a simple extension to this study.

3-D VOLUME PREPARATION

After acquiring the MRI data, it was necessary to prepare the volumes. These were created by adding the area of interest (the phalangeal bones of the index finger) for each slice of MRI data. Since each slice contains a 2-D representation of the phalanges, adding them creates the composite 3-D volume. All volume rendering was completed utilizing a DMI MAXIVIEW 3-D dedicated workstation (MAXIVIEW, Dimensional Medicine, Inc., Minnetonka, MN) and its accompanying software.

The MAXIVIEW workstation was created specifically as a tool for processing medical imaging modality data. It accepts image data from Computed Tomographic (CT) systems, Digital Subtraction Angiography (DSA) systems, and MRI systems. This system allows 3-D reformatting, resectioning and multi-planar reformatting for processing images. In addition to creating the volumes, MAXIVIEW also proved valuable for viewing, calibrating, and measuring the volumes.

The overall problem with the thresholding of MRI data during volume rendering deserves further discussion. The reconstruction sequence of computer workstations such as the MAXIVIEW depends largely upon its ability to extract as much surface detail as possible in two dimensions (ie, differentiate between the surface of the proximal phalanx and the surrounding tissues in a given slice) and to then add these surfaces for a 3-D representation (Vannier and Geist, [10]) using MRI, CT, or DSA data. However, as the resolution of the individual slices decreases, the resolution of the corresponding volume likewise decreases. This fact makes CT an excellent choice for rendering. It is based on attenuation values for X-rays, called Hounsfield numbers, which offer a stark contrast between bone and soft tissue. However, CT still depends on X-ray attenuation, which makes MRI attractive for repetitive

studies of this type, owing to its lack of ionizing radiation. But MRI suffers from its lower resolution of the border between bone and soft tissue (compared to CT), which often leads to difficulties in thresholding. This will become less of a problem as the contrast of MRI scanners' images increases.

Thresholding the images is the key step in rendering volumes. The images contain gray scale computed information based on a combination of hydrogen density, T1 and T2 relaxation times (MRI) or Hounsfield numbers (CT). This gray scale information is then utilized to determine what material is present inside a 3-D voxel. Voxels which contain the correct values are retained for inclusion in the volume, while others remain blank. It follows that the size of the voxel itself proves to be an overall limit to the volume's resolution. In this study, the typical volume was approximately 0.4 mm in each dimension (x,y,z). After the volume is computed, the next step is the shading process. An initial viewing direction is chosen. The 3-D view in this direction is projected onto a 2-D plane, called the image plane, for display on the CRT.

Rendering the phalanges for this study was the next step. In an effort to maximize the resolution of the volumes, the markers and the bones were rendered separately. This created a separate representation for each, but the positions relative to each other remained fixed in the global coordinate system of the MRI scanner. For each slice of a pose, the appropriate bones were selected and thresholded. A second set of bone markers was added to the bone's rendered volume to ensure that the volume was correctly aligned while measuring in the 3-D mode (see Figures 3-5). After the volumes for the bones were created, the volumes for the restraint device's water markers were computed. The water markers served to calibrate and validate the measurements and algorithms for this study. A second set of markers were also produced with the water marker volumes to ensure alignment, just as we did with the phalanx volumes.

In order to analyze the motion of rigid bodies, we used the calculations and methods devised by several authors [4,8,9]. The spatial coordinates of landmark positions (a minimum of three on each rigid body in each position) can be calculated from the measurement tools of the DMI. These coordinates then comprise the information necessary to derive the transformation matrix describing the motion, which is taken to be a screw motion. A screw motion can be described by a rotation matrix and a translation vector, or by the position of the screw axis, the angle of rotation about this axis, and the translation along this axis. This method is a fairly robust method of determining the motion of the rigid body, but does suffer from errors induced by scaling errors and random measurement errors (noise).

While a comprehensive treatment of the derivation of Spoor and Veldpaus' methods is not feasible in this study, several key points need to be clarified. First, for this method, three or more non-collinear points are needed in the first and second positions, with no initial approximation needed. The translation vector **(v)** and the rotation matrix **(R)** describe the movement of a rigid body from position 1 to position 2. The rotation matrix has the following properties:

$$R^T R = I \qquad (1)$$

where **I** is the 3x3 identity matrix and **T** denotes transposition. The vectors describing each point in the first position $(\mathbf{a}_i)$ and those describing the points in the second position $(\mathbf{q}_i)$ are related by

$$q_i = Ra_i + v \qquad (2)$$

Since the unknown quantities in (2) are **R** and **v**, a method must be used

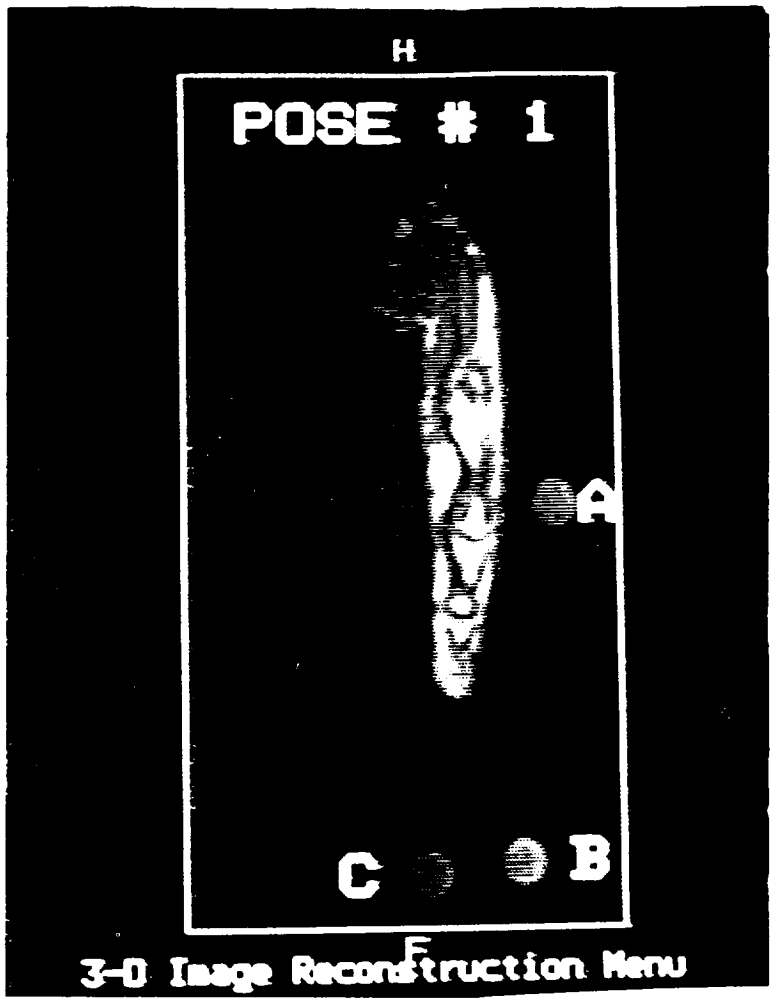

Fig 2 - A representative image of a "slice" of the left index finger in the restraint device. A,B, and C show the markers.

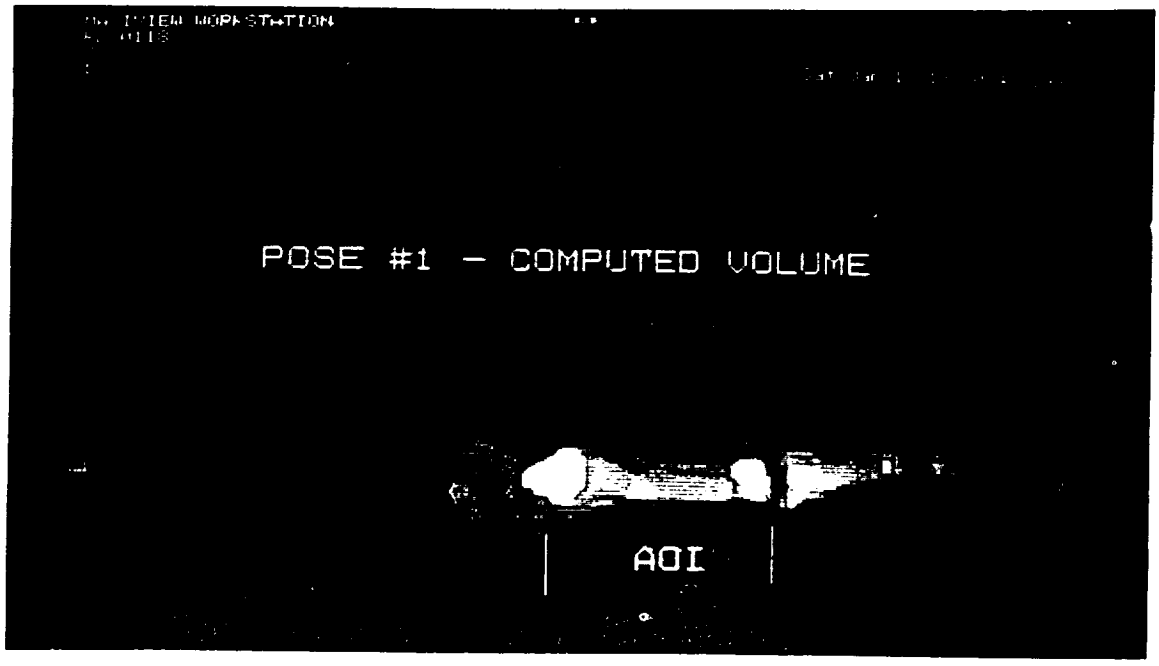

Fig 3 - The rendered volume in the first pose.

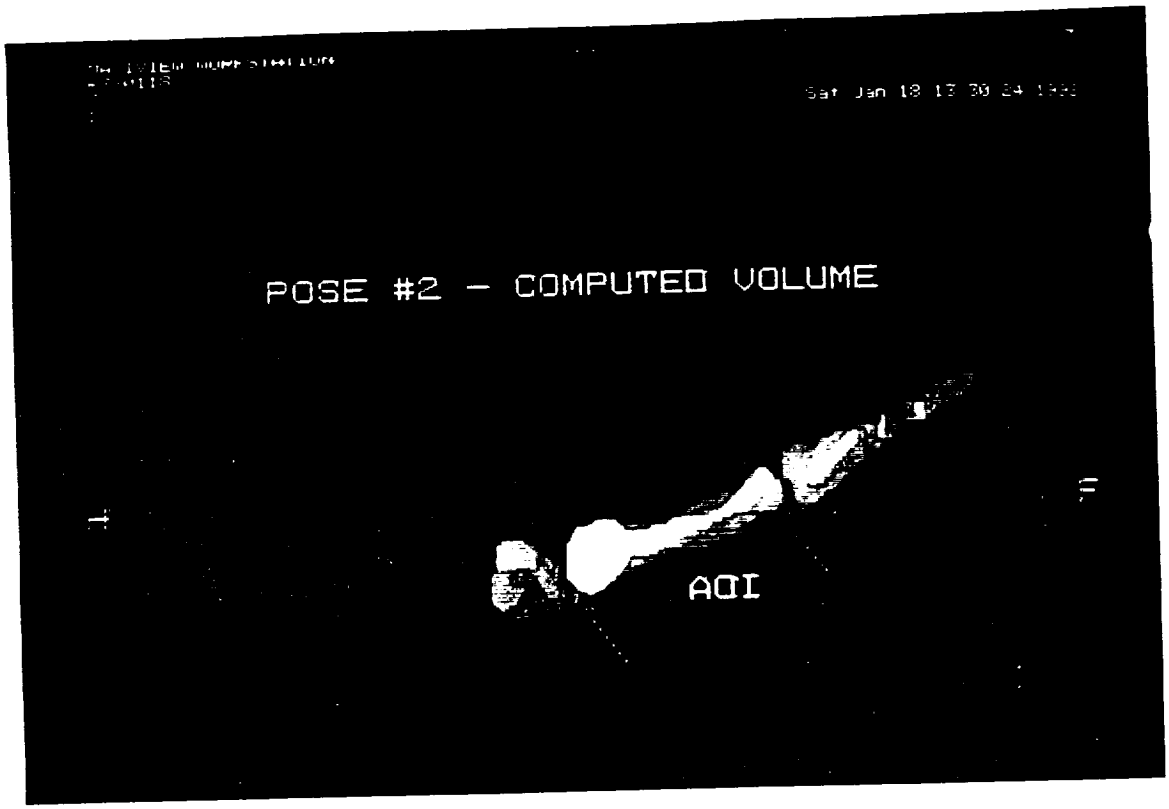

Fig 4 - The rendered volume in the second pose.

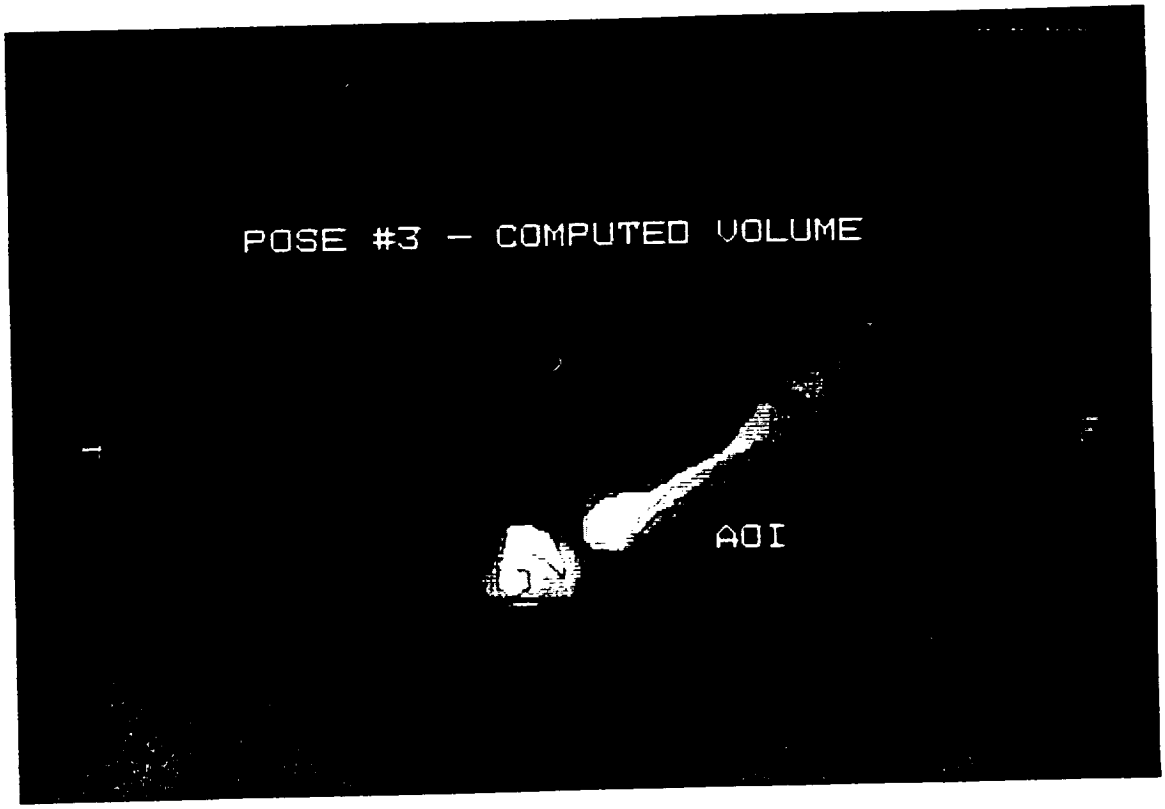

Fig 5 - The rendered volume in the third pose.

to obtain values for them by using the measurements of the points in the first and second positions. A computer program was written (Peterson, [8]) which takes the three-dimensional coordinates from two positions of the rigid body and then computes the transformation matrix in the form of

$$T=\begin{vmatrix} R_{11} & R_{12} & R_{13} & 0 \\ R_{21} & R_{22} & R_{23} & 0 \\ R_{31} & R_{32} & R_{33} & 0 \\ v_i & v_j & v_k & 1 \end{vmatrix} \quad (3)$$

where the 3x3 matrix in the upper left describes the rotation **(R)** of the body, and **v** denotes the translation vector. Once the transformation matrix is determined, the methods of analyzing the motion can be one of several in existence. The method of Spoor and Veldpaus utilizes the symmetrical and anti-symmetrical portions of the rotation matrix to determine the body's motion about the helical axis, with

$$2*n*\sin(\theta)=\begin{vmatrix} R_{32}-R_{23} \\ R_{13}-R_{31} \\ R_{21}-R_{12} \end{vmatrix} \quad (4)$$

The angular rotation is given by

$$\sin(\theta)=1/2\sqrt{(R_{32}-R_{23})^2+(R_{13}+R_{31})^2+(R_{21}-R_{12})^2} \quad (5)$$

The rotation is also given by

$$\cos(\theta)=(1/2)*(R_{11}+R_{22}+R_{33}-1) \quad (5a)$$

Now that the angle is known, returning to equation (4) yields **(n)**, the unit vector along the helical axis.

For the translation analysis, one must again derive an expression based upon the transformation matrix. The translation vector, **v**, is taken from the transformation matrix. The following information determines the necessary information:

$$[1-\cos(\theta)]\,nn^T=[(R+R^T)-\cos(\theta)I]/2=|b_1 b_2 b_3| \quad (6)$$

where $\mathbf{b_i}$ are three element columns. Another value for **n** is determined from

$$b_i^T=\max(b_1^T b_1, b_2^T b_2, b_3^T b_3);\ n=\pm\frac{b_i}{\sqrt{b^T b_i}} \quad (7)$$

where **n** will be in the same direction as that derived from (4), but a scaling factor different in magnitude. The values for a point on the axis and the translation on the axis are then found from

$$t=n^T*v \quad (8)$$

and

$$s=(-1/2)*n*(n*v)+\frac{\sin(\theta)}{(2(1-\cos(\theta))}*n*v \quad (9)$$

where **s** represents a radius vector of a point on the helical axis, and **t** is the translation along the helical axis. Noteworthy is the fact that the translation vector is quite sensitive to measurement errors and noise, while the rotation matrix is rather robust and yielded highly accurate results.

DATA ANALYSIS/RESULTS

The angles of rotation about the helical axis for the respective position changes for this study were

ANGLES OF ROTATION - POSE #3 MARKERS	
Restraint Device	- 52.0 deg
2-D Slice Image	- 52.9 deg
3-D Volume	- 52.7 deg

Table 1 - Calibration Results

quite accurate, as were the calibration results utilizing the markers. Each marker set for the poses was rendered into a 3-D volume, just as the phalanx voxels were rendered. However, the water marker volumes were created for one slice of image data only. This was

to ensure that a clear rotation about one axis alone was visible, thus further validating the measurements of the DMI and the accuracy of the transformation matrix software. From the slice containing the markers (see Figure 2), measurements of the markers for pose #3 were determined for the angle B-A-C. This angle was then compared to the angle produced by measuring landmark positions from the rigid body A-B (notionally position 1) moving to A-C (notionally to position 2). The results are listed in Table 1. Furthermore, the unit vector along the helical axis for the rotation of Pose #3 was $n = [0\ 0\ 1]^T$, thus showing that for the markers, a simple 2-D rotation occurred in the z-axis, which proves valuable later.

After checking the process using the water markers, we then measured and analyzed the rigid body motion of the landmark positions on the proximal phalanx. The measurements were taken in the (x,y,z) coordinates and then transformed into the transformation matrix. From this, as in the case of the markers, we determined the motion of the phalanx about the helical axis using Spoor and Veldpaus algorithms. Seven landmark positions defined each rigid body motion, with future efforts geared toward increasing the number of landmark positions for increased accuracy and reliability. The results are listed in Table 2.

From-To (deg)	1	2	3
1 - 2	21.3	20.4	21.3
2 - 3	12.4	14.0	12.7
1 - 3	32.6	32.9	33.5

Table 2 - The 3-D rotations for three trials.

The overall consistency of the results above can be readily observed. The fact that the accuracy of the transformation increases as the magnitude of motion increases is a point of interest for future work. Also, as in the case of the markers, the motion was primarily two-dimensional about the z-axis, as expected. The small rotation in the x and y axes can be attributed mainly to the alignment of the subject hand. Random measurement errors also played a role. The mean and standard deviation of the movements are listed in Table 3.

From-To	Mean	Deviation(deg)
1-2	21.1	.8
2-3	13.0	.7
1-3	33.5	.4

Table 3 - Statistical Analysis.

CONCLUSION

As noted earlier, future work in this area includes ongoing power-assisted glove work. A subject could wear the EVA glove inside the magnet, placing the hand within the radiofrequency coil. By stopping a subject at various stages of the motion required to perform a task, high resolution imaging of the entire had and glove volume could be performed at each stage. The transformations of the entire hand's members could then be analyzed. The effect of using the glove compared to non-glove motion could also be studied. Other areas of possible interest include those involving potential applications of injury-related analysis of the hand. One major subject in this field is study of individual joint kinematics leading to injury suffered during certain repetitive activities, such as those encountered by a computer programmer while entering data at a keyboard.

Our research proved that MRI is

a feasible tool for kinematic analysis of rigid bodies. The process was very slow for this initial study, due to several factors, but subsequent studies will be completed much more quickly. The screw motion analysis of the proximal phalanx in this research produced results that were both reliable and repeatable for the proximal phalanx and should yield the same results for whole hand analysis, a future goal of the group. While other methods do exist, such as electrical goniometry, computed tomography, etc., only MRI offers a safe means of producing accurate results for in vivo analysis.

REFERENCES

1. Chao E.Y. and Morrey B.F., "Three-Dimensional Rotation of the Elbow", Journal of Biomechanics, Volume 11, pp. 57-73, 1978.

2. Haase, A. "Snapshot FLASH MRI. Applications to T1, T2, and Chemical-Shift Imaging." Magnetic Resonance Medicine 1990; 13:77-89.

3. Jones, J.P. "Physics of the MR Image: From the Basic Principles to Image Intensity and Contrast, in Magnetic Resonance Imaging: Vol. II, Physical Principles and Instrumentation, eds. Partain, C.L. et al., W.B. Saunders Company, Philadelphia, PA pp. 1003-1028.

4. Kinzel G.L. et al., "Measurement of the Total Motion Between Two Body Segments- I. Analytical Development", Journal of Biomechanics, Volume 5, pp. 93-105, 1972.

5. Kinzel G.L. et al., "Measurement of the Total Motion Between Two Body Segments - II. Description of Application", Journal of Biomechanics, Volume 5, pp. 283-293, 1972.

6. Larsen R.J. and Marx M.L., Mathematical Statistics and Its Applications, Prentice-Hall, Englewood Cliffs, New Jersey, 1986.

7. Mugler, J.P. and Brookeman J.R., "Three-Dimensional Magnetization Prepared Gradient Echo Imaging",society of Magnetic Resonance in Medicine Abstract Book, 1990, p. 432.

8. Peterson S.W., Measurement and Analysis of Human Joint Motion, Ph.D. Thesis, University of Minnesota, December 1985.

9. Spoor C.W. and Veldpaus F.E., "Rigid Body Motion Calculated from Spatial Co-ordinates of Markers", Journal of Biomechanics, Volume 13, pp. 391-393.

10. Vannier M.W. and Geist D., "PC-Based 3-D Reconstruction of Medical Images", Computer and Graphics, Volume 13, No. 2, 1989, pp 135-143.

MAGNETIC RESONANCE IMAGING AS A TOOL FOR EXTRAVEHICULAR ACTIVITY ANALYSIS

R. Dickenson, C. Lorenz[1], S. Peterson, A. Strauss, J. Main

Departments of Mechanical Engineering and Radiology and Radiological Sciences[1]

Vanderbilt University, USA

Paper # IAF/IAA-92-0254

43rd CONGRESS OF THE
INTERNATIONAL ASTRONAUTICAL FEDERATION

August 28-September 5, 1992/Washington, DC

MAGNETIC RESONANCE IMAGING AS A TOOL FOR EXTRAVEHICULAR ACTIVITY ANALYSIS

R. Dickenson* , C. Lorenz[1], S. Peterson, A. Strauss, J. Main

Departments of Mechanical Engineering and Radiology and Radiological Sciences[1]

Vanderbilt University, USA

Abstract

The purpose of this research is to examine the value of magnetic resonance imaging (MRI) as a means of conducting kinematic studies of the hand for the purpose of extravehicular activity (EVA) capability enhancement. After imaging the subject hand using a magnetic resonance scanner, the resulting 2-D slices were reconstructed into a 3-D model of the proximal phalanx of the left hand. Using the coordinates of several landmark positions, one is then able to decompose the motion of the rigid body. MRI offers highly accurate measurements due to its tomographic nature without the problems associated with other imaging modalities for in vivo studies.

I. Introduction

The study of the movement of the phalanges of the hand using a different imaging modality was the goal of this study. Various methods exist for determining the 3-D rotation and translation of the bones, such as x-ray projection, goniometers, sonic digitization, etc. MRI offers the advantage of being a safe, accurate means of studying joint motions in vivo.

As with other studies of this type, one starts with the data acquisition phase and then processes the acquired data to produce meaningful results. The MRI scanner was the means of data acquisition for this study, with the resulting 2-D images serving as the basis for the remainder of the study.

II. Data Acquisition Methods

The data for this study came from MR images of a subject's left hand. The entire hand was imaged, but for the purposes of this study, only the index finger was analyzed. The study focused on the rotation and translation characteristics of the proximal phalanx and its relation to the MCP joint, so only the portions of the images pertaining to these areas were used. A restraint device was constructed to ensure that both random hand motion and vibratory noise were minimized during imaging. Although random hand motion can vary from one individual to the next, the magnitude of this motion is very small. Over the image acquisition period, this type of motion results in negligible position error. The

* Research Assistant, Mechanical Engineering

device was designed to ensure that the index finger was separated from the other fingers in a fixed position. Six preset angles of rotation were possible using this device, of which three were used for this study. Since MR images' signal intensity is based on density of certain atoms (hydrogen in this case), markers containing water were placed on the restraint. Two of the markers were attached to the bottom of the device, while the third was attached to the hinged portion, just past the tip of the index finger (see Fig 2) The markers appear as circles, with A denoting the marker beneath the hinge, B showing the marker affixed to the tip of the base, and C showing the marker at the fingertip. These markers allowed calibration of the procedure and a means for determining the accuracy of the group's results.

MRI is used widely for its tomographic capabilities, high spatial resolution, and ability to produce high contrast between different tissue types. The physics of MRI are among the most complicated of all the current imaging modalities [2,3,7]. Briefly, the basic MR process involves placing a subject into a strong uniform magnetic field in the bore of a large magnet, which typically has a field strength on the order of 1.0-1.5 Tesla. This field aligns the net magnetic spin of the individual atoms. In order to produce a usable signal, these aligned magnetic spins must be perturbed. A radiofrequency (RF) pulse is applied at the resonant frequency of the atomic spin of interest (hydrogen is usually chosen due to its abundance). The spins are moved away from their preferred axis of rotation by the energy imparted by the RF pulse. The spins will try to realign with their original axis of rotation (along the bore of the magnet), and as they realign, they emit a RF signal. This signal can be decomposed into its frequency and phase components which are related to the location in the subject from which the signal was measured. The magnitude of the signal is proportional to the signal intensity generated by the various structures in the image. This magnitude is, in turn, related to the density of hydrogen atoms in the tissue and the realignment (relaxation) parameters of the tissue studied. These parameters are called T1, the longitudinal relaxation time, and T2, the transverse relaxation time. The density of the hydrogen atoms determines the material present in a given 3-D volume of space. This information is then projected onto a 2-D display for viewing (Figure 1). The image data can be manipulated to reorient the slices in different orientations for further analysis.

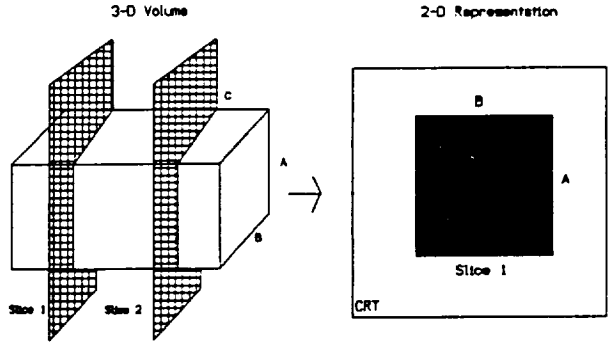

Figure 1 - Diagram showing the 3-D slices of a volume depicted on a 2-D CRT display.

The programs used to control the MR scanner to create images are called pulse sequences. Each type of pulse sequence provides different contrast between various tissue

types or has different spatial resolution or signal-to-noise properties. The most traditional (and slowest) type of pulse sequence is the spin echo pulse sequence. There are also many pulse sequences designed to provide essentially the same tissue contrast or signal-to-noise ratio as spin echo sequences, but in a fraction of the time. Since our goal was to optimize speed, image quality, resolution, and tissue contrast, we used a variation of a fast pulse sequence called TurboFLASH. The scanner used was a 1.5T clinical unit (Siemens Magnetom SP, Iselin, NJ). In order to obtain approximately isotropic image volume elements (voxels), we used a volumetric acquisition version of TurboFLASH known as MPRAGE (Magnetization Prepared Rapid Acquisition Gradient Echo). With this sequence, we obtained acceptable spatial resolution (1-2 mm) images through the entire hand with good differentiation between tissue types, and an acceptable signal-to-noise ratio in approximately 7 minutes. The pulse sequence parameters used were TR = 6 msec, flip angle = 10 degrees, acquisition matrix = 130 x 256 x 128, and a field of view = 250 mm.

Figure 1 demonstrates the tomographic capability of MRI. Since a volume of image data of up to 30 cm^3 can be acquired using the particular radiofrequency coil chosen for this study, imaging the hand in an EVA glove will be a simple extension to this study.

III. 3-D Volume Preparation

After acquiring the MRI data, it was necessary to prepare the volumes. These were created by adding the area of interest (the phalangeal bones of the index finger) for each slice of MRI data. Since each slice contains a 2-D representation of the phalanges, adding them creates the composite 3-D volume. All volume rendering was completed utilizing a DMI MAXIVIEW 3-D dedicated workstation (MAXIVIEW, Dimensional Medicine, Inc., Minnetonka, MN) and its accompanying software.

The MAXIVIEW workstation was created specifically as a tool for processing medical imaging modality data. It accepts image data from Computed Tomographic (CT) systems, Digital Subtraction Angiography (DSA) systems, and MRI systems. This system allows 3-D reformatting, resectioning and multi-planar reformatting for processing images. In addition to creating the volumes, MAXIVIEW also proved valuable for viewing, calibrating, and measuring the volumes.

The overall problem with the thresholding of MRI data during volume rendering deserves further discussion. The reconstruction sequence of computer workstations such as the MAXIVIEW depends largely upon its ability to extract as much surface detail as possible in two dimensions (ie, differentiate between the surface of the proximal phalanx and the surrounding tissues in a given slice) and to then add these surfaces for a 3-D representation (Vannier and Geist, [10]) using MRI, CT, or DSA data. However, as the resolution of the individual slices decreases, the resolution of the corresponding volume likewise decreases. This fact makes CT an excellent choice for rendering. It is based on attenuation values for X-rays, called Hounsfield numbers, which offer a stark contrast between bone and soft tissue. However, CT still depends on X-ray attenuation, which makes MRI attractive for repetitive studies of this type, owing to its lack of ionizing radiation. But MRI suffers from its lower resolution of

the border between bone and soft tissue (compared to CT), which often leads to difficulties in thresholding. This will become less of a problem as the contrast of MRI scanners' images increases.

Thresholding the images is the key step in rendering volumes. The images contain gray scale computed information based on a combination of hydrogen density, T1 and T2 relaxation times (MRI) or Hounsfield numbers (CT). This gray scale information is then utilized to determine what material is present inside a 3-D voxel. Voxels which contain the correct values are retained for inclusion in the volume, while others remain blank. It follows that the size of the voxel itself proves to be an overall limit to the volume's resolution. In this study, the typical volume was approximately 0.4 mm in each dimension (x,y,z). After the volume is computed, the next step is the shading process. An initial viewing direction is chosen. The 3-D view in this direction is projected onto a 2-D plane, called the image plane, for display on the CRT.

Rendering the phalanges for this study was the next step. In an effort to maximize the resolution of the volumes, the markers and the bones were rendered separately. This created a separate representation for each, but the positions relative to each other remained fixed in the global coordinate system of the MRI scanner. For each slice of a pose, the appropriate bones were selected and thresholded. A second set of bone markers was added to the bone's rendered volume to ensure that the volume was correctly aligned while measuring in the 3-D mode (see Figures 3-5). After the

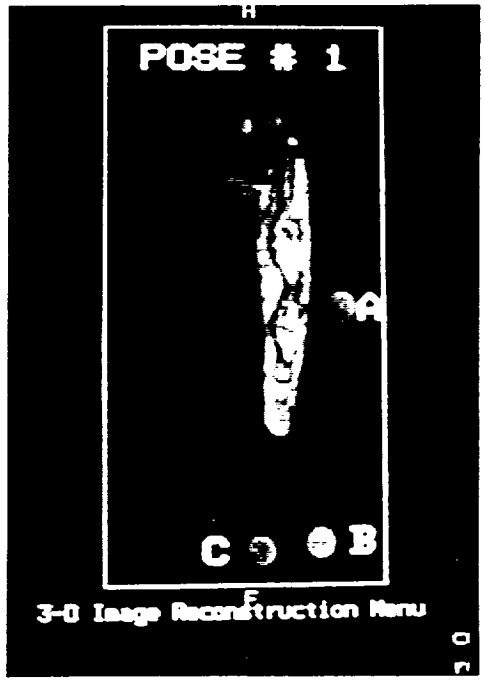

Figure 2 - A representative image of a "slice" of the left index finger in the restraint device. A,B, and C show the markers.

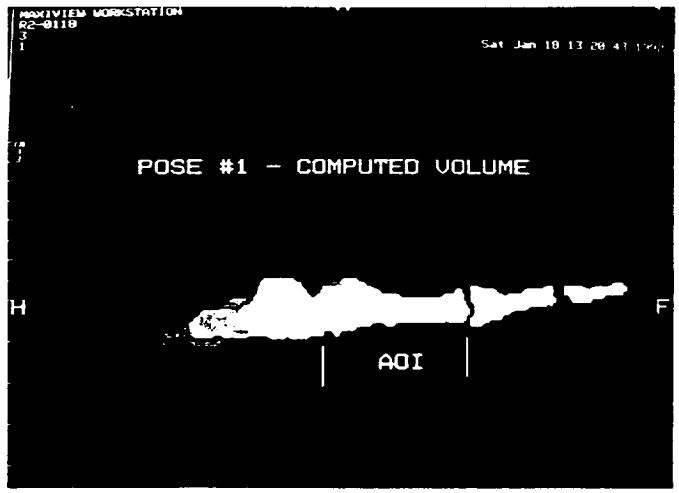

Figure 3 - The rendered volume in the first pose.

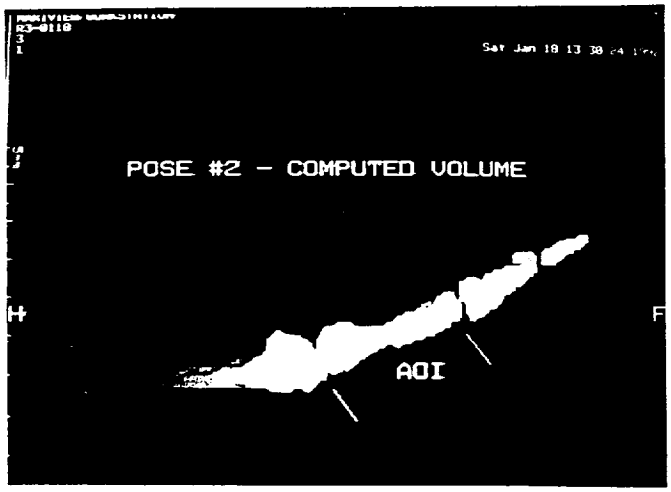

Figure 4 - The rendered volume in the second pose.

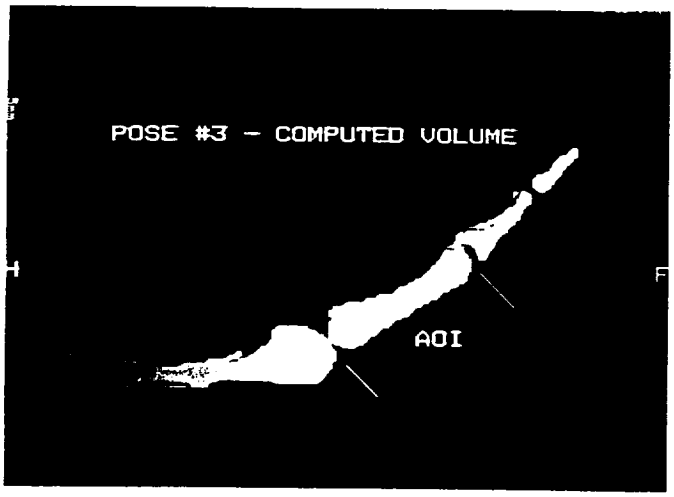

Figure 5 - The rendered volume in the third pose.

volumes for the bones were created, the volumes for the restraint device's water markers were computed. The water markers served to calibrate and validate the measurements and algorithms for this study. A second set of markers were also produced with the water marker volumes to ensure alignment, just as we did with the phalanx volumes.

In order to analyze the motion of rigid bodies, we used the calculations and methods devised by several authors [4,8,9]. The spatial coordinates of landmark positions (a minimum of three on each rigid body in each position) can be calculated from the measurement tools of the DMI. These coordinates then comprise the information necessary to derive the transformation matrix describing the motion, which is taken to be a screw motion. A screw motion can be described by a rotation matrix and a translation vector, or by the position of the screw axis, the angle of rotation about this axis, and the translation along this axis. This method is a fairly robust method of determining the motion of the rigid body, but does suffer from errors induced by scaling errors and random measurement errors (noise).

While a comprehensive treatment of the derivation of Spoor and Veldpaus' methods is not feasible in this study, several key points need to be clarified. First, for this method, three or more non-collinear points are needed in the first and second positions, with no initial approximation needed. The translation vector (**v**) and the rotation matrix (**R**) describe the movement of a rigid body from position 1 to position 2. The rotation matrix has the following properties:

$$R^T R = I \qquad (1)$$

where **I** is the 3x3 identity matrix and **T** denotes transposition. The vectors describing each point in the first position ($\mathbf{a}_i$) and those describing the points in the second position ($\mathbf{q}_i$) are related by

$$q_i = Ra_i + v \qquad (2)$$

Since the unknown quantities in (2) are **R** and **v**, a method must be used to obtain values for them by using the measurements of the points in the first and second positions. A computer program was written (Peterson, [8]) which takes the three-dimensional coordinates from two positions of the rigid body and then computes the transformation matrix in the form of

$$T = \begin{vmatrix} R_{11} & R_{12} & R_{13} & 0 \\ R_{21} & R_{22} & R_{23} & 0 \\ R_{31} & R_{32} & R_{33} & 0 \\ v_i & v_j & v_k & 1 \end{vmatrix} \qquad (3)$$

where the 3x3 matrix in the upper left describes the rotation **(R)** of the body, and **v** denotes the translation vector. Once the transformation matrix is determined, the methods of analyzing the motion can be one of several in existence. The method of Spoor and Veldpaus utilizes the symmetrical and anti-symmetrical portions of the rotation matrix to determine the body's motion about the helical axis, with

$$2 * n * \sin(\theta) = \begin{vmatrix} R_{32} - R_{23} \\ R_{13} - R_{31} \\ R_{21} - R_{12} \end{vmatrix} \qquad (4)$$

The angular rotation is given by

$$\sin(\theta) = \frac{1}{2}\sqrt{(R_{32}-R_{23})^2 + (R_{13}-R_{31})^2 + (R_{21}-R_{12})^2} \qquad (5)$$

The rotation is also given by

$$\cos(\theta) = (1/2) * (R_{11} + R_{22} + R_{33} - 1) \qquad (5a)$$

Now that the angle is known, returning to equation (4) yields **(n)**, the unit vector along the helical axis.

For the translation analysis, one must again derive an expression based upon the transformation matrix. The translation vector, **v**, is taken from the transformation matrix. The following information determines the necessary information:

$$[1-\cos(\theta)]\, nn^T = [(R + R^T) - \cos(\theta) I]/2 = |b_1 b_2 b_3| \qquad (6)$$

where $\mathbf{b}_i$ are three element columns. Another value for **n** is determined from

$$b_i^T b_i = \max(b_1^T b_1, b_2^T b_2, b_3^T b_3); \; n = \pm \frac{b_i}{\sqrt{b_i^T b_i}} \qquad (7)$$

where **n** will be in the same direction as that derived from (4), but a scaling factor different in magnitude. The values for a point on the axis and the translation on the axis are then found from

$$t = n^T * v \qquad (8)$$

and

$$s = (-1/2) * n * (n * v) + \frac{\sin(\theta)}{(2(1-\cos(\theta)))} * n * v \qquad (9)$$

where **s** represents a radius vector of a point on the helical axis, and **t** is the translation along the helical axis. Noteworthy is the fact that the translation vector is quite sensitive to measurement errors and noise, while the rotation matrix is rather robust and yielded highly accurate results.

IV. Data Analysis/Results

The angles of rotation about the helical axis for the respective position changes for this study were quite accurate, as were the calibration results utilizing the markers. Each marker set for the poses was rendered into a 3-D volume, just as the phalanx voxels were rendered. However, the water

ANGLES OF ROTATION - POSE #3 MARKERS	
Restraint Device	- 52.0 deg
2-D Slice Image	- 52.9 deg
3-D Volume	- 52.7 deg

Table 1 - Calibration Results

marker volumes were created for one slice of image data only. This was to ensure that a clear rotation about one axis alone was visible, thus further validating the measurements of the DMI and the accuracy of the transformation matrix software. From the slice containing the markers (see Figure 2), measurements of the markers for pose #3 were determined for the angle B-A-C. This angle was then compared to the angle produced by measuring landmark positions from the rigid body A-B (notionally position 1) moving to A-C (notionally to position 2). The results are listed in Table 1. Furthermore, the unit vector along the helical axis for the rotation of Pose #3 was $n = [0\ 0\ 1]^T$, thus showing that for the markers, a simple 2-D rotation occurred in the z-axis, which proves valuable later.

After checking the process using the water markers, we then measured and analyzed the rigid body motion of the landmark positions on the proximal phalanx. The measurements were taken in the (x,y,z) coordinates and then transformed into the transformation matrix. From this, as in the case of the markers, we determined the motion of the phalanx about the helical axis using Spoor and Veldpaus algorithms. Seven landmark positions defined each rigid body motion, with future efforts geared toward increasing the number of landmark positions for increased accuracy and reliability. The results are listed in Table 2.

From-To (deg)	1	2	3
1 - 2	21.3	20.4	21.3
2 - 3	12.4	14.0	12.7
1 - 3	32.6	32.9	33.5

Table 2 - The 3-D rotations for three trials.

The overall consistency of the results above can be readily observed. The fact that the accuracy of the transformation increases as the magnitude of motion increases is a point of interest for future work. Also, as in the case of the markers, the motion was primarily two-dimensional about the z-axis, as expected. The small rotation in the x and y axes can be attributed mainly to the alignment of the subject hand. Random measurement errors also played a role. The mean and standard deviation of the movements are listed in Table 3.

From-To	Mean	Deviation(deg)
1-2	21.1	.8
2-3	13.0	.7
1-3	33.5	.4

Table 3 - Statistical Analysis.

V. Conclusion

As noted earlier, future work in this area includes ongoing power-assisted glove work. A subject could wear the EVA glove inside the magnet, placing the hand within the radiofrequency coil. By stopping a subject at various stages of the motion required to perform a task, high resolution imaging of the entire had and glove volume could be performed at each stage. The transformations of the entire hand's members could then be analyzed. The effect of using the glove compared to non-glove motion could also be studied. Other areas of possible interest include those involving potential applications of injury-related analysis of the hand. One major subject in this field is study of individual joint kinematics leading to injury suffered during certain repetitive activities, such as those encountered by a computer programmer while entering data at a keyboard.

Our research proved that MRI is a feasible tool for kinematic analysis of rigid bodies. The process was very slow for this initial study, due to several factors, but subsequent studies will be completed much more quickly. The screw motion analysis of the proximal phalanx in this research produced results that were both reliable and repeatable for the proximal phalanx and should yield the same results for whole hand analysis, a future goal of the group. While other methods do exist, such as electrical goniometry, computed tomography, etc., only MRI offers a safe means of producing accurate results for in vivo analysis.

Acknowledgements

The authors wish to acknowledge the funding for this research effort, which was provided by the NASA Office of Aeronautics and Space Exploration and the National Space Grant College and Fellowship Program.

References

1. Chao E.Y. and Morrey B.F., "Three-Dimensional Rotation of the Elbow", Journal of Biomechanics, Volume 11, pp. 57-73, 1978.

2. Haase, A. "Snapshot FLASH MRI. Applications to T1, T2, and Chemical-Shift Imaging." Magnetic Resonance Medicine 1990; 13:77-89.

3. Jones, J.P. "Physics of the MR Image: From the Basic Principles to Image Intensity and Contrast, in Magnetic Resonance Imaging: Vol. II, Physical Principles and Instrumentation, eds. Partain, C.L. et al., W.B. Saunders Company, Philadelphia, PA pp. 1003-1028.

4. Kinzel G.L. et al., "Measurement of the Total Motion Between Two Body Segments- I. Analytical Development", Journal of Biomechanics, Volume 5, pp. 93-105, 1972.

5. Kinzel G.L. et al., "Measurement of the Total Motion Between Two Body Segments - II. Description of Application", Journal of Biomechanics, Volume 5, pp. 283-293, 1972.

6. Larsen R.J. and Marx M.L., Mathematical Statistics and Its Applications, Prentice-Hall, Englewood Cliffs, New Jersey, 1986.

7. Mugler, J.P. and Brookeman J.R., "Three-Dimensional Magnetization Prepared Gradient Echo Imaging",society of Magnetic Resonance in Medicine Abstract Book, 1990, p. 432.

8. Peterson S.W., Measurement and Analysis of Human Joint Motion, Ph.D. Thesis, University of Minnesota, December 1985.

9. Spoor C.W. and Veldpaus F.E., "Rigid Body Motion Calculated from Spatial Co-ordinates of Markers", Journal of Biomechanics, Volume 13, pp. 391-393.

10. Vannier M.W. and Geist D., "PC-Based 3-D Reconstruction of Medical Images", Computer and Graphics, Volume 13, No. 2, 1989, pp 135-143.

SAE TECHNICAL
PAPER SERIES

911382

MR Imaging of Hand Microcirculation as a Potential Tool for Space Glove Testing and Design

Trista A. Niemann
Mechanical Engineering Dept.
Vanderbilt Univ.

Christine H. Lorenz
Department of Radiology and Radiological Sciences
Vanderbilt Univ.

Steven W. Peterson and Alvin M. Strauss
Mechanical Engineering Dept.
Vanderbilt Univ.

Reprinted from: Space Station and Advanced EVA (SP-872)

The Engineering Society For Advancing Mobility Land Sea Air and Space®
INTERNATIONAL

21st International Conference on
Environmental Systems
San Francisco, California
July 15-18, 1991

400 COMMONWEALTH DRIVE, WARRENDALE, PA 15096-0001 U.S.A.

The papers included in this volume are abstracted and indexed in the SAE Global Mobility Database.

ISSN 0148-7191

Persons wishing to submit papers to be considered for presentation or publication through SAE should send the manuscript or a 300 word abstract of a proposed manuscript to: Secretary, Engineering Activity Board, SAE.

Printed in U.S.A.

911382

MR Imaging of Hand Microcirculation as a Potential Tool for Space Glove Testing and Design

Trista A. Niemann
Mechanical Engineering Dept.
Vanderbilt Univ.

Steven W. Peterson and Alvin M. Strauss
Mechanical Engineering Dept.
Vanderbilt Univ.

Christine H. Lorenz
Department of Radiology and Radiological Sciences
Vanderbilt Univ.

ABSTRACT

The task of evaluating and designing space gloves requires accurate biomechanical characterization of the hand. The availability of magnetic resonance (MR) imaging has created new opportunities for in vivo analysis of physiological phenomena such as the relationship between circulation and fatigue.

An MR imaging technique originally proposed to quantitatively evaluate cerebral perfusion has been modified to evaluate the capillary microcirculation in hand muscles. An experimental protocol was developed to acquire perfusion-weighted images in the hand before and after various levels of exercise. Preliminary results on the feasibility of applying the MR imaging technique to the study of microcirculation and fatigue in the hand are presented. The potential of this method for space glove testing and design is also discussed.

INTRODUCTION

Astronauts experience considerable performance-limiting hand fatigue during EVA. For the future of the space program, improved glove designs as well as improved methods for evaluating the space gloves are crucial. Biomechanical characterization of the hand is needed to effectively evaluate and design spacesuit gloves. The use of MR imagery has provided new methods for analyzing physiological systems.

MR is a relatively new imaging modality which is capable of obtaining multiple qualitatively different images of the same anatomic region each emphasizing a different fundamental parameter of the tissue (1)*. MR data from the hand (or any other sample) is generated by placing the hand in a magnetic field which aligns the spin states of the hydrogen molecules. Radio waves are then used to vibrate the nuclei out of their aligned positions. The resonant response of the atomic nuclei is measured by recording the strength of the radiation emitted by the atomic nuclei as their spin states realign with the magnetic field. The time required for this realignment process to occur can also be measured and can be used to obtain images. This response is dependent on several factors: the strength of the magnetic field, the frequency of the radio wave, and the type and arrangement of the atomic nuclei present in the sample volume. In the imaging device, spatial information is determined by generating magnetic field gradients within the anatomical segment. By varying the gradients, images of slices of different thicknesses through the segment can be obtained. By tuning the scanning device the information content in the image can be determined (2). Figure 1 is an MR image.

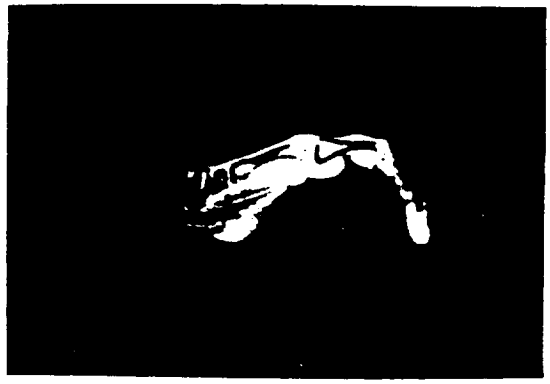

Figure 1. MR image of a section through the finger.

*Numbers in parentheses designate references at the end of the paper

Quantitative imaging of the capillary microcirculation, referred to as perfusion/diffusion imaging, is a relatively new MR technique originally proposed by Le Bihan (3) which has been modified for applications in several organ systems (4, 5). This technique is in development at Vanderbilt University Medical Center's Department of Radiology and Radiological Sciences. The images generated by this technique theoretically reflect local variations in the capillary microcirculation and brownian motion of water molecules in the tissues. The images can be quantitatively analyzed based on the theory that the signal in areas of greater perfusion will be more attenuated than the signal in areas of lesser perfusion (4). Perfusion imaging can provide a useful noninvasive method for quantitative evaluation of parameters related to capillary blood flow.

The purpose of this study was to investigate the feasibility of using this technique in determining the relationship between blood perfusion and muscle fatigue. The existence of a viable relationship would provide a powerful tool for the assessment of glove performance. During rest only 20 to 25 percent of the muscle capillaries are open. As the muscle exercises, normally dormant capillaries open dramatically to increase the supply of oxygen and nutrients to the muscle fibers (capillary recruitment) (6). The increase in capillary blood flow resulting from the exercise (and possibly a decrease in blood flow once the muscle is fatigued) should be detectable using this technique.

The perfusion imaging technique currently allows the selection of only a single plane for imaging. Therefore, the flexor pollicis brevis muscle of the thumb was selected for imaging because the muscle is easily identified in the MR images. Another reason for selection was the indication that this muscle experienced fatigue during dynamic gripping tasks. In the "Extravehicular Activities Study", physiological fatigue was assessed by recording electromyographic (EMG) signals from the thumb flexor. The fatigue of the muscle was objectively measured by analyzing the change in the frequency components of the EMG signal that occurred when the muscle contraction was repeated. Fatigue in the thumb flexor muscle during a gripping task was found to be significant, especially when a pressurized glove was worn (7).

EXPERIMENTAL METHOD

In order to determine if the MR perfusion imaging technique would be practical and reliable for the study of hand fatigue, several constraints concerning the MR scanner, the exercise protocol, and the MR perfusion imaging technique had to be considered in designing the experimental method for this study.

DESIGN CONSTRAINTS - First, the MR scanner does not allow the subject much room for movement of any type. Figure 2 is a diagram of a typical MRI facility. The small diameter of the bore limits the available space required for exercising the hand. The 'best' arrangement found was with the subject in a supine position with his hand behind his head within the RF coil. This position provided the most comfort and ease of motion for the subject while exercising.

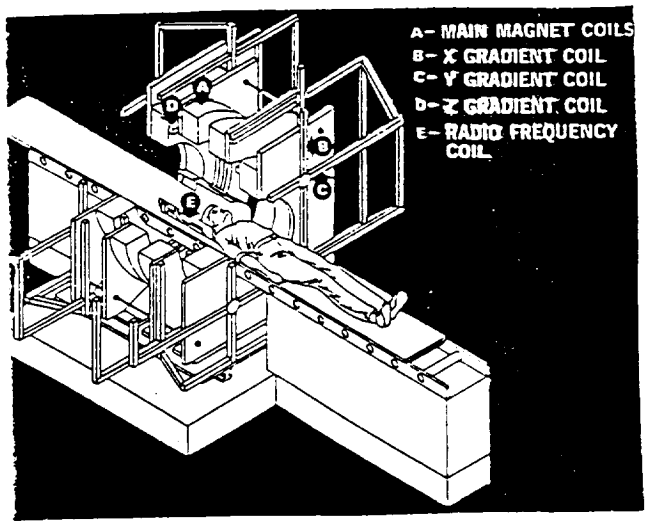

Figure 2. A typical MRI scanner.

The second constraint involved choosing an exercise device compatible with the 1.5 Tesla Magnet of the MR scanner. This magnet is extremely strong (10,000 times stronger than the Earth's magnetic field). Any exercise device made of ferromagnetic material was therefore automatically excluded from evaluation. The non-ferromagnetic exerciser chosen was the Thumbciser™ by North Coast Medical, Inc. The Thumbciser™, shown in Figure 3, is entirely plastic and rubber and works well to fatigue the flexor pollicis brevis muscle.

Another concern was the extreme sensitivity of perfusion imaging to motion. Since the pulse sequences used in this technique are sensitive to microscopic motion, any large motions (greater than 1mm) during image acquisition completely destroy the results. Quality images (ones with reduced noise and no motion artifact) are possible only if the segment being imaged is completely still. To keep the hand totally immobilized, a plaster hand grip device was designed. The plaster hand grip was mounted on a

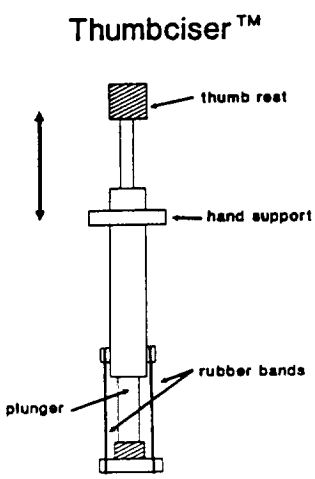

Figure 3. The Thumbciser™ with slight modifications including hand rest and additional rubber band support

wooden base covered in Play-Doh®. The Play-Doh® was necessary to fix the apparatus to the MR bed and to dampen the vibrations caused by the MR scanner during imaging.

The last constraint was imaging time. Each perfusion-weighted image takes approximately 1 minute to complete. To accurately quantitate the increase in perfusion after exercise, multiple images are necessary. Because of the time required for each image, only a limited number of images can be acquired before the effects of the exercise have subsided. This limitation will be explored in further detail in the discussion section.

EXERCISE PROTOCOL - The exercise protocol consisted of two phases. Prior to imaging, a plaster cast of the subject's grip was made. Next, the subject's maximum voluntary contraction (MVC) was recorded with the subject in the supine position, arm extended behind the head. The Thumbciser™ attached to a force gauge measured the MVC. Using the Thumbciser™, the subject then performed as many repetitions as possible at 50% MVC until fatigue made a full contraction impossible. The repetitions were done in time with a tone at a rate of one contraction every three seconds. The total number of repetitions, Rmax, was recorded. Also prior to imaging, the subject (while in a supine position) practiced moving his hand back and forth between the grip and exerciser to become accustomed to the motion.

The next part of the study was completed using a 1.5-Tesla MR imager (Magnetom 63; Siemens, Iselin, NJ). First, the subject was properly positioned in the scanner on his back, arm behind the head. The Thumbciser™ and plaster grip were placed within reach of the subject's hand. Next, the subject placed his hand in the grip, and a baseline set of perfusion/diffusion-weighted images of the thumb muscles was taken. Then the exercise sequence was started (all contractions were done at 50% MVC). For this preliminary study only one exercise set, at 100% Rmax, was done. After the exercise was completed and the muscles fatigued, a post-exercise MR image set was taken.

In order for the images to be meaningful, the re-positioning of the hand after exercise must be extremely accurate. The reproducibility of image intensity is also of utmost importance in determining the reliability of this technique. To evaluate the reproducibility of both position and image intensity, the subject removed and replaced his hand in the grip several times. After each repetition a set of perfusion/ diffusion-weighted images was taken.

RESULTS

Three criteria were used to determine whether the study of the relationship between muscle fatigue and perfusion was feasible using this newly modified perfusion imaging technique: repositioning accuracy, reproducibility of signal intensity, and significant changes in apparent diffusion coefficient (ADC) before and after exercise. With the feasibilty of this technique confirmed, the applications to space glove testing and design can be explored.

The hand images created before and after movement were subtracted to determine repositioning accuracy. The muscles of interest typically shifted between 1 and 3 mm (3-7% of muscle width). The average intensity in the baseline images (N=3) was 75.4 +/- 0.6. The same reproducibility test was done to evaluate the perfusion/diffusion-weighted images. The average intensity of the images with the most sensitivity to motion (N=3) was 67.8 +/- 2.6. The technique is therefore reproducible both in positioning and quantitative values, and should be adequate for future use in evaluating fatigue.

The apparent diffusion coefficient (ADC) which theoretically includes effects due to both diffusion and perfusion was calculated according to IVIM theory (3) before and after exercise to determine if a difference could reliably be seen. Before exercise the ADC was 1.24×10^{-3} mm^2/sec and after exercise the ADC was 1.64×10^{-3} mm^2/sec. For reference, the ADC in water is about 2×10^{-3} mm^2/sec and in brain and kidney

between 1 and 2 x 10^{-3} mm^2/sec (4, 5). Figure 4 shows the image intensity versus the gradient factor b, where b is a measure of the sensitivity of the image to microscopic motion of protons.

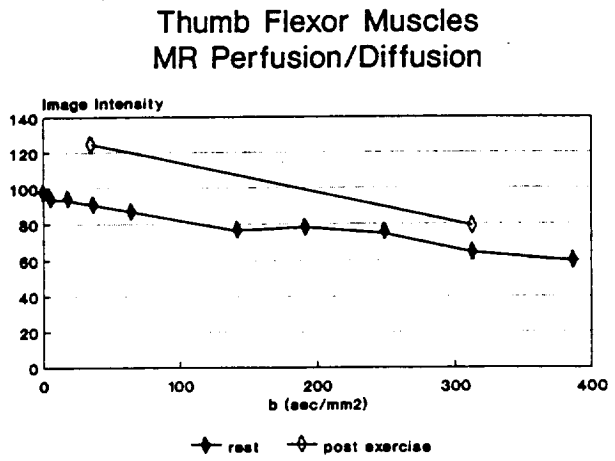

Figure 4. MR Perfusion/Diffusion
increasing gradient factor than the intensity of tissue with lesser perfusion (3).

According to IVIM theory, the intensity of tissue with greater perfusion will decrease more rapidly with increasing gradient factor than the intensity of tissue with lessor perfusion (3). The absolute intensities are not important; it is the rate of change of intensity that is related to microcirculatory effects.

DISCUSSION

This preliminary study showed that using perfusion imaging techniques to explore the relationship between microcirculation and fatigue is feasible. The data is reproducible in terms of positioning and image intensity measurements. The ADC was also shown to increase significantly after exercise.

Because of the time limitations during imaging related to exercise effects, we were limited to use of the ADC as a measure of change. As mentioned earlier, the ADC is related to both perfusion and diffusion effects. Diffusion increases suggest changes in cell metabolic activity occurring because of the exercise. So, even though this technique is currently unable to separate perfusion from diffusion, the increase in ADC should be significant with respect to muscle fatigue.

A follow-up study has been planned using similar experimental methods. An attempt will be made to show a gradual increase in the apparent diffusion coefficient with fatigue. This will be accomplished by having multiple subjects follow the exercise procedures described below. Prior to imaging, a plaster cast will be made, and the MVC and Rmax will be obtained. On the imaging day, the subject will have a baseline MR image set taken before the exercise sequence begins. The Thumbciser™ will be used to perform 33% of the Rmax at a rate of one contraction every three seconds followed by a second image set. The next exercise set will consist of 66% of Rmax followed by a third image set. The last exercise set will consist of 100% of Rmax to completely fatigue the muscles of interest, followed by the last image set. Our theory is that the gradual increase in exercise (up to the point of fatigue) will show a gradual increase in the ADC. The point at which fatigue sets in or performance is limited may be detectable by the change in the ADC. These studies will also serve to further evaluate the reproducibility of the technique and its ability to detect small changes in blood flow.

The perfusion imaging technique's success in quantitatively measuring muscle fatigue could provide valuable information in the field of space glove testing and design. A second follow-up study currently being designed will measure fatigue of the hand inside a simulated space glove in order to determine specific points of blood flow changes when performing various EVA-type tasks. These tests will provide objective, quantitative measures of fatigue as well as information on the precise location of the fatigue. The contributions of various muscle groups to debility will also be investigated. Glove performance evaluations using space gloves currently in development at this research institute are also being planned.

And, as MR technology improves and imaging time decreases, the acquisition of multiple images allowing the separation of perfusion and diffusion effects may be possible. With other advances in MR imaging and in vivo MR spectroscopy, specific metabolites may be detected and quantified with respect to their relationship to muscle fatigue.

ACKNOWLEDGEMENTS

The authors wish to acknowledge the sponsorship of this project by the NASA Office of Aeronautics and Exploration Technology and additional support from

the NASA National Space Grant College and Fellowsip Program.

REFERENCES

1. DeLaPaz, Robert, "Computerized Analysis and Information Extraction of Medical Magnetic Resonance Images (MRI)", SPIE Vol. 902 Three-Dimensional Imaging and Remote Sensing Imaging, 1988, pp. 151-154.

2. Crooks, Lawrence, "An Introduction to Magnetic Resonance Imaging", IEEE Engineering in Medicine and Biology Magazine, September, 1985, pp. 8-15.

3. Le Bihan D, Breton E, Lallemand D, et al, "MR Imaging of Intravoxel Incoherent Motions: Applications to Diffusion and Perfusion in Neurological Disorders", Radiology 1986; 161: pp. 401-407.

4. Powers T, Lorenz CH, Holburn GE, and Price RR, "Renal Artery Stenosis: In Vivo Perfusion MR Imaging", Radiology, 1991; 178: pp. 543-548.

5. Lorenz CH, Pickens DR, Puffer DB and Price RR. "Magnetic Resonance Perfusion/Diffusion Phantom Experiments," Magn Reson Med 1991, in press.

6. Guyton, Arthur, Textbook of Medical Physiology, 7th Edition, Philadelphia: Saunders, 1986: pp. 133, 230, 336, 1009-1013.

7. O'Hara, J. and Briganti, M., "Extravehicular Activities Limitations Study, Vol. II, Establishment of Physiological and Performance Criteria for EVA Gloves", NASA Document N89-17393: pp. 4-30 to 5-43.

"A Preliminary Structural Analysis of Space-Based Inflatable Tubular Frame Structures" was presented at the First European Joint Conference on Engineering Systems Design and Analysis - Aerospace Technology Session, June 29 - July 3, 1992, Istanbul, Turkey.

A Preliminary Structural Analysis of Space-Based Inflatable Tubular Frame Structures

J. A. Main S. W. Peterson A. M. Strauss

Dept. of Mechanical Engineering
Vanderbilt University
Box 1592, Station B
Nashville, TN 37235 USA

ABSTRACT

The use of inflatable structures has often been proposed for aerospace and planetary applications. The advantages of such structures include low launch weight and easy assembly. This paper proposes the use of inflatables for applications requiring very large frame structures intended for aerospace use.

In order to consider using an inflated truss the structural behavior of the inflated frame must be examined. The statics of inflated tubes as beams has been discussed in the literature, but the dynamics of these elements has not received much attention. In an effort to evaluate the vibration characteristics of the inflated beam a series of free vibration tests of an inflated fabric cantilever were performed. Results of the tests are presented in this paper and models for system behavior posed.

NOMENCLATURE

a_n	constant in natural frequency calculation
l	inflated beam length (m)
p	beam inflation pressure (Pa)
r	radius of inflated beam (m)
t	time (s)
x	beam coordinate from beam tip (m)
y	beam deflection (m)
E	beam fabric modulus (N/m)
I	inflated beam moment of inertia (m^3)
Kin	kinetic energy (joules)
M	applied bending moment (N-m)
N	axial stress resultant (N/m)
Pot	potential energy (joules)
V_1	volume of beam when undeflected (m^3)
V_2	volume of beam at maximum deflection (m^3)
μ	beam mass per unit length (kg/m)
ρ	radius of curvature (m)
θ	angular position (radians)
ω	angular frequency (radians/s)

INTRODUCTION

Interest in using inflatable structures in space exists because their basic characteristics (Leonard, 1974) solve many engineering problems that the structural designer is faced with in space. Pneumatic structures consist of no more than a few layers of fabric and can be launched into space in their uninflated state, so the launch penalty associated with them is very low. Also, they can be prefabricated, packed, and then deployed in space by pressurization. There are questions, however, about the safety and durability of inflated structures in the space environment.

The initial space-based application of inflated structures, also called pneumatic structures, was ECHO-1, launched in August of 1960. ECHO-1 was a 30 m diameter metallized mylar balloon that was used as a passive telecommunications satellite. Similar pneumatic structures were sent aloft as ECHO-2 in 1964 and PAGEOS-1 in 1966.

Examples of more complex space-based inflated structures that go a step beyond the simple spherical balloons used in ECHO and PAGEOS were designed and tested by the Goodyear Aerospace Corporation under contract from NASA during the Apollo and Skylab programs in the 1960's and 70's. These included the Lunar Stay Time Extension Module (Tynan, 1965), MOBY DICK (French, 1967), and the D021 airlock (Manning and Jurich, 1973).

Numerous proposals have also been made to use more complex inflatables for large space structures such as precision antenna reflectors (Girard et al., 1982; Reibaldi, 1985; Authier and Hill, 1985; Bernasconi and Reibaldi, 1986; Williams, 1988), solar concentrators (Mikulas and Hedgepeth, 1989; Grossman and Williams, 1989), orbiting hangars (Ohkami et al., 1986), and inflatable construction forms (Kaden and Pense, 1988). It has also been suggested that inflatable segments be used to replace the solid portions of the space shuttle robot arm to reduce arm inertia and minimize required storage space (McCarty, 1990).

In 1962 Frei Otto's Tensile Structures was first published, a work that was largely devoted to outlining numerous past, present and future applications of pneumatic structures. Otto presents scores of intriguing ideas for novel applications of pneumatic structures. Of particular interest to this investigation are the concepts that use inflated cylindrical beams as structural members. The choice of the inflated cylinder as structural member is natural: a piece of fabric sewn into a closed tube will assume the shape of a cylinder when internally

'pressurized. The ease of fabrication and ability to span distances and carry loads make the inflated cylinder the natural pneumatic analog to the elastic beam. Reenforcing this analogy are Otto's conceptual designs that include inflated cylindrical beams as members in planar and space trusses.

Current strategies for open frame structures intended for aerospace use include both deployable and erectable structures. Deployable trusses are those that are folded or packed and then remotely expanded upon reaching orbit. Erectable trusses use standardized beam elements that connect into a node fixture. The strength and reliability of the solid members of these truss designs make them the practical choice for the truss component in current space station designs. However, when future needs require construction of extremely large truss structures, perhaps with dimensions measured in kilometers rather than meters, the amount of material to be lifted and the extravehicular activity required for construction of solid element trusses may become prohibitive. The advantages of inflatables may outweigh their shortcomings in these applications.

ANALYSIS OF THE INFLATED BEAM: STATICS

If the inflatable truss structure concept is to be successfully implemented structural models must be developed to predict both their static and dynamic behavior in the space environment. Structural analysis of inflated circular-cylindrical beams has been performed using a number of different strategies. Linear shell analyses have been used to model the buckling behavior and shear deflections(Leonard et al., 1960; Topping, 1964; Bulson, 1973) of inflated members. Stiffness of inflated cantilever beams has also been modelled with nonlinear methods (Douglas, 1969) and variational methods have been used with shell models of inflated beams to determine beam deflections under a variety of loads (Steeves, 1975). Comer and Levy (1963) modelled the behavior of an inflated cantilever beam in a manner similar to conventional beam theory. The following deflection analysis of the inflated beam closely follows the method used by Comer and Levy with some modifications to make the results more applicable to fabric structures. These changes include the use of stress resultants instead of stress and expressing fabric modulus in terms of force per unit width. This was done because fabric thickness can only be vaguely correlated with load carrying ability.

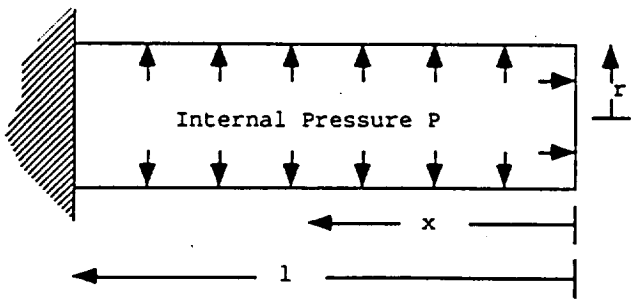

Figure 1. Sketch of the inflated cantilever.

Figure 1 shows a sketch of an inflated cantilever beam. An arbitrary loading of this beam can be expressed as applied moments that are a function of the beam coordinate x. A model of an inflated structure must accommodate both slack and taut regions in the fabric. In the taut regions, or when the axial stress in a given cross-section of the fabric of an inflated beam remains tensile around the complete circumference, the stress distribution illustrated in Figure 2 is assumed.

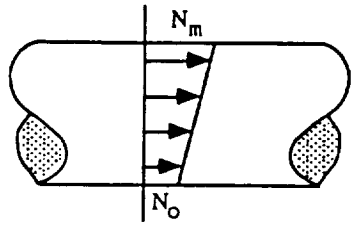

Figure 2. The stress distribution in the fabric of the inflated beam in regions where no wrinkling is present.

In these regions the value of the axial stress resultant in the beam skin is defined as

$$N = N_o \left(\frac{1 + \cos\theta}{2}\right) + N_m \left(\frac{1 - \cos\theta}{2}\right) \qquad (1)$$

In this expression θ is measured around the circumference of the beam from the point where $N = N_o$.

When the applied moment exceeds the value $\pi r^3 p/2$ the bending stress cancels the axial stress in the fabric skin on the concave side of the beam and wrinkling will begin in that region. The fabric wrinkles because it is incapable of resisting compressive loads. In these regions the stress distribution illustrated in Figure 3 is assumed.

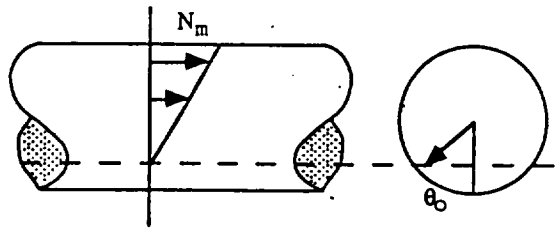

Figure 3. The stress distribution in the fabric of the inflated beam in regions where wrinkling occurs.

In these regions the stress resultant in the axial direction is the fabric skin is

$$N = \left(\frac{\cos\theta_o - \cos\theta}{1 + \cos\theta_o}\right) N_m \qquad \pi > \theta > \theta_o$$

$$N = 0 \qquad \theta_o > \theta > 0 \qquad (2)$$

For the balance of moments about a transverse axis through the center of the beam a distance x from the tip

$$M(x) = -2 \int_0^{\pi} N\, r^2 \cos\theta \, d\theta \qquad (3)$$

When $M > \pi r^3 p/2$ equations 2 and 3 can be combined to give

$$N_m = \frac{2\,M(x)\,(1 + \cos\theta_o)}{r^2\,(2\pi - 2\theta_o + \sin 2\theta_o)} \qquad (4)$$

For a balance of axial forces on the endplate

$$p\pi r^2 = 2\int_0^{\pi} N\, r\, d\theta \qquad (5)$$

Again considering the regions containing wrinkled fabric, equations 2 and 5 can be combined to give

$$N_m = \frac{p\pi r\,(1 + \cos\theta_o)}{2\,((\pi - \theta_o)\cos\theta_o + \sin\theta_o)} \qquad (6)$$

Equating the expressions for Nm in equations 4 and 6 yields

$$\frac{M(x)}{pr^3} = \frac{\pi\,(2\pi - 2\theta_o + \sin 2\theta_o)}{4\,((\pi - \theta_o)\cos\theta_o + \sin\theta_o)} \qquad (7)$$

Considering now the regions where no wrinkling of the cross section occurs, substitution of equation 1 into equation 3 gives

$$N_m - N_o = 2\,M(x)/\pi r^2 \qquad (8)$$

Substituting equation 1 into equation 5 yields

$$N_m + N_o = pr \qquad (9)$$

Combining equations 8 and 9 yields

$$N_m = (M(x)/\pi r^2) + (pr/2) \qquad (10)$$

The curvature of a beam element that is part of a wrinkled region is given by

$$\frac{1}{\rho} = \frac{(N_m/E)}{r(1 + \cos\theta_o)} \qquad (11)$$

Substituting in the expression for N_m in equation 4 yields

$$\frac{1}{\rho} = \frac{2\,M(x)}{E\,r^3(2\pi - 2\theta_o + \sin 2\theta_o)} \qquad (12)$$

The curvature of elements in the unwrinkled regions is given by

$$\frac{1}{\rho} = \frac{(N_m - N_o)}{2\,E\,r} \qquad (13)$$

Substituting equation 8 into equation 13 yields

$$\frac{1}{\rho} = \frac{M(x)}{\pi\,r^3\,E} \qquad (14)$$

Equations 12 and 14 can be combined and the approximation $1/\rho = d^2y/dx^2$ applied so that the entire system of equations can be expressed in the following form:

$$\frac{d^2y}{dx^2} = \frac{M(x)}{E\,I} \qquad (15)$$

$$I = r^3\,(\pi - \theta_o + (\sin 2\theta_o)/2) \quad \text{for } M > \pi p r^3/2$$

$$I = \pi\, r^3 \quad \text{for } M < \pi p r^3/2$$

For the regions of the beam that are wrinkled ($M > \pi r^3 p/2$) equation 7 must be used to determine the angle θ_o that corresponds with the applied moment. Beam deflections can be obtained by numerically solving the differential equation of bending.

ANALYSIS OF THE INFLATED BEAM: DYNAMICS

Dynamic modelling methods that have been applied to inflated beams include spring-inertia models and simple potential energy models (Main et al., 1991). Accurate dynamic models of space-based structures are important because unexpected vibration problems have been encountered in orbiting structures that have compromised the sensitivity of the instruments they carry, and unexpected dynamic effects could also compromise structural integrity.

In the previous section an analysis method for the inflated cantilever was outlined that is analogous to the shear-moment method of elastic beam analysis. Expanding on this analogy, Leonard (1988) suggested that elastic beam flexural modes be used to approximate the lower natural frequencies of an inflated beam. The expression for the natural frequency of the nth mode of vibration of a solid elastic cantilever beam is

$$\omega_n = a_n\sqrt{(E\,I)/(\mu\,l^4)} \qquad (16)$$

The constant a_n equals 3.52 and 22.0 for the first and second modes, respectively (Den Hartog, 1985).

Despite the similarities between the two systems, there are important characteristics that distinguish the inflated beam from the elastic beam. In particular, the effects of the change in volume and the associated change in pressure of the the enclosed gas of the beam should be examined as the physical cause of a natural oscillation of the inflated cantilever.

One method of determining the frequency of vibration of a dynamic system is to consider the balance between the kinetic and potential energies. In the inflated beam the pressurization medium is compressed and expands as the enclosed volume changes during each cycle, thus changing the potential energy of the system.

To determine the potential energy stored as the volume of the beam changes during each cycle the undeformed and deformed volumes of the beam must be calculated. Consider the element of the inflated beam sketched in Figure 4.

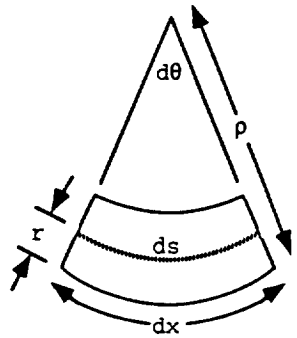

Figure 4. An element of an inflated beam.

The undeformed volume of this element is

$$dV_1 = \pi r^2 \, dx \tag{17}$$

The deformed volume of the beam can be approximated by assuming the beam fabric to be inextensible. The length of the centerline is then related to the element length as follows.

$$dx - ds = r \, d\theta \tag{18}$$

Multiplying through by the cross-sectional area of the beam allows the volume difference between the undeformed and deformed element to be determined.

$$dV_1 - dV_2 = \pi r^3 \, d\theta \tag{19}$$

From the geometry of the deformed element we have $d\theta = dx/\rho$. Further incorporating this and the approximation $1/\rho = d^2y/dx^2$ into equation 19 yields

$$dV_1 - dV_2 = \pi r^3 \left(\frac{d^2y}{dx^2}\right) dx \tag{20}$$

Combining this result with equation 17 and integrating yields expressions for both the undeformed and deformed volumes of the beam.

$$V_1 = \pi r^2 l$$
$$V_2 = \pi r^2 l - \int_0^l \pi r^3 \left(\frac{d^2y}{dx^2}\right) dx \tag{21}$$

If we assume the process of compression and expansion of the gas in the beam to be quasi-static, the potential energy stored in the gas during each compression cycle is

$$Pot = -p_1 V_1 \ln\left(\frac{V_2}{V_1}\right) \tag{22}$$

The total kinetic energy of the inflated fabric cantilever in free vibration is the sum of the kinetic energies of each element dx.

$$dKin = \frac{1}{2} (\mu \, dx) (y\omega)^2 \tag{23}$$

This expression assumes that each point on the beam vibrates such that

$$y(x,t) = y_o(x) \sin\omega t \tag{24}$$

The expression for the total kinetic energy of the beam is therefore

$$Kin = \frac{1}{2} \mu\omega^2 \int_0^l y^2 \, dx \tag{25}$$

Equating the expressions for the beam potential and kinetic energies yields the following expression for beam natural frequency.

$$\omega^2 = \frac{-2 \, p_1 V_1 \ln\left(\frac{V_2}{V_1}\right)}{\mu \int_0^l y^2 \, dx} \tag{26}$$

To solve this equation for a particular vibration amplitude the uniform inertial load level necessary for deflecting the beam the desired amount must be determined. This is done by iteratively solving equations 15 and 7 for a range of uniform loads until the load that results in the desired tip deflection is determined. Once this load level is determined and the numerical solution to the beam deflection differential equation has been obtained, the results can be substituted into equation 26 and the frequency of vibration due to the expansion and compression of the gas determined. Vibration frequencies for a range of amplitudes can be obtained by repeating this procedure over a range of load levels.

EXPERIMENTAL

An inflated cylindrical cantilever beam was constructed by combining an outer rip-stop nylon restraint layer with an internal gastight vinyl bladder. (See Figure 5) The resulting structure had a length of 1.0605 m and was 0.0928 m in diameter. The base of the cantilever was solidly mounted to a large building column and a free vibration test was performed. Slight beam curvature was noted due to gravity resulting in a downward tip deflection of approximately 2 cm. The beam vibration was initiated by horizontally displacing the tip of the cantilever approximately 5 cm and then releasing it. This initial deflection was chosen with reference to the results of the previous investigators to be well short of the level that would cause beam buckling. A free vibration spectrum was obtained by mounting a Bruel and Kjear Model 4366 accelerometer on the tip of the beam. All tests were performed with the beam pressurized to 69 kPa (10 PSI).

NUMERICAL AND EXPERIMENTAL RESULTS

The expression for beam natural frequency in equation 16 was used to determine the lower natural frequencies of the inflated beam. Tensile tests on the beam restraint fabric demonstrated that it had a modulus of approximately 30,000 N/m. The masses of the fabric restraint, vinyl bladder, and the enclosed nitrogen gas combined to give a beam mass per unit length of 0.092 kg/m. With these results the first and second modes of vibration were calculated to be 4.60 and 28.76 Hz, respectively.

The frequency of vibration due to the projected change in the volume of the beam was calculated from equation 26. The beam curvatures and displacements were calculated from equation 15 by assuming that the beam is subject to a uniform load of a magnitude necessary for a given tip deflection. Since the displacements and curvatures of the beam are dependent upon the magnitude of the applied uniform load, the vibration frequency calculated from those parameters is amplitude dependent. The differential equation solver DASSL was used to find the curvatures and displacements along the length of the beam for each incremental load level. Solutions were generated for a range of amplitudes up to the 5 cm maximum amplitude.

The resulting amplitude vs. frequency plot and the two lowest natural frequencies of the beam are shown in Figure 6. The curves are truncated at the 5 cm amplitude level to correspond with the initial tip deflection of the beam during the free vibration tests. The predicted frequency of vibration of 4.60 Hz is easily identifiable in the experimental spectrum. The second mode, at 28.76 Hz, is less evident. The peak from 40 to 57 Hz seems to correspond well with the gas compression/expansion model curve in the 1 to 3 cm amplitude range.

SUMMARY

Comparison of the model results with the experimentally obtained free vibration spectrum of the inflated cantilever indicate that accurate predictions of the frequencies of vibration for the lower modes can indeed be made using conventional beam flexural modes. There does exist approximately a 16% discrepancy between the calculated and measured frequency of the first mode. Considering the complexity of the system and the assumptions necessary for development of the model it is the opinion of the authors that this difference is not unreasonable.

The correspondence between the gas compression/expansion model and the experimental data is encouraging, but not yet conclusive as to whether or not the corresponding peak in the experimental spectrum is due to this physical process. A definitive answer to this question might be obtained by repeating the free vibration test and simultaneously recording the pressure variations inside the beam.

Figure 5. Photo of inflated cantilever test assembly.

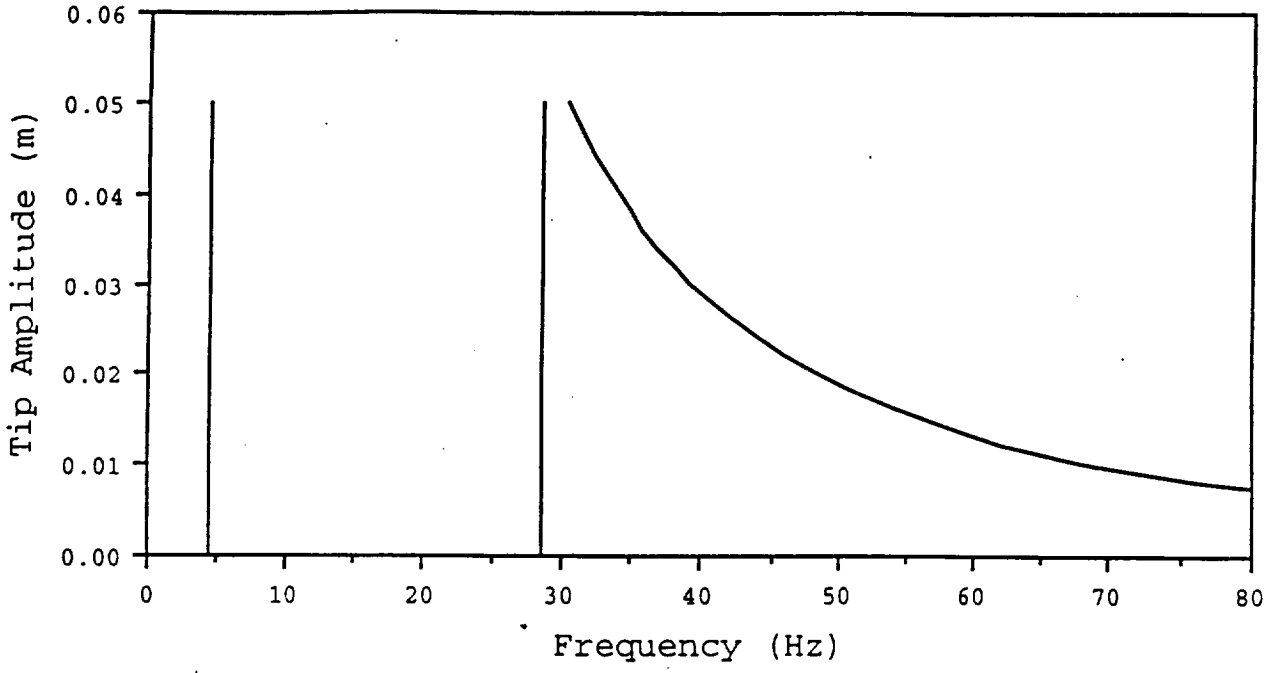

Figure 6. Plot showing the calculated frequencies of vibration of the inflated cantilever. The two spikes on the left are first and second modes of vibration according to beam theory. The curve on the right shows the amplitude dependent vibration frequencies of the beam from the gas compression/expansion model.

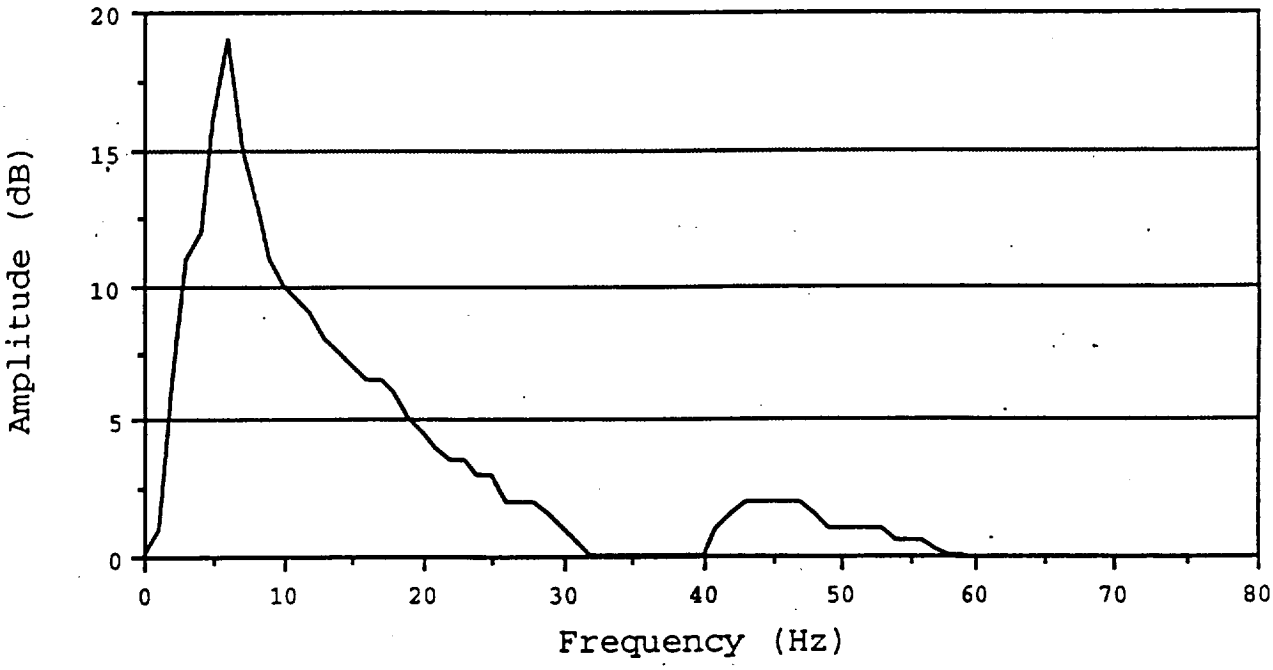

Figure 7. Experimentally obtained free vibration spectrum of the inflated cantilever test specimen. The initial tip amplitude of the beam was 5 cm.

ACKNOWLEDGEMENTS

The authors would like to thank the NASA Office of Aeronautics and Exploration Technology and the NASA National Space Grant College and Fellowship Program.

REFERENCES

Authier, B., and Hill, L., "Large Inflatable Parabolic Reflectors in Space," Instrumentation for Submillimeter Spectroscopy 598 (1985): 126-132.

Bernasconi, M. C. , and Reibaldi, G. G., "Inflatable, Space-Rigidized Structures: Overview of Applications and Their Technology Impact," Acta Astronautica 14 (1986): 455-465.

Bulson, P. S., "Design Principles of Pneumatic Structures," The Structural Engineer 51 (June 1973): 209-215.

Comer, R. L., and Levy, S., "Deflections of an Inflated Circular-Cylindrical Cantilever Beam," AIAA Journal 1 (July 1963):1652-1655.

Den Hartog, J. P., Mechanical Vibrations (Mineola NY, Dover, 1985), 141-147.

Douglas, W. J. "Bending Stiffness of an Inflated Cylindrical Cantilever Beam," AIAA Journal 7 (July 1969): 1248-1253.

French, R. J., A Feasibility Investigation of Expandable Structures Module for Orbital Experiment - Artificial G, (Goodyear Aerospace Report under NASA contract), NTIS, N67-30000.

Girard, L., Bloetscher, F., and Stimler, F., Innovative Structures for Space Applications, (Goodyear Aerospace Report GAC 19-1563, October 1982), NTIS, N84-25757.

Grossman, G., and Williams, G., "Inflatable Concentrators for Solar Propulsion and Dynamic Space Power," in Solar Engineering - 1989, Proceedings of the Eleventh Annual ASME Solar Energy Conference held in San Diego, CA, April, 1989.

Kaden, R. A., and Pense, L. D., "Planetary Base Inflatable Form Construction," in Engineering, Construction, and Operations in Space, Proceedings of Space 88 held in Albuquerque, NM, August 1988.

Leonard, J. W., "State-of-the-Art in Inflatable Shell Research," ASCE Journal of the Engineering Mechanics Division 1 (February 1974): 17-25.

Leonard, J. W., Tension Structures (New York NY, McGraw-Hill, 1988), 246-247.

Leonard, R. W., Brooks, G. W., and McComb, H. G. Jr., Structural Considerations of Inflatable Reentry Vehicles (NASA Technical Note D-457, September 1960).

McCarty, L. H., "Inflatable Arm Segments May Lighten Shuttle's Manipulator System," Design News (April 9, 1990): 150-151.

Main, J. A., Peterson, S. W., Strauss, A. M., "Design of Space-Based Inflatable Tubular Frame Structures," in Paper Presented at the International Design for Extreme Environments Assembly in Houston, TX in November 1991.

Manning, L., and Jurich, L., Expandable Airlock Experiment (DO21) and the Skylab Mission, (Goodyear Aerospace Report under U. S. Air Force contract, September 1972), NTIS, N73-15896.

Mikulas, M. M., and Hedgepeth, J. M., "Structural Concepts for Very Large (400-Meter-Diameter) Solar Concentrators," in Second Beamed Space-Power Workshop, Proceedings of a NASA workshop at Langley Research Center, Hampton, VA, February 1989, NTIS, N90-10153.

Ohkami, Y., Matsumoto, K., Kida, T., IIda, T., and Sakai, J., "An Enclosed Hangar Concept for Large Spacecraft Servicing at Space Station," in Proceedings: 15th International Symposium on Space Technology and Science held in Tokyo, Japan, May 1986.

Otto, F., Tensile Structures (Cambridge MA, MIT Press, 1962), 86-87.

Reibaldi, G. G., "Inflatable Technology in Orbit Demonstration Within the European Space Agency Programs," in 25th International Conference on Space held in Rome, Italy, March 1985.

Steeves, E. C., A Linear Analysis of the Deformation of Pressure Stabilized Tubes (U. S. Army Natick Laboratories report, AD/A-006 493, January 1975), NTIS, N75-32513.

Topping, A. D., "Shear Deflections and Buckling Characteristics of Inflated Members," Journal of Aircraft 1 (Sept.-Oct. 1964): 289-293.

Tynan, C. W. Jr., "Lunar Stay Time Extension Module," in Selected Papers on Environmental and Attitude Control of Manned Spacecraft, (NASA, June 1965), NTIS, N67-14250.

Williams, G., "Inflatable Antennas for Microwave Power Transmission," in Free-Space Power Transmission, Proceedings of a NASA workshop at Lewis Research Center, Cleveland, Ohio, March 1988, NTIS, N90-21799.

SAE TECHNICAL
PAPER SERIES

Power Assist EVA Glove Development

John A. Main, Steven W. Peterson, and Alvin M. Strauss
Vanderbilt Univ.

SAE The Engineering Society For Advancing Mobility Land Sea Air and Space®
INTERNATIONAL

22nd International Conference
on Environmental Systems
Seattle, Washington
July 13-16, 1992

400 COMMONWEALTH DRIVE, WARRENDALE, PA 15096-0001 U.S.A.

All SAE papers, standards, and selected books are abstracted and indexed in the SAE Global Mobility Database.

ISSN 0148-7191

Printed in USA

Power Assist EVA Glove Development

John A. Main, Steven W. Peterson, and Alvin M. Strauss
Vanderbilt Univ.

ABSTRACT

Structural modelling of the EVA glove indicates that flexibility in the metacarpophalangeal (MCP) joint can be improved by selectively lowering the elasticity of the glove fabric. Two strategies are used to accomplish this. One method uses coil springs on the back of the glove to carry the tension in the glove skin due to pressurization. These springs carry the loads normally borne by the glove fabric, but are more easily deformed. An active system was also designed for the same purpose and uses gas filled bladders attached to the back of the EVA glove that change the dimensions of the back of the glove and allow the glove to bend at the MCP joint, thus providing greater flexibility at this joint. A threshold control scheme was devised to control the action of the joint actuators. Input to the controller was provided by thin resistive pressure sensors placed between the hand and the pressurized glove.

The pressure sensors consist of a layer of polyester film that has a thin layer of ink screened on the surface. The resistivity of the ink is pressure dependent, so an extremely thin pressure sensor can be fabricated by covering the ink patch with another layer of polyester film and measuring the changing resistance of the ink with a bridge circuit. In order to sense the force between the hand and the glove at the MCP joint a sensor was placed on the palmar face of the middle finger. The resultant signal was used by the controller to decide whether to fill or exhaust the bladder actuators on the back of the glove. The information from the sensor can also be used to evaluate the effectiveness of a given control scheme or glove design since the magnitude of the measured pressures gives some idea of the torque required to bend a glove finger at the MCP joint.

Tests of this actuator, sensor, and control system were conducted in an 57.2 kPa glove box by performing a series of 90 degree finger bends with a glove without an MCP joint assembly, a glove with the coil spring assembly, and with the four fingered actuated glove. The tests of these three glove designs confirm the validity of the model.

INTRODUCTION

One of the primary difficulties in designing a more flexible metacarpophalangeal (MCP) joint for the EVA glove is the geometry of the hand and the complexity of the surrounding fabric structure, i. e. the glove itself. Fabric structures do not lend themselves easily to structural modelling in the conventional sense: while fabric is approximately linearly elastic in tension it wrinkles in response to compressive loads. With some simplification, however, a workable structural model of the MCP joint can be devised.

Examination of a pressurized fabric glove indicates that the region surrounding the hand at the MCP joint is analogous to a pressurized tube. Although dependant upon the geometry of the palm bar and the tightness of fit, the cross-section of the glove at this point can be approximated by an ellipse. For the purposes of this discussion the EVA glove at the MCP joint can, without loss of generality, be simplified further by representing it by a pressurized fabric tube with a circular cross section.

NOMENCLATURE

p	beam inflation pressure (Pa)
r	radius of inflated beam (m)
x	axial beam coordinate (m)
E	beam fabric modulus (N/m)
I	inflated beam moment of inertia (m^3)
M	applied bending moment (N-m)
N	axial stress resultant (N/m)
ρ	radius of curvature (m)
θ	angular position (radians)

ANALYSIS OF THE EVA GLOVE MCP JOINT

Comer and Levy (1963) modelled bending of cylindrical membrane structures in a manner analogous to conventional beam theory. The following structural analysis closely follows the method used by Comer and Levy with some modifications to make the results more

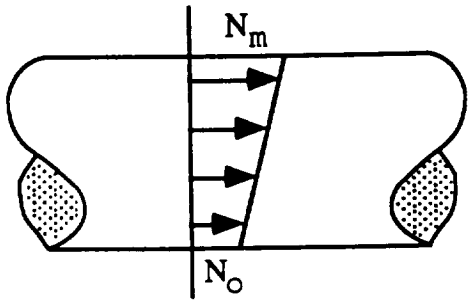

Figure 1. The stress distribution in the fabric of the glove MCP joint in regions where no wrinkling is present.

applicable to fabric structures. These changes include the use of stress resultants instead of stress and the expression of the fabric modulus in terms of force per unit width.

Figure 1 shows a sketch of an idealized EVA glove MCP joint. It is a simple cylindrical fabric structure supported by internal pressure. An arbitrary loading of the joint can be expressed by applied moments that are functions of the axial coordinate x. A model of an inflated structure must accommodate both slack and taut regions in the fabric. In the taut regions, where the axial stress in a given cross-section of the fabric of the glove remains tensile around the complete circumference, the stress distribution illustrated in Figure 1 is assumed.

In these regions the value of the axial stress resultant in the glove fabric is defined as

$$N = N_o \left(\frac{1 + \cos\theta}{2}\right) + N_m \left(\frac{1 - \cos\theta}{2}\right) \qquad (1)$$

In this expression θ is measured around the circumference of the beam from the point where $N = N_o$. (i.e. if the glove is loaded in flexion, $N = N_o$ on the palmar side of the glove)

When the applied moment from the hand exceeds the value $\pi r^3 p/2$ the bending stress just cancels the axial stress in the fabric skin on the palmar side of the glove and wrinkling will begin in that region. The fabric wrinkles because it is incapable of resisting compressive loads. In these regions the stress distribution illustrated in Figure 2 is assumed.

In these regions the stress resultant in the axial direction in the fabric skin is

$$N = \left(\frac{\cos\theta_o - \cos\theta}{1 + \cos\theta_o}\right) N_m \qquad \pi > \theta > \theta_o$$

$$N = 0 \qquad \theta_o > \theta > 0 \qquad (2)$$

For the balance of moments about a transverse axis through the center of the glove

$$M(x) = -2 \int_0^{\pi} N r^2 \cos\theta \, d\theta \qquad (3)$$

When $M > \pi r^3 p/2$ equations 2 and 3 can be combined to give

$$N_m = \frac{2 M(x) (1 + \cos\theta_o)}{r^2 (2\pi - 2\theta_o + \sin 2\theta_o)} \qquad (4)$$

For a balance of axial forces on any given cross section

$$p\pi r^2 = 2 \int_0^{\pi} N r \, d\theta \qquad (5)$$

Again considering the regions containing wrinkled fabric, equations 2 and 5 can be combined to give

$$p\pi r^2 = 2 \int_0^{\pi} N r \, d\theta \qquad (5)$$

Equating the expressions for N_m in equations 4 and 6 yields

$$\frac{M(x)}{pr^3} = \frac{\pi (2\pi - 2\theta_o + \sin 2\theta_o)}{4 ((\pi - \theta_o)\cos\theta_o + \sin\theta_o)} \qquad (7)$$

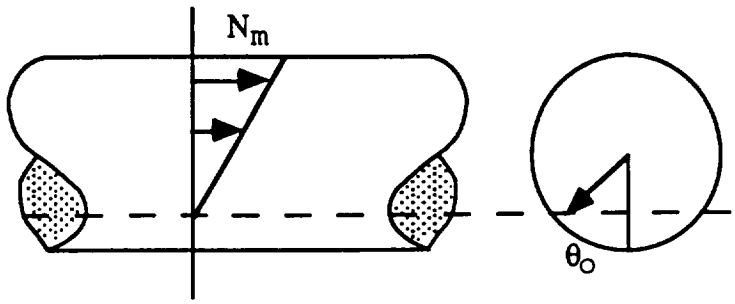

Figure 2. The stress distribution in the fabric of the EVA glove in regions where wrinkling occurs.

Considering now the regions where no wrinkling of the cross section occurs, substitution of equation 1 into equation 3 gives

$$N_m - N_o = 2\,M(x)/\pi r^2 \qquad (8)$$

Substituting equation 1 into equation 5 yields

$$N_m + N_o = pr \qquad (9)$$

Combining equations 8 and 9 yields

$$N_m = (M(x)/\pi r^2) + (pr/2) \qquad (10)$$

The curvature of the glove joint that is wrinkled is given by

$$\frac{1}{\rho} = \frac{(N_m/E)}{r(1+\cos\theta_o)} \qquad (11)$$

Substituting in the expression for N_m in equation 4 yields

$$\frac{1}{\rho} = \frac{2\,M(x)}{E\,r^3(2\pi - 2\theta_o + \sin 2\theta_o)} \qquad (12)$$

The curvature of the joint when no wrinkling is present is given by

$$\frac{1}{\rho} = \frac{(N_m - N_o)}{2\,E\,r} \qquad (13)$$

Substituting equation 8 into equation 13 yields

$$\frac{1}{\rho} = \frac{M(x)}{\pi\,r^3\,E} \qquad (14)$$

Equations 12 and 14 can be combined so that the model of the simplified glove MCP joint subject to a bending moment can be expressed in the following form:

$$\frac{1}{\rho} = \frac{M(x)}{E\,I} \qquad (15)$$

$$I = r^3\,(\pi - \theta_o + (\sin 2\theta_o)/2) \quad \text{for } M > \pi pr^3/2$$

$$I = \pi\,r^3 \quad \text{for } M < \pi pr^3/2$$

When wrinkling occurs at the joint ($M > \pi r^3 p/2$) equation 7 must be used to determine the angle θ_o that corresponds to the applied moment. Different geometries that might be more representative of the actual EVA glove can also be accommodated in this model simply by substituting the appropriate moment of inertia for the MCP joint cross-section.

GLOVE DESIGN

In terms of the model embodied in equation 15, the goal of the EVA glove designer is to achieve a given joint curvature ($1/\rho$) while minimizing the necessary moment (M) that must be supplied by the hand. One way to accomplish this (Main et al., 1991) is to supply a moment from exterior actuators to reduce the contribution necessary from the hand. The model also supports current efforts (Kosmo et al., 1988; Spampinato et al., 1990) to design and construct closer fitting gloves since, for a given glove curvature, the required applied moment from the hand can be reduced by lowering the moment of inertia (I) of the glove cross section. The lowest moment of inertia would be the closest fitting glove possible. Examination of equation 15 leads to another technique for reducing the applied moment necessary to bend the MCP joint. This is accomplished by reducing the elasticity (E), or spring constant, of the glove itself. One of the advantages of increasing joint mobility in this fashion is that, since the modifications are made only to the part of the glove that is in tension, the only hardware additions necessary are on the back of the hand. This means that hand/tool coupling is not compromised by the addition of hardware to the palm. The goal of this investigation was to reduce MCP stiffness in this fashion and verify the validity of the model in the process.

A unique glove was designed and constructed specifically for testing this concept. As shown in Figures 3 and 4, the test glove consists of a fabric restraint layer over a latex inner glove. The glove includes a palm bar to prevent ballooning, a strap over the back of the hand to further tighten the glove over the palm, and tucked fabric finger joints for finger mobility. An important feature of this glove is the inclusion of a large pleat that extends from the edges of the palm over the knuckles on the back of the hand. The effect of this pleat is to give the glove a pressurized neutral position with the fingers flexed approximately 60 degrees at the MCP joint.

The glove was designed to accept three distinct dorsal assemblies which change the characteristics of the MCP joint. These assemblies were mounted on the glove at attachment points at the base of each finger and a large velcro mount on the glove wrist. Each assembly has the effect of changing the neutral position of the glove fingers to a zero flexion angle. The simplest of the three dorsal assemblies is a panel of fabric that attaches to the wrist and is laced into the finger attachment points. This version (see Figure 5) is considered the standard version and is intended to be analogous to a pressurized glove without any MCP joint modifications.

A coil spring dorsal assembly was also constructed (see Figure 6) and represents an attempt to increase MCP joint flexibility by lowering the spring constant of the load bearing structure on the back of the glove. The springs chosen for this assembly (SPEC Model E0360-039-2000, k=0.508 N/mm, free length=50.8 mm, diameter=9.14 mm) have a spring

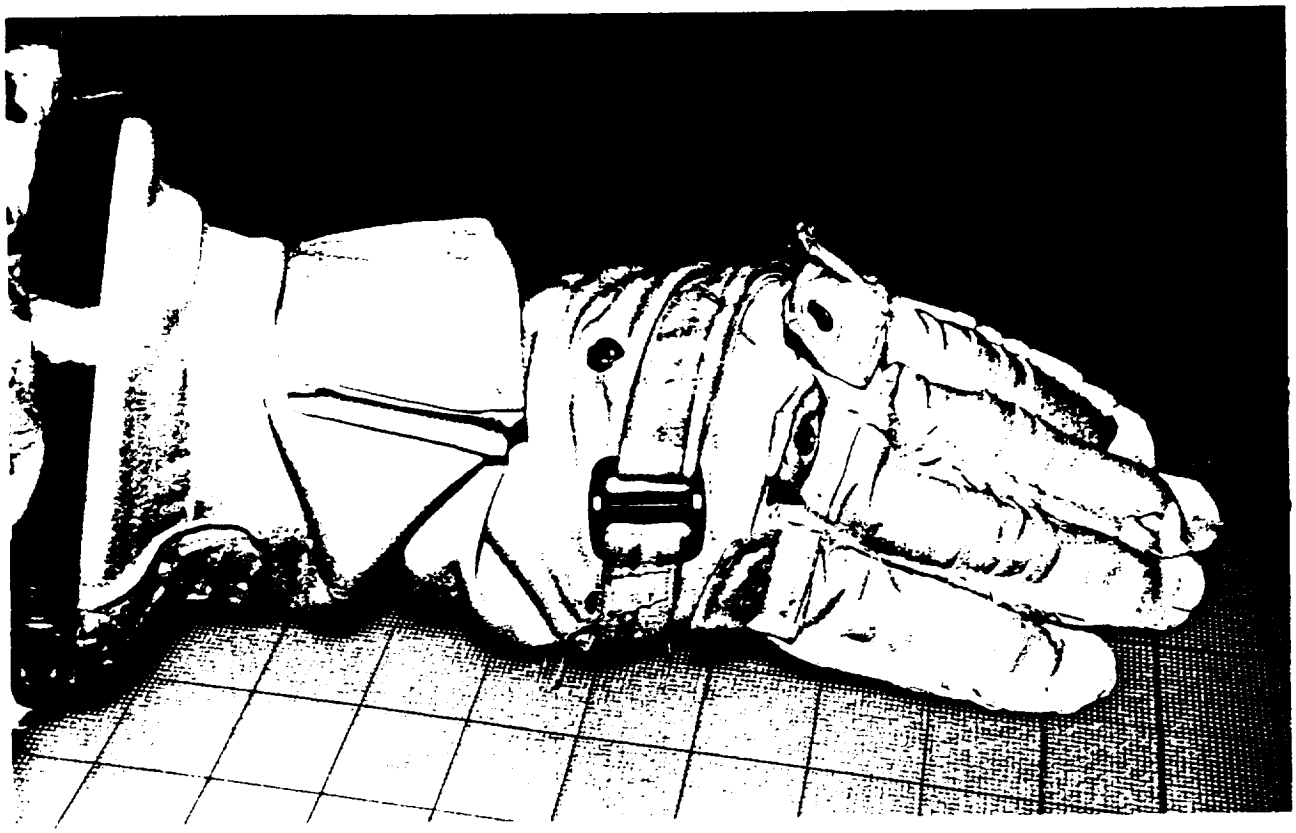

Figure 3. Photo of test glove without a dorsal assembly.

constant significantly less than the fabric panel in the standard version.

A pneumatic actuator assembly was also constructed (see Figure 7) and was intended to further reduce the spring constant of the dorsal assembly by inclusion of an active subsystem. The design of the actuator is shown in Figure 8. The neoprene tubes enclosed in the nylon sleeves have a spring constant that is approximately the same as the coil springs in the previously described dorsal assembly. There is, however, the added capability of extending the actuator by pressurizing it. The nylon sleeves are cut very long and thin (maximum diameter 15 mm) so that, upon pressurization, the bladder will stretch and the actuator will lengthen, allowing the glove MCP joint to flex. The actuator is controlled using glove/finger contact pressure measurements obtained from a thin pressure sensor (Tekscan Button Sensor, see Figure 9) placed between the hand and the glove at the base of the middle finger of the right hand. The Tekscan sensor consists of a layer of polyester film that has a thin layer of ink screened on the surface. The resistivity of the ink is pressure dependent, so an extremely thin pressure sensor can be fabricated by covering the ink patch with another layer of polyester film and measuring the resistance change of the sensor with a bridge circuit. The stock Tekscan sensor has a thickness of 0.15 mm. After lead attachment and application of a protective layer of insulating tape the sensor assembly has a thickness of 0.51 mm.

The control strategy for the active system is illustrated in Figure 10. As the hand moves against the glove no action is taken by the control system until an upper pressure threshold (V_p) is exceeded. At that point the pressurization valve opens and the actuator fills, allowing the finger to flex. The actuator extends to the point that the pressure between the hand and glove is reduced below the threshold V_p, closing the pressurization valve. When the hand extends back toward neutral position the pressure sensor reading will drop further and go below the lower threshold (V_e). In this region the controller opens the exhaust valve.

The schematic of the controller circuit is included as Figure 11. The circuit consists of a bridge circuit for pressure measurement and an operational amplifier (NTE 857) to isolate the bridge as well as to amplify the signal. The function of the remainder of the circuit is summarized in Table 1. The two 311 voltage comparators are set to switch from a HIGH state to LOW when the signal from the finger pressure sensor exceeds their preset thresholds, V_p and V_e. The output of the comparators is connected to a pair of logic gates that control the action of the pressurization and exhaust valves. The NOR gate controls the action of the pressurization valve and the AND gate the exhaust valve.

Figure 4. Photo of test glove in the 57.2 kPa glove box without a dorsal assembly. Note the neutral position of the MCP joint.

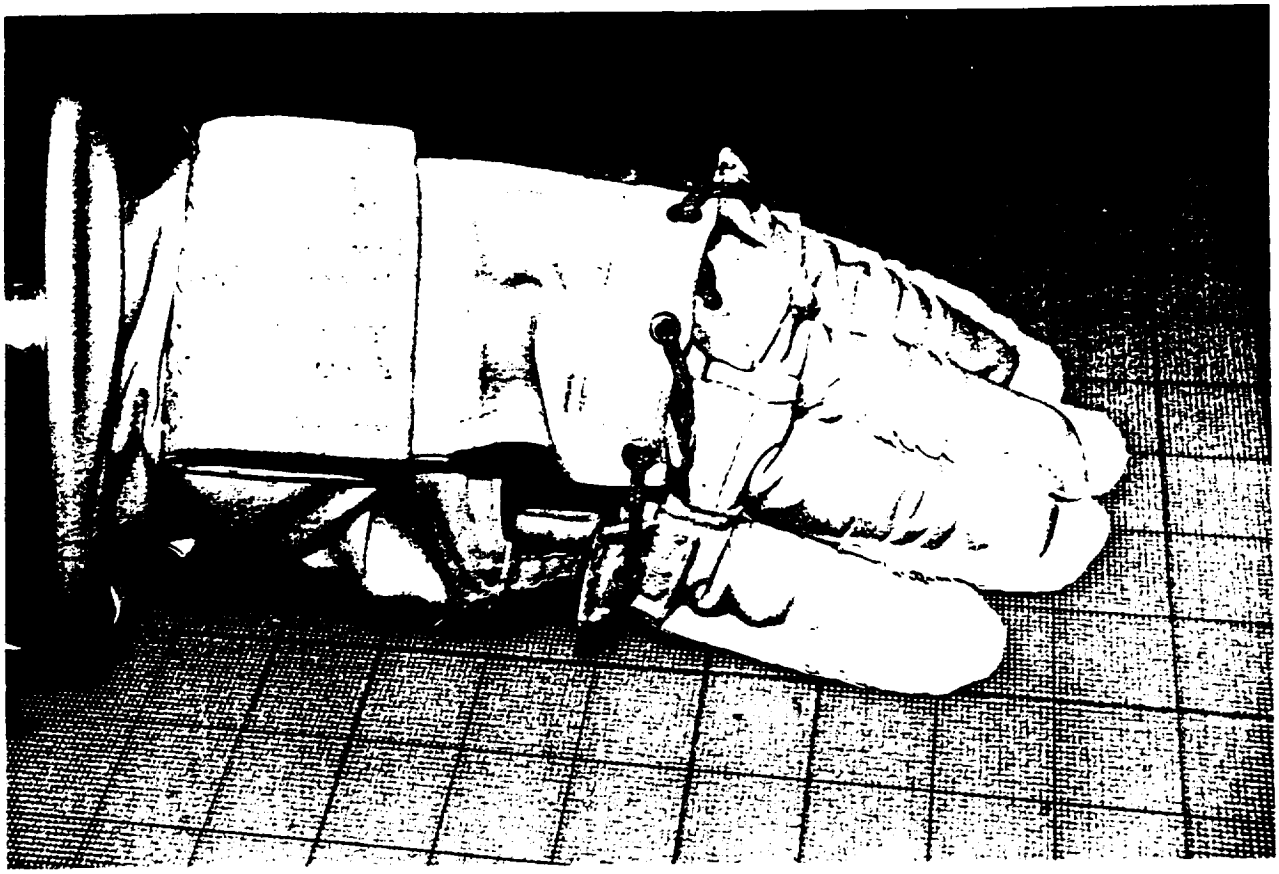

Figure 5. Test glove with the fabric panel dorsal assembly.

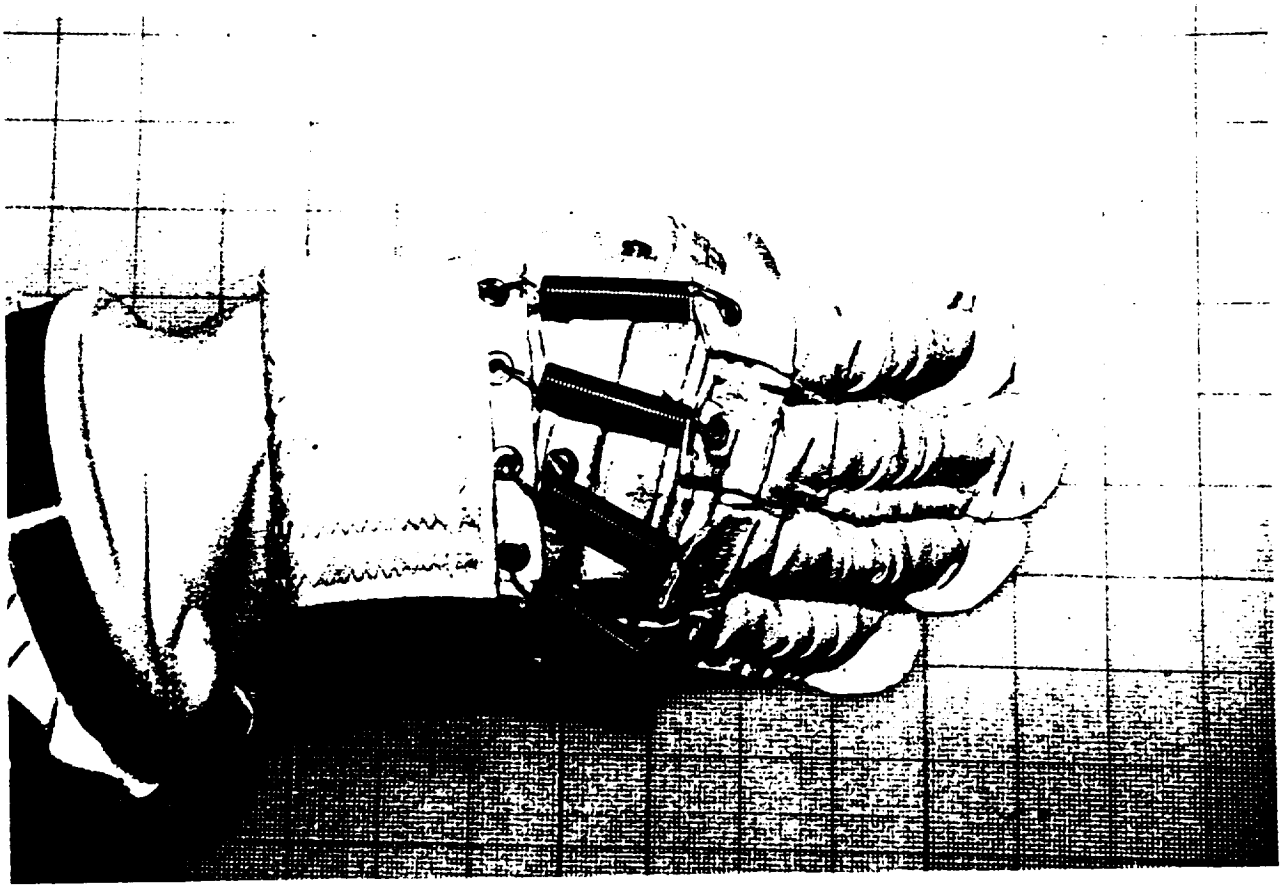

Figure 6. Test glove with the coil spring dorsal assembly.

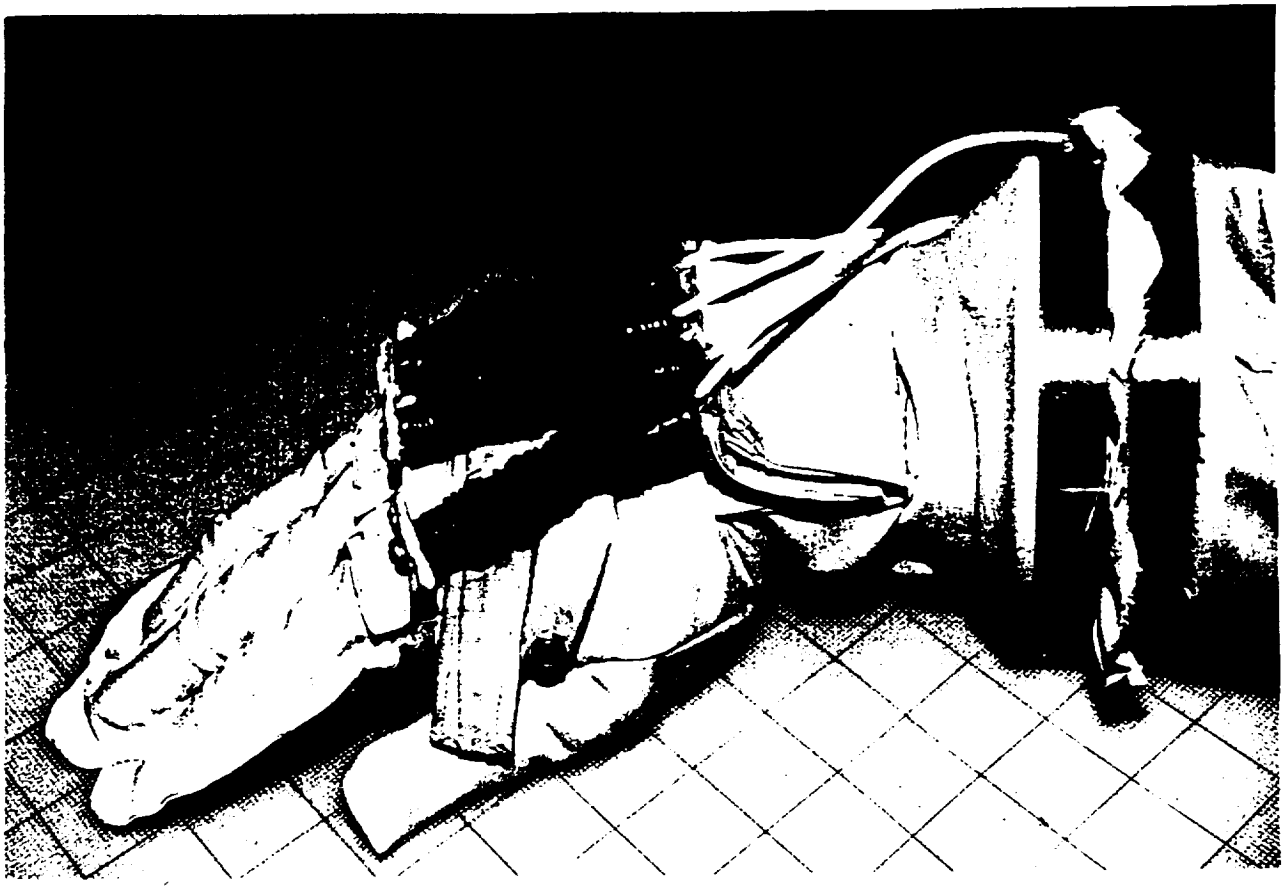

Figure 7. Test glove with pneumatic actuator dorsal assembly.

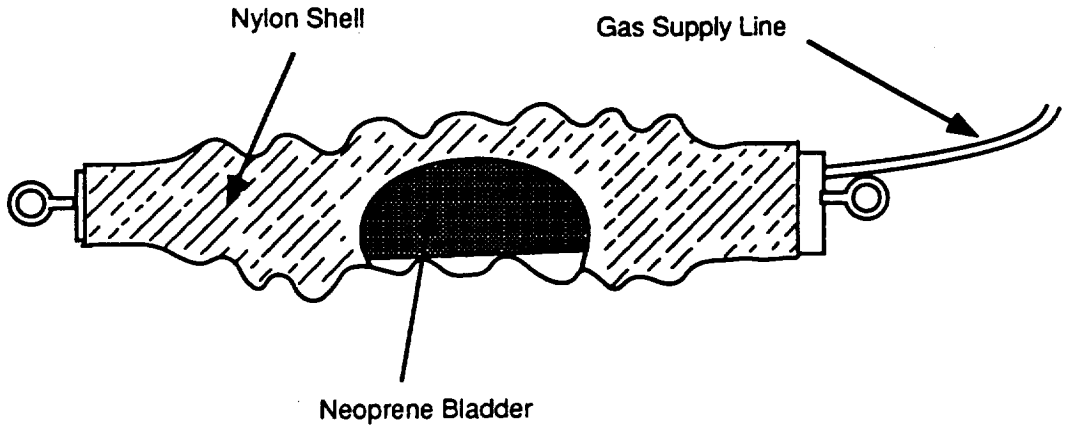

Figure 8. Sketch of pneumatic actuator.

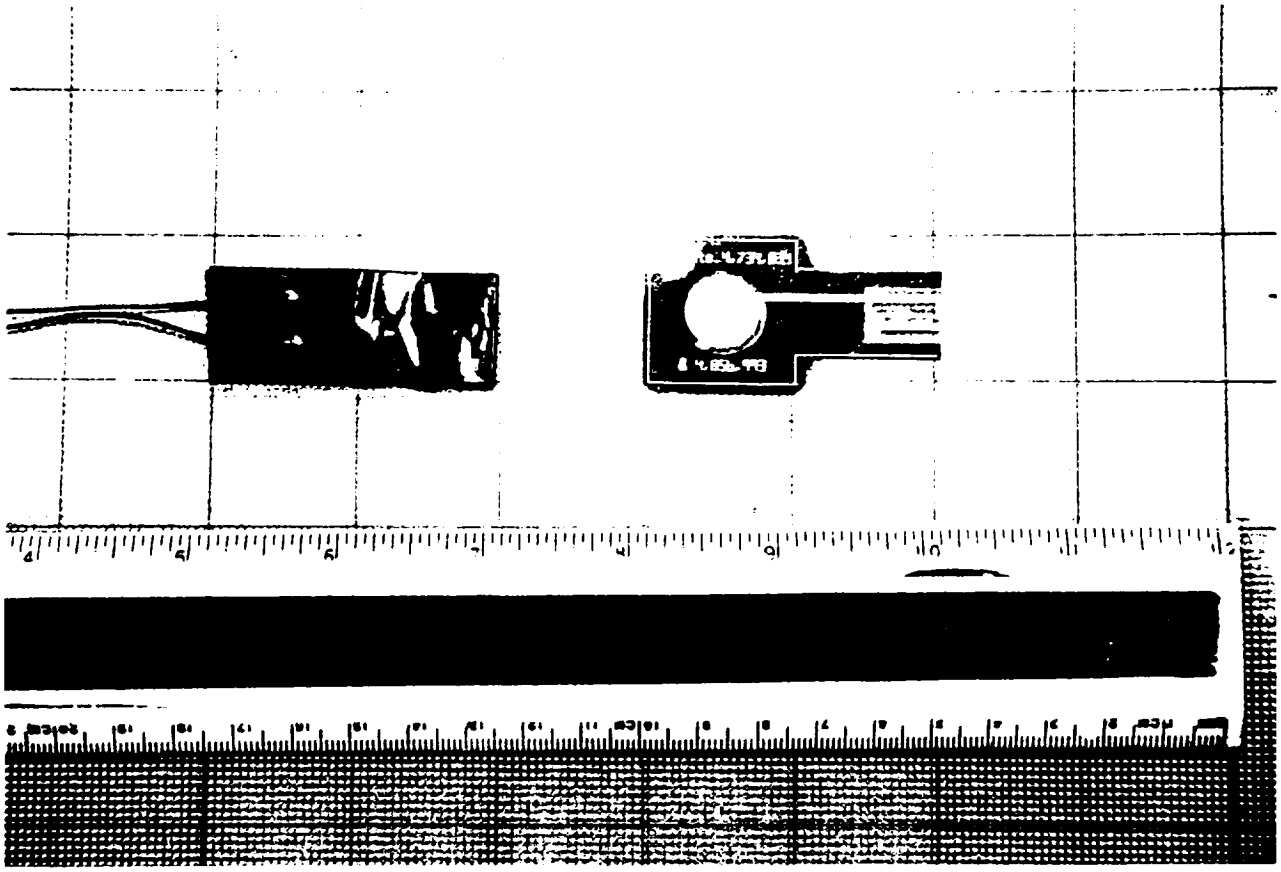

Figure 9. Photo of Tekscan, Inc., pressure sensor. Stock version (right) and after lead attachment (left).

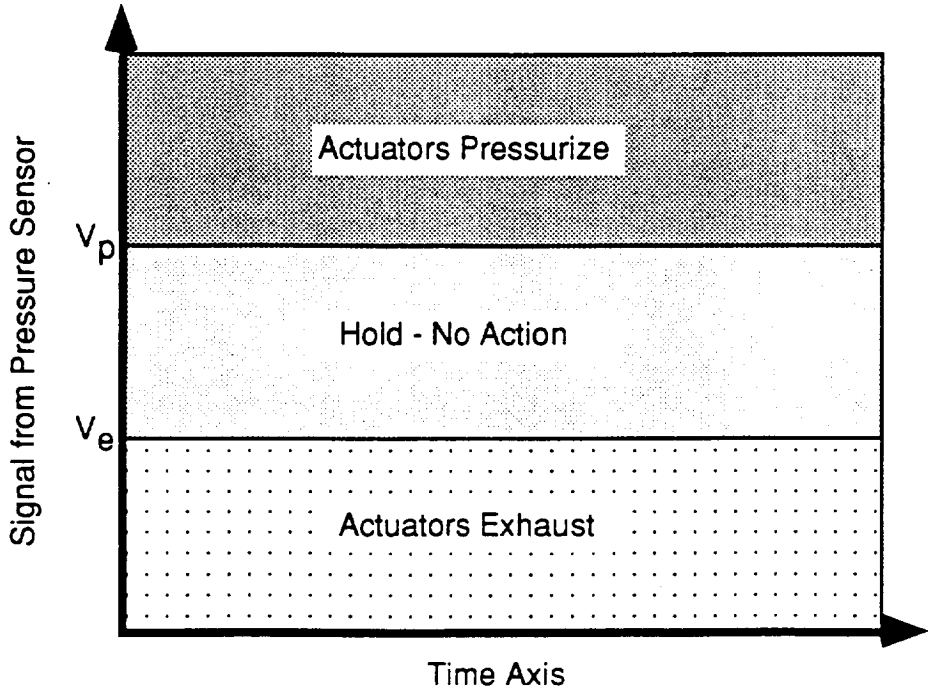

Figure 10. Plot showing control system actions relative to pressure sensor input and threshold settings.

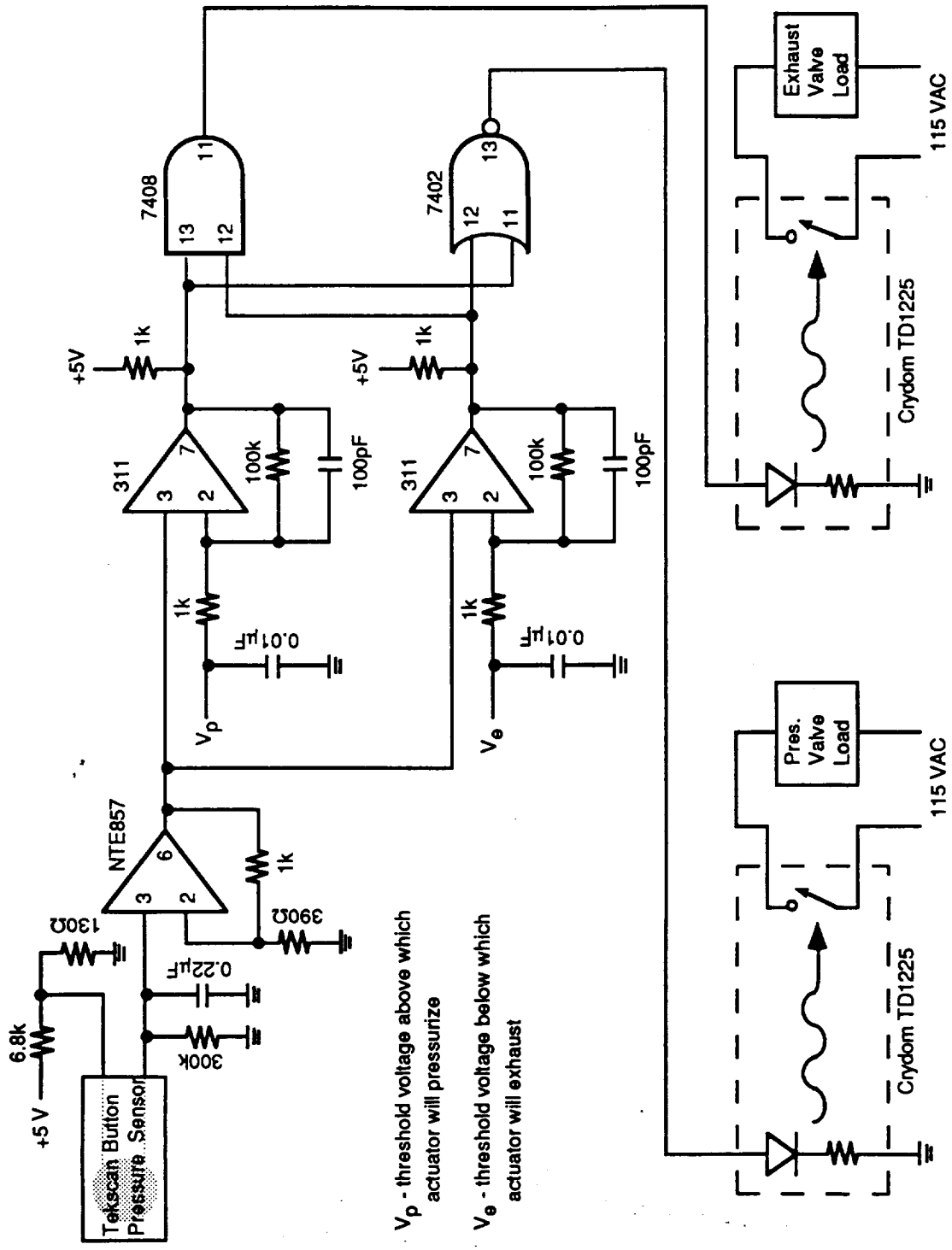

Figure 11. Schematic of sensor and control system.

Table 1. Pneumatic Actuator Controller Truth Table.

Sensor Output	Voltage Comp. set at V_e	Voltage Comp. set at V_p	Exhaust Valve (AND)	Pres. Valve (NOR)
$< V_e$	High	High	ON	OFF
$> V_e$ and $< V_p$	Low	High	OFF	OFF
$> V_p$	Low	Low	OFF	ON

EXPERIMENTAL

Tests of all three glove embodiments consisted of a series of 90 degree flexions of all four fingers. The target frequency for the finger bends was 0.5 Hz. Data was collected at 0.1 second intervals from the Tekscan sensor mounted the base of the palmar face of the middle finger (see Figure 12). The sensor had been previously calibrated so that the voltage output of the conditioning circuit could be translated into finger pressure. A test series consisted of twenty 90 degree bends of the glove MCP joint including all four fingers. Repeatability was insured in the bending task by placing a target object in the glove box in a position where finger contact with the object yielded a 90 degree flexion of the MCP joint.

Tests of the glove with the pneumatic actuator assembly required setting the pressurization and exhaust thresholds prior to the test. For the data presented here Vp and Ve were set to 33.4 mV and 20.5 mV, respectively. These voltage levels correspond to 89.5 kPa and 47.2 kPa on the sensor calibration curve. Photos of each glove version at neutral inflated position and with fingers flexed at the MCP joint are included as Figures 13 through 18. A plot of typical sensor pressure readings during the 90 degree flexion test is included as Figure 19.

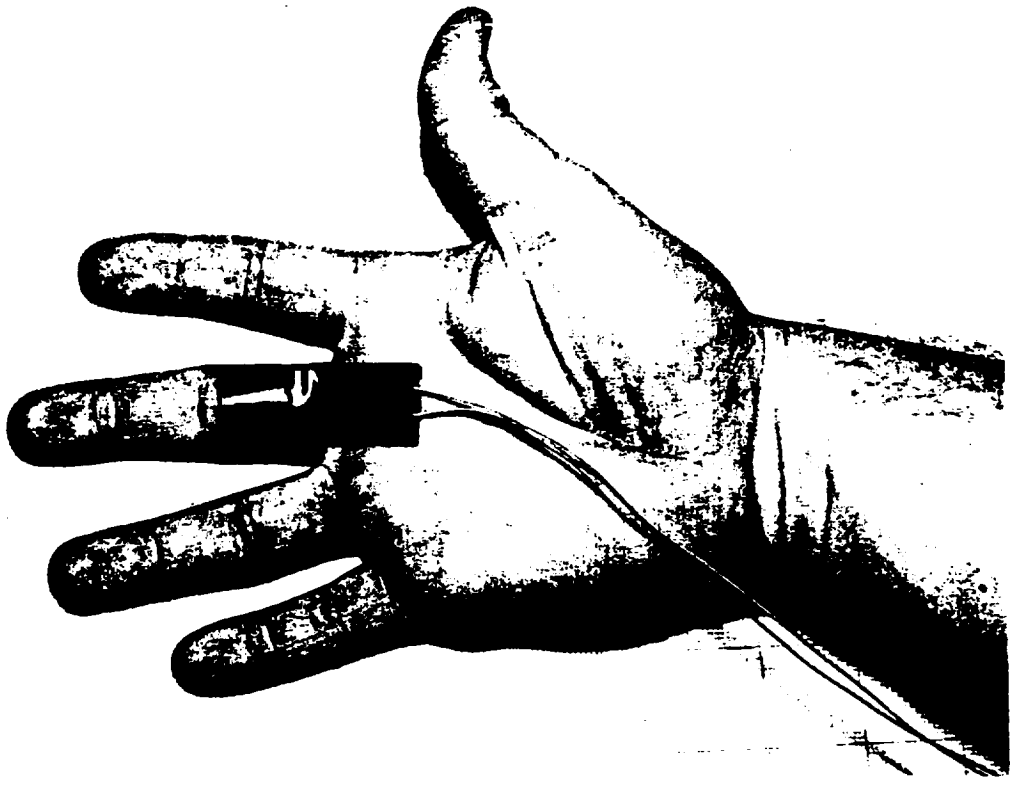

Figure 12. Photo showing sensor application to hand.

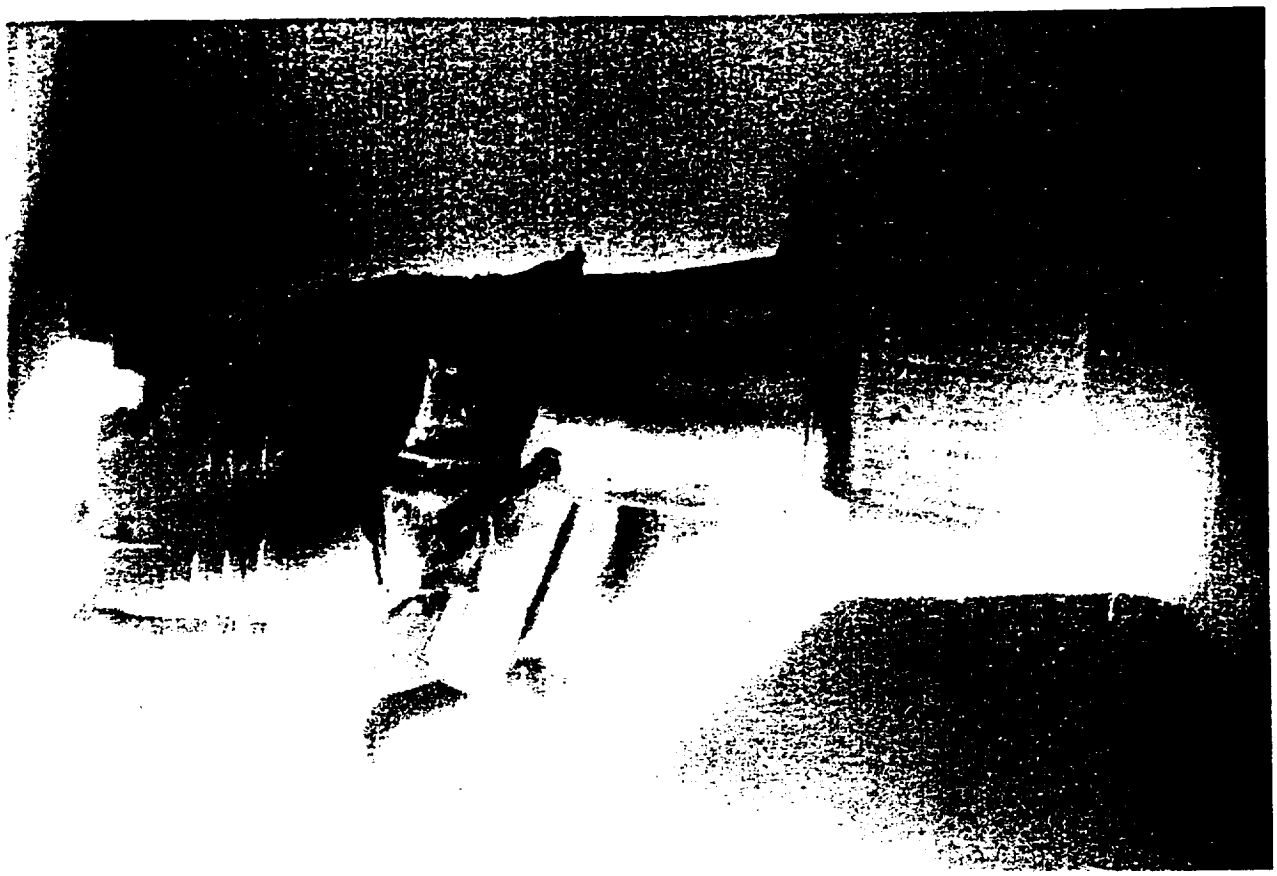

Figure 13. Photo showing the fabric panel version in the pressurized neutral position.

Figure 14. Photo of the fabric panel version in the glove box showing the MCP joint finger flexion.

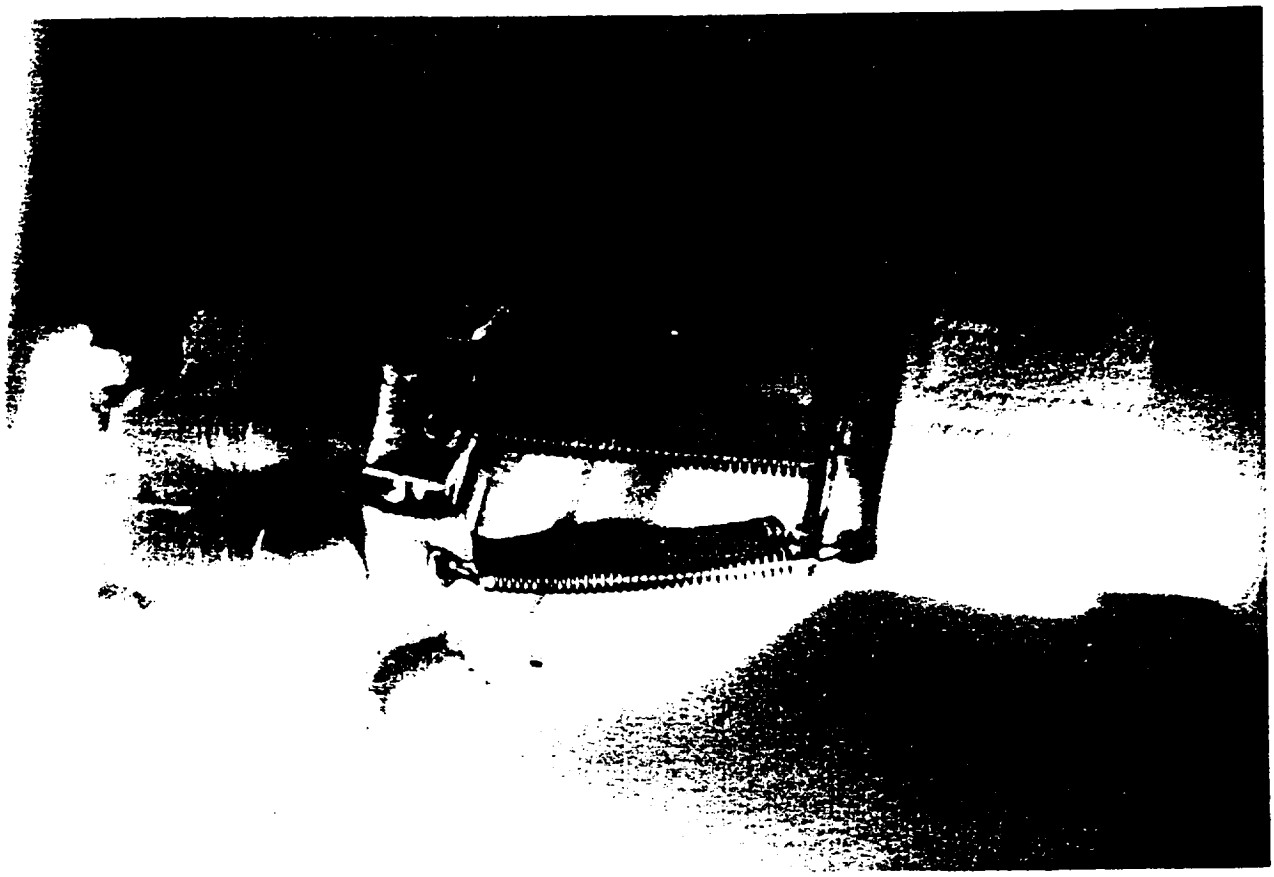

Figure 15. Photo showing the coil spring version in the pressurized neutral position.

Figure 16. Photo of the coil spring version in the glove box showing MCP joint finger flexion.

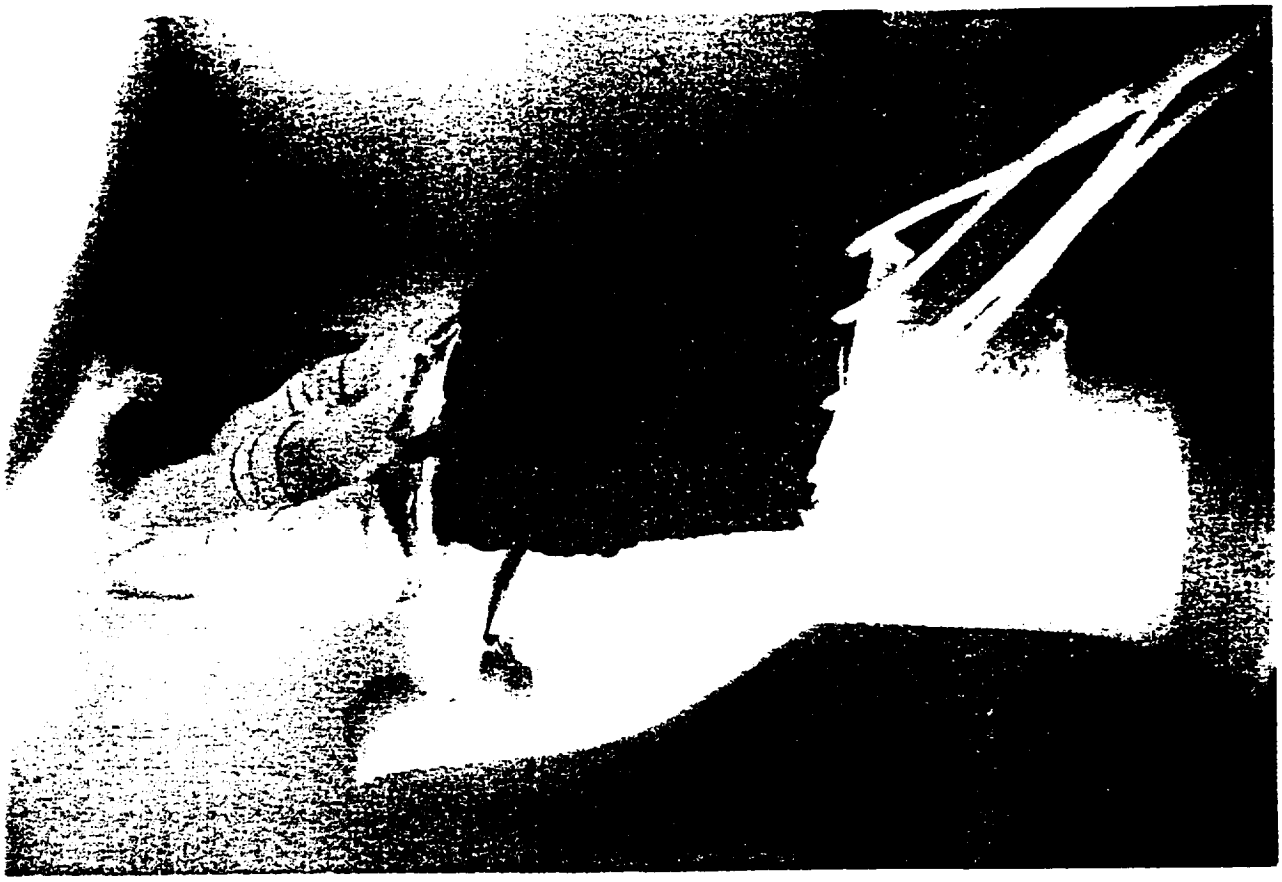

Figure 17. Photo showing the pneumatic actuator version in the pressurized neutral position.

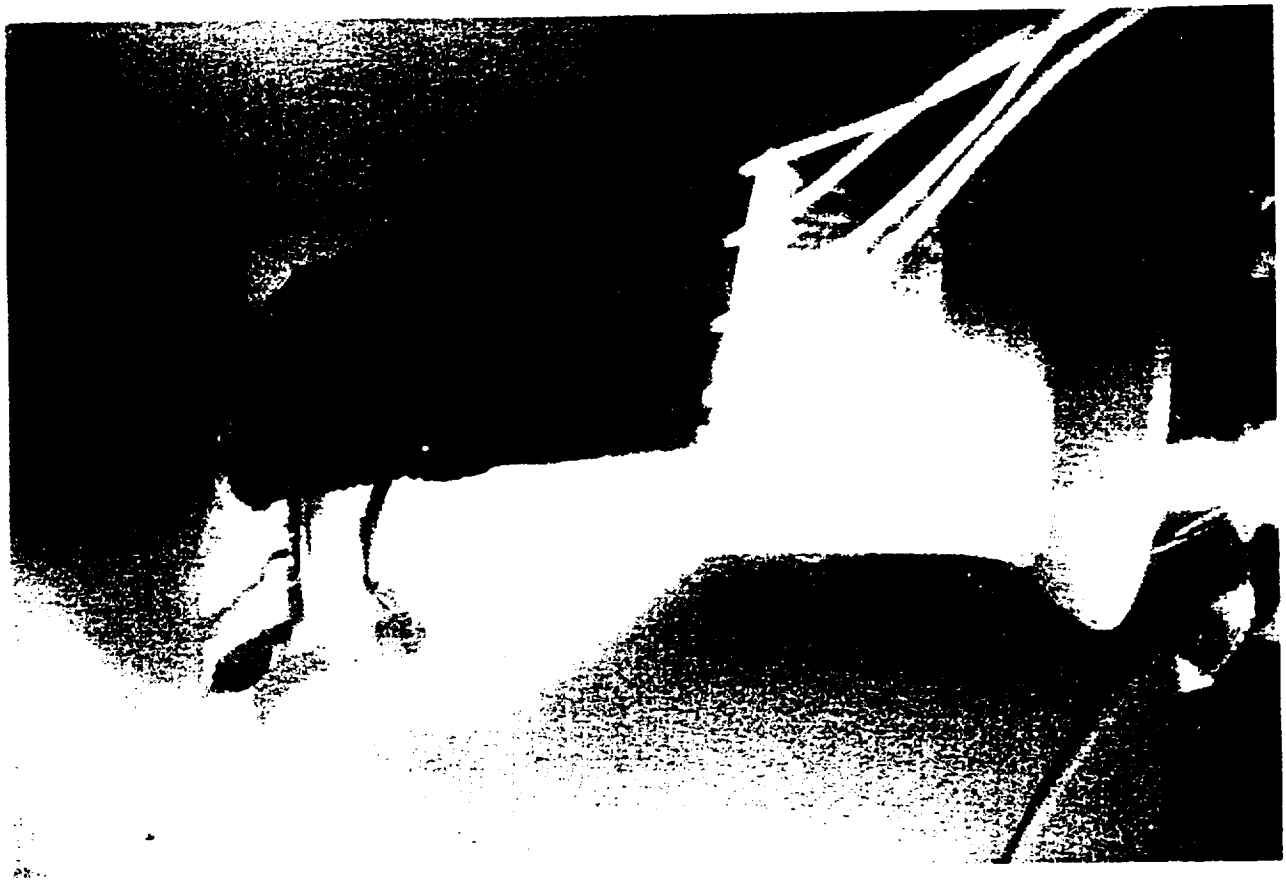

Figure 18. Photo of the pneumatic actuator version in the glove box showing MCP joint finger flexion.

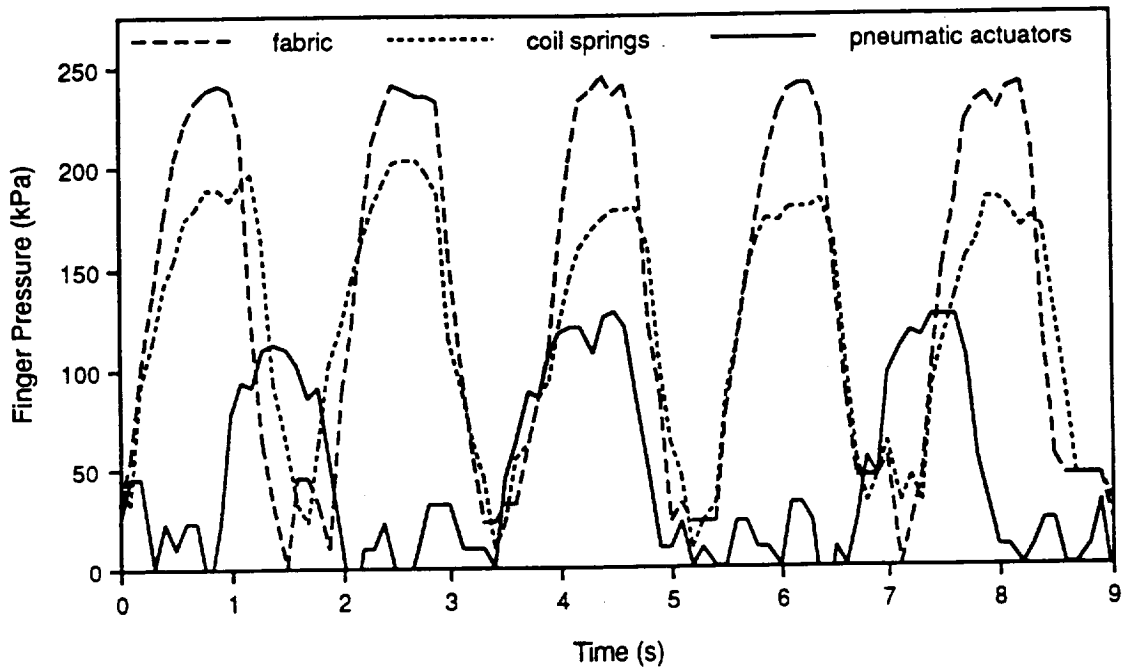

Figure 19. Plot of the pressure between the middle finger and the pressurized test glove during the 90 degree flexion task for the three different dorsal assemblies.

DISCUSSION

A summary of the peak pressures measured between the middle finger and the test glove for each glove version is included as Table 2. The data presented in the table was generated from the last nine cycles of each test because the data from early in the tests was very erratic. This appears to be caused by a "settling" period that takes place in the glove assembly after each glove box evacuation. The average of the peak pressures measured by the sensor during the flexion tests of the glove with the fabric panel was 237 kPa. By simply replacing the fabric panel with the coil spring assembly the average peak finger pressure dropped 20% to 190 kPa. This assembly also has the advantage of being very low in profile, each spring being no more than 10 mm in diameter.

An even greater drop in the measured peak finger pressure was found with the pneumatically actuated glove. When the actuators were in use the average peak pressure during bending was found to be 140 kPa . This represents a 41% drop in the resistance of the glove to bending when compared to the fabric panel glove. The increased scatter (S.D. 18.3 kPa) of the maximum finger pressures in the test of this glove version stems from the flow of compressed nitrogen to and from the glove actuators. This generates additional mechanical noise in the glove structure that is reflected in the pressure sensor readings. The tests of the glove with the pneumatic actuators also showed that this version had a lower maximum 90 degree flexion rate than either the fabric panel or coil spring versions. The data for the actuated glove presented in Figure19 represents the maximum rate attainable for this version. The time required for

Table 2. Summary of Peak Pressure Data from Finger/Glove Contact Pressure Sensor.

Glove Version	Average Maximum Finger Pressure	Standard Deviation
Fabric Panel	237 kPa	9.3 kPa
Coil Spring Assembly	190 kPa	9.1 kPa
Pneumatic Actuators	140 kPa	18.3 kPa

exhausting the actuators during the extension phase of each cycle limited the maximum attainable frequency to approximately 0.37 Hz. The pneumatic actuators have the further disadvantage of requiring a pressurized gas supply and gas supply lines for the actuators.

The data obtained in this study qualitatively supports the structural model developed previously. The coil spring assembly, with a lower spring constant than the fabric panel, resulted in less torque required to bend the joint. A further reduction in the spring constant of the dorsal portion of the glove at the MCP joint through the use of active pneumatic components resulted in even a greater improvement in joint flexibility.

Given the validity of the pressurized glove model presented here, there exists an opportunity to lower the joint torque of the glove still further. Examination of Equation 15 indicates that the ideal assembly for the dorsal portion of the glove would be able to carry the load that is present in the glove fabric due to pressurization, yet have an extremely low spring rate. Such components exist and are generally referred to as constant force or negator springs. Future investigations are planned to evaluate the usefulness of these components in high mobility pressurized glove joints. Future investigations must also determine the effects on glove fit and and overall suit performance of allowing the back of the glove to change dimensions to increase glove flexibility.

ACKNOWLEDGEMENTS

The authors would like to acknowledge the support of the NASA Office of Aeronautics and Exploration Technology and the NASA National Space Grant College and Fellowship Program.

BIBLIOGRAPHY

Comer, R. L., and Levy, S., "Deflections of an Inflated Circular-Cylindrical Cantilever Beam," AIAA Journal 1 (July 1963):1652-1655.

Kosmo, J. J., Bassick, J. and Porter, K., "Development of Higher Operating Pressure Extravehicular Space-Suit Assemblies," proceedings of the 18th Intersociety Conference on Environmental Systems in San Francisco, CA, July 11-13, 1988, SAE Paper #881102.

Main, J. A., Peterson, S. W., and Strauss, A. M., "A Prototype Power Assist EVA Glove," proceedings of the 21st International Conference on Environmental Systems in San Francisco, CA, July 15-18, 1991, SAE Paper #911384.

Spampinato, P., Cadogan, D., McKee, T., and Kosmo, J., "Advanced Technology Application in the Production of Spacesuit Gloves," proceedings of the 20th Intersociety Conference on Environmental Systems in Williamsburg, VA, July 9-12, 1990, SAE Paper #901322.

SAE TECHNICAL
PAPER SERIES

911384

A Prototype Power Assist EVA Glove

John A. Main, Steven W. Peterson, and Alvin M. Strauss
Department of Mechanical Engineering
Vanderbilt Univ.
Nashville, TN

Reprinted from: Space Station and Advanced EVA (SP-872)

SAE The Engineering Society For Advancing Mobility Land Sea Air and Space®
INTERNATIONAL

21st International Conference on
Environmental Systems
San Francisco, California
July 15-18, 1991

400 COMMONWEALTH DRIVE, WARRENDALE, PA 15096-0001 U.S.A.

The papers included in this volume are abstracted and indexed in the SAE Global Mobility Database.

ISSN 0148-7191

Persons wishing to submit papers to be considered for presentation or publication through SAE should send the manuscript or a 300 word abstract of a proposed manuscript to: Secretary, Engineering Activity Board, SAE.

Printed in U.S.A.

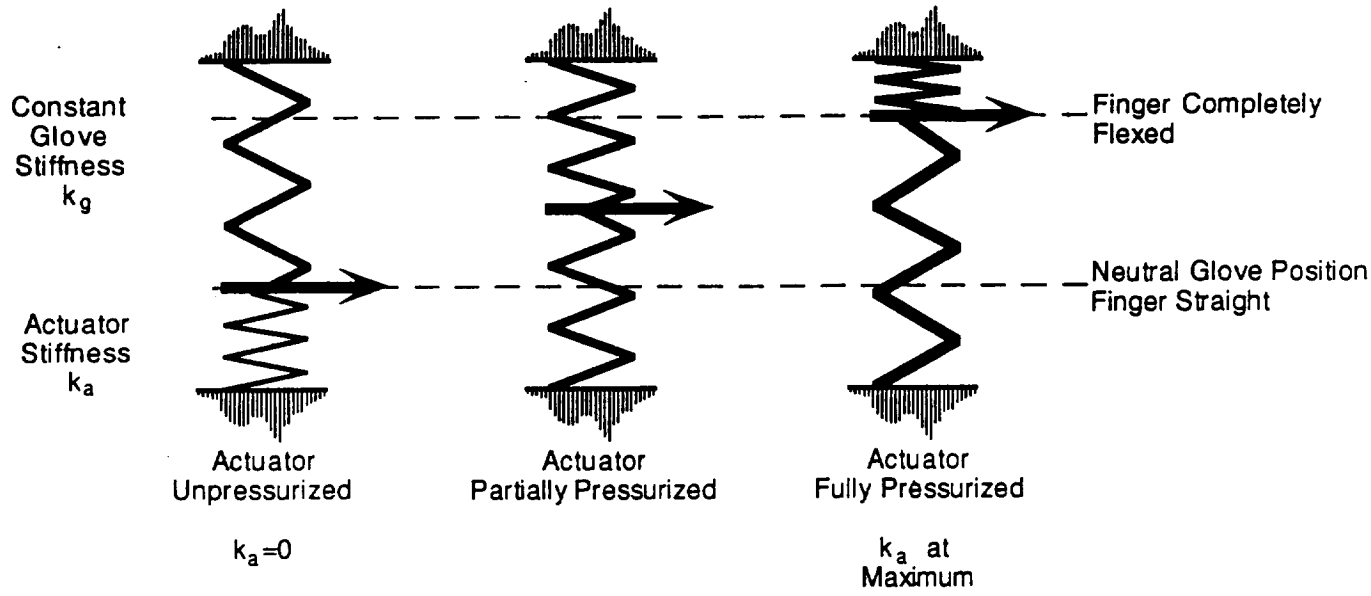

Figure 1. Spring model of inflated glove/actuator system.

to the two spring system illustrated in Figure 1. The glove MCP joint can be accurately modeled as a constant stiffness spring since the nominal inflation pressure remains constant at 57.2 kPa (8.3 PSI). The spring in opposition to the glove stiffness spring represents the pneumatic actuator. This spring has a variable stiffness that depends on the pressurization level of the actuator.

Behavior of the glove/actuator system can be illustrated with this simple model in the following fashion. When the actuator is unpressurized the stiffness associated with it (k_a) is essentially zero and the glove assumes the neutral inflated position. As the actuator is pressurized k_a increases and the equilibrium position of the system changes. This change in equilibrium position represents the bending of a given finger at the MCP joint. When the actuator is fully pressurized k_a is at a maximum and thus the fingers have deflected the maximum amount.

Examination of the opposing spring model leads to two important conclusions. First, the neutral position of the actuated glove joint should be flat and straight. This will allow the actuator to move the finger through the entire range of motion. It is the actuator, not the cut of the glove pattern, that will bend the glove into a position that corresponds to the neutral position of the human hand. Second, the kinematics of the actuator must mimic the kinematics of the gloved hand. The path that the actuator must follow begins with the glove neutral position and follows the motion of the bending finger. Because the glove stiffness is always non-zero the mounted actuator will always face opposition. Therefore it will never reach the neutral position it would reach if not mounted on the glove. For this reason the unmounted neutral position of the inflated actuator should be a shape that would bend the fingers beyond the desired maximum. When the neutral positions of the two substructures are defined in this fashion they can then work in opposition and the finger can move to any position between the two desired extremes.

According to this model then, the actuator design problem is one of designing an inflated structure that, when mounted on the back of a pressurized glove, will inflate and bend in the same fashion as a finger bends. Efforts to accomplish this task have led to an evolution of sorts in pressure glove actuator design.

The first series of actuators tested followed the concept illustrated in Figure 2. This actuator consists of a plain fabric base and a tucked fabric superstructure sewn together to form a cylinder. A gastight flexible bladder is placed inside the fabric

cylinder to contain the pressurization medium and is connected to the gas reservoir via a flexible tube. As the actuator is pressurized the excess fabric along the top of the actuator allows expansion while the plain base does not. The net effect is that the structure takes on a "U" shape when pressurized.

A number of actuators of this type were constructed and tested on a pressurized restraint

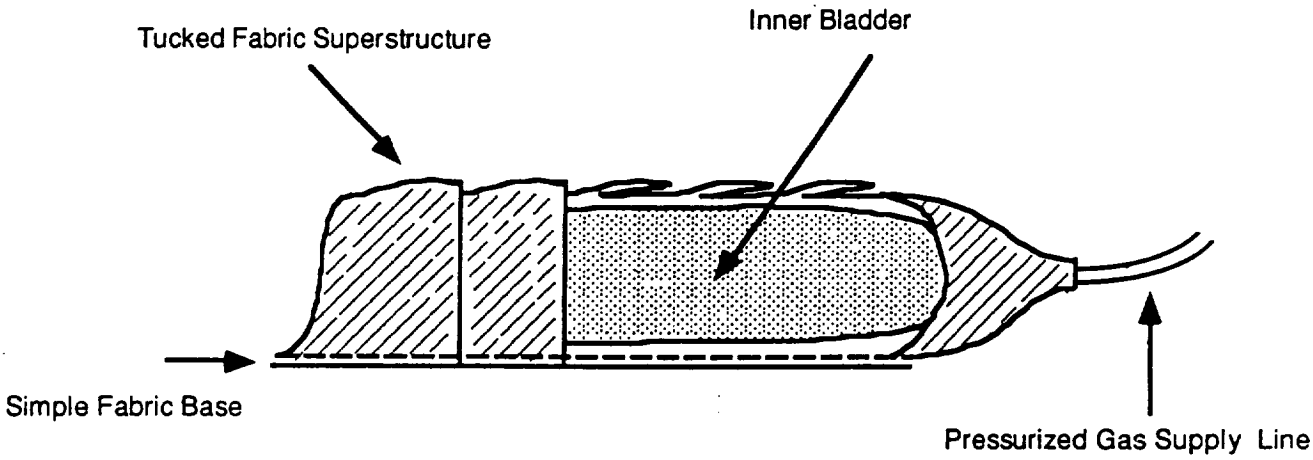

Figure 2. First generation actuator concept.

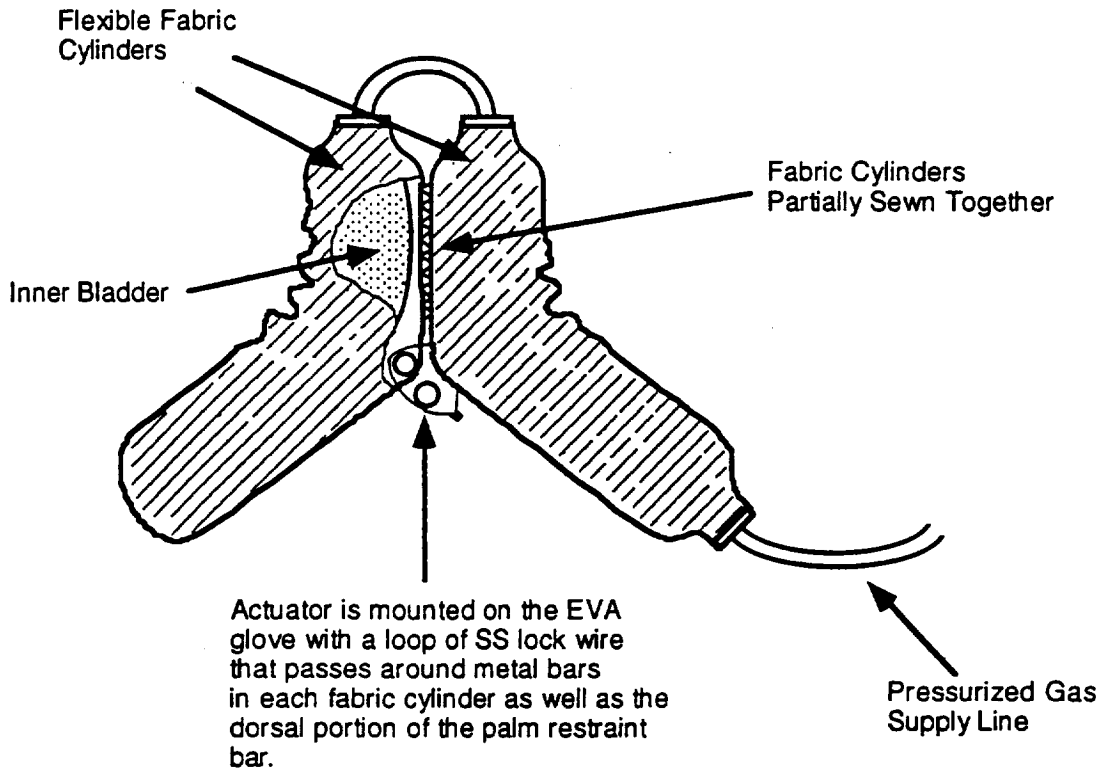

Figure 3. Second generation actuator concept.

mockup with disappointing results. Although the actuators pressurize to the desired "U" shape when unmounted, they do not exert enough force to bend a finger at the MCP joint any appreciable amount. This is true even at actuator pressures exceeding 413.5 kPa (60 PSI) with the 57.2 kPa (8.3 PSI) glove mockup. It was evident from these early tests that a radical change in the actuator design concept was necessary.

A second generation of actuators was developed from the experience gained from the first unsuccessful attempts. Illustrated in Figure 3, it consists of two inflatable fabric cylinders that are securely attached to each other for approximately 1/3 of their length. The gastight bladder inside the fabric cylinders are connected to each other and the gas reservoir by a network of tubes. When this actuator is pressurized the cylinders will stiffen and move together in a fashion somewhat like that of a pair of tweezers. Pressures of approximately 413.5 kPa (60 PSI) were necessary to bend in 60 degree flexion all four fingers of the glove mockup. This design provides a vastly increased range of motion between the unpressurized and pressurized states when compared to the first generation actuator. It also provides a large increase in the magnitude of the bending force that the actuator is capable of producing. Early tests on this actuator configuration were promising enough that a right-handed prototype of the powered glove was constructed including four independent MCP joint actuators. (See Figure 4)

Figure 4. Photo of prototype glove with four MCP joint finger actuators.

GLOVE PROTOTYPE

The prototype glove is intended to be a reasonable approximation of the restraint and bladder components of the current NASA EVA gloves. Tucked fabric interphalangeal joints are included as is a palm bar that completely encircles the hand at the level of the MCP joint. No attempt was made to duplicate the thumb assembly of the NASA EVA glove so the prototype thumb is similar to that of a conventional glove.

For optimum performance of the actuation system the placement of the palm restraint bar is critical. It must be built into the glove so that it does not interfere with MCP joint flexion on the palmar face of the hand and it must be situated slightly distal from the MCP joint knuckle on the dorsal face. The MCP joint actuators are mounted to the dorsal portion of the palm restraint bar so accurate placement of the bar is critical.

A breadboard manual actuation control system was constructed to facilitate evaluation of the glove prototype. The action of each finger actuator is controlled by two valves. One valve controls the pressurization of the actuator and thus the bending of the finger, the other exhausts the actuator, allowing the finger to return toward the neutral glove position. A schematic of the pneumatic system is included as Figure 5.

All the valves used in the system breadboard were two-way normally closed solenoid valves. This choice was made for reasons of convenience. From the point of view of maximum system safety it would be prudent to use normally closed valves for the control of the pressurized gas and normally open valves for exhaust control. This will ensure, in the case of a complete loss of power, that the actuators will not charge and, if already charged, will exhaust and relax the glove.

Figure 6 is a photo of the actuator controller breadboard. The four manifold mounted valves at the top center of the plate are the pressurization valves for each actuator. The manifold is connected to the gas reservoir and pressurized to 413.5 kPa (60

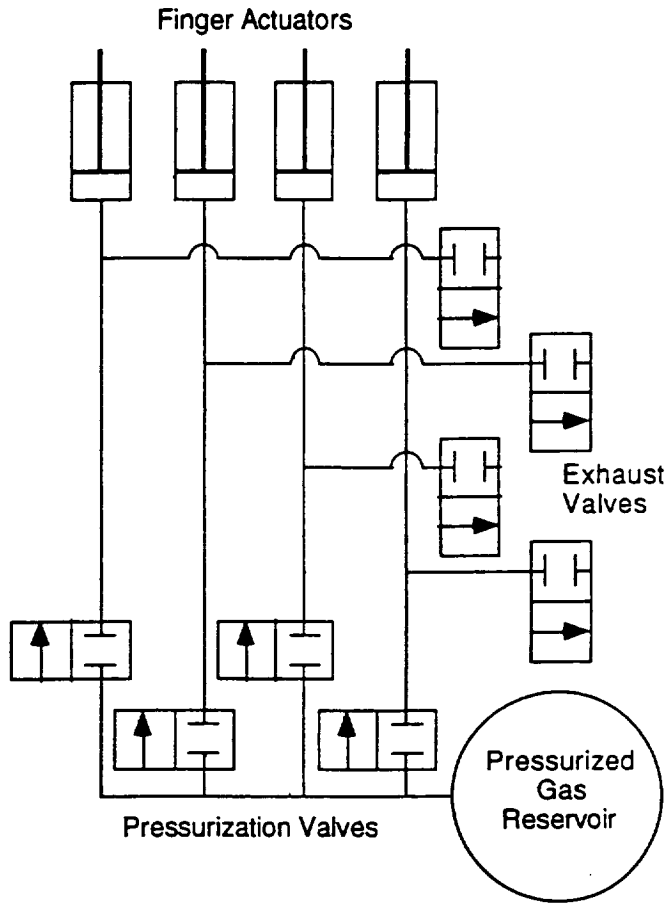

Figure 5. Schematic of pneumatic control system.

PSI). Each of the 1/16" I.D. lines leading away from the manifold connects to a single actuator. The four satellite valves shunted off the pressure lines by tee connectors are the actuator exhaust valves. With this valve configuration each actuator can be pressurized or evacuated independently, thus preserving the independence of finger motions. Valve action and thus actuator response is controlled by the double row of microswitches in the lower right hand corner of the breadboard, the lower row controlling actuator pressurization and the upper row exhaust.

Preliminary evaluations of this actuation and control system were conducted in a glove box evacuated to 57.2 kPa (8.3 PSI). (See Figure 7) The goal of these evaluations was to determine if hand fatigue due to MCP joint flexion is reduced in the actuated glove as compared to an unactuated glove.

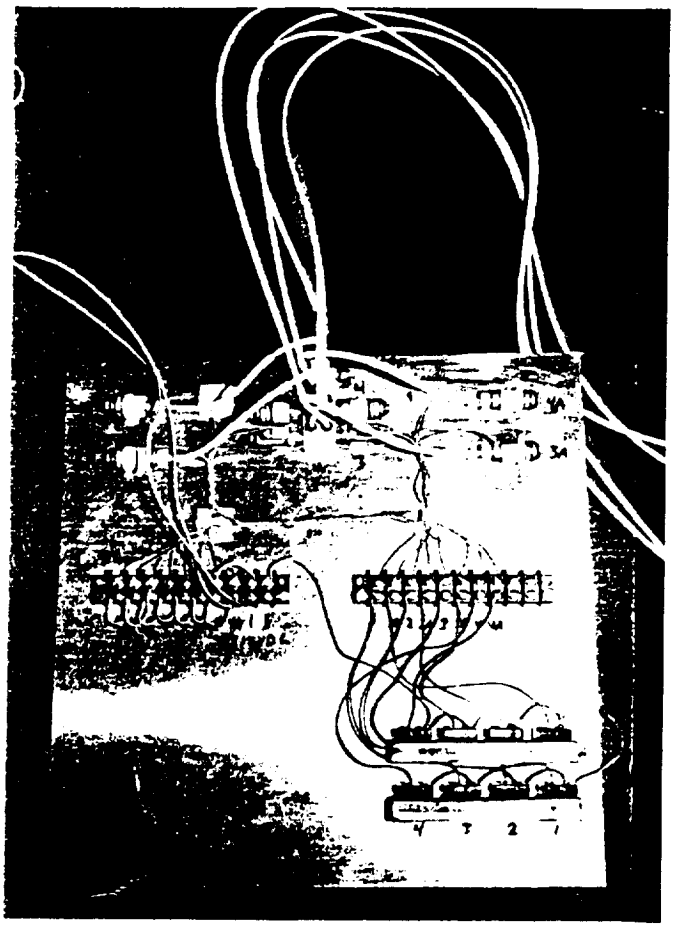

Figure 6. Photo of control system breadboard.

Using the prototype glove with the actuators disabled it was found that the hand rapidly fatigues after only a few rapid cycles of approximately 60 degree MCP joint flexion. Although the stiffness of this glove mockup is certainly greater than that of the production EVA gloves this exercise does serve to illustrate the MCP joint stiffness problem. When the actuation system was activated the 60 degree flexion task could be accomplished indefinitely without muscle fatigue. During the actuated glove tests the wearer placed the right hand in the glove prototype and operated the control switches with the left. In this fashion the cyclic 60 degree flexion of the four fingers was accomplished. Some discomfort was noted during the actuated glove tests due to the pressure of the actuators on the fingers. Approximately 1 second is required for a full flexion-relaxation cycle. The limiting factor in this response time is the rather low flow coefficient of the control valves. Dramatic improvement in the response time is easily obtainable with better valve selection.

Repeated use of the powered glove in the glove box over a period of a few weeks also made evident some necessary hardware modifications. The most critical problem encountered is the wear and tear on the actuator mounts that eventually reduces the effectiveness of the actuators. The small metal supports that are placed in the actuator cylinder to provide an anchor point for the mounting wire pull through the cylinder fabric after repeated use. This allows the actuator to pull away from the glove and eventually reduces the maximum angle of bend of the actuated glove from 60 to approximately 45 degrees. Replacement of the small metal supports with curved members that better conform with the inflated actuator shape should alleviate this problem. Other improvements needed in future iterations include reduction of the profile of the finger actuators and improvement of the time response of the system by incorporating larger diameter pressure lines.

Figure 7. Prototype testing in the glove box.

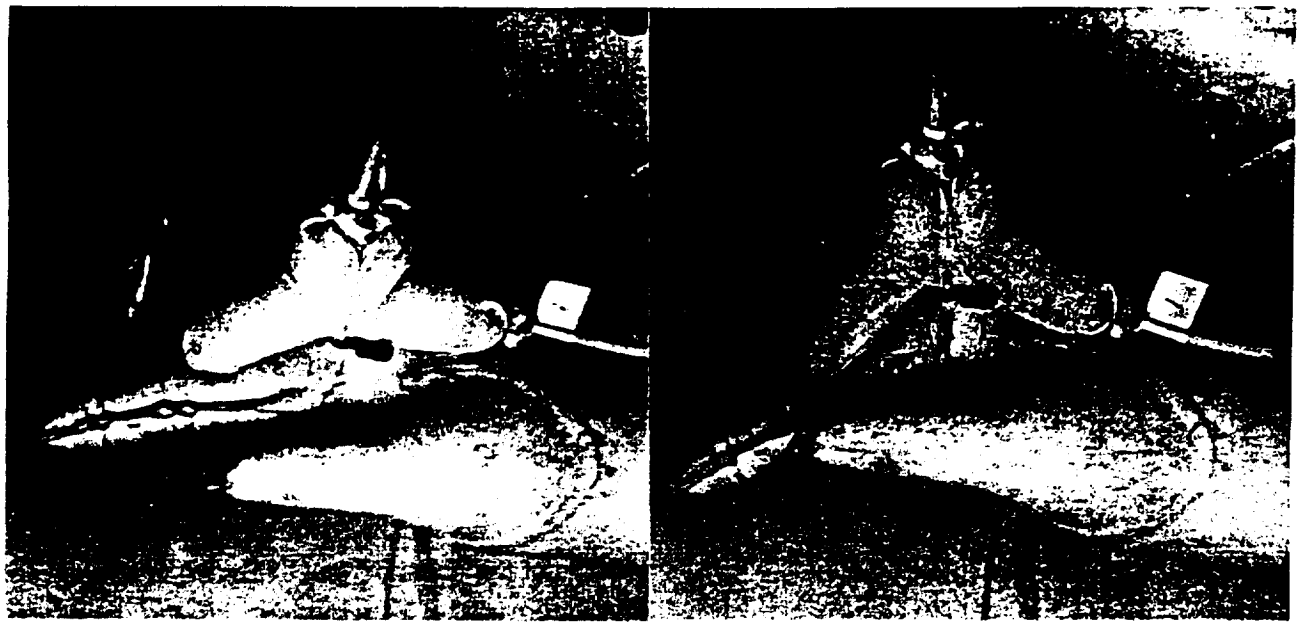

Figure 8. Photos of the prototype glove with actuators unpressurized (left) and pressurized (right).

SENSORS AND CONTROL SYSTEM

With the stated goal of building a powered glove that will mimic the motions of the enclosed hand, the issue of actuator control becomes at least as important as that of actuator design. A simple on-off control system for the above actuation system is proposed here that is intended to maximize system reliability by minimizing the number of system components and using simple decision making procedures.

In order to mimic hand movements these movements must be detected in some fashion. Miniature pressure sensors mounted between the inflated glove and the palmar and dorsal faces of the proximal phalanx of each finger provide a measure of the force each finger is applying to the glove and is thus an indication of desired hand motion. Placing sensors on each finger assures that the independence of finger movements provided by the separate finger actuators is preserved.

The signals generated by these sensors are used to control the actuator pressurization and exhaust valves. Each sensor signal has a threshold level that defines whether a signal is considered high or low. The actions taken by the control system for a given set of sensor outputs are listed in Table 1. For example, in order to bend one finger toward the palm the wearer begins to move the finger against the glove. This causes a signal to be generated from the pressure sensor on the palmar face of the finger. The control valve between the actuator on that finger and the gas reservoir opens at the point where the signal from the pressure sensor exceeds the predetermined threshold. This causes the actuator to pressurize and the finger to bend. In order to stop

Table 1. Control System responses to given finger sensor signals

Input Signal		System Response	
Palmar Sensor	Dorsal Sensor	Pressurization Valve	Exhaust Valve
0	0	CLOSED	CLOSED
1	0	OPEN	CLOSED
0	1	CLOSED	OPEN
1	1	CLOSED	CLOSED

the finger motion the wearer relaxes slightly so that the signal from the pressure sensor again falls below the threshold and the flow of gas from the reservoir is halted. The sensor on the dorsal face of the finger is included so that when pressure is applied to it the exhaust control valve opens and the finger moves back toward the neutral glove position.

It is necessary to define one more condition in the sensor array truth table. This condition occurs when there is pressure on both sensors and both exceed their threshold levels, as will happen when the actuators pressurize when the wearer is grasping an object. According to the previously defined control rules, when a situation like this occurs gas would flow through an open pressurization valve and out an open exhaust valve. A fourth state is defined to avoid this situation that keeps both the pressurization and exhaust valves closed when both sensor signals are high.

Current work in the area of sensors and controls is focussing on finding a suitable pressure sensor for this application. A major problem that must be overcome is the fact that production miniature sensors often have thin, fragile leads that will not survive long inside the glove. Other problems anticipated when sensors are mounted inside the glove are the effects of temperature variations and perspiration on the sensors.

DISCUSSION

Future work on the pneumatically actuated pressure suit glove will necessarily concentrate on improvement of the already successfully evolving actuator design and the implementation of the proposed sensor and control systems. This actuation and control system holds great promise to reduce hand fatigue due to grasping tasks and increase EVA productivity. A reduced emphasis on close glove fit and custom pattern creation for every wearer may be a by-product of successful implementation of this system that could result in a significant reduction in the cost of EVA outfitting. However, the cost savings could easily be offset by other advantages of close glove fit such as comfort, tactility, and dexterity.

The proposed system has the advantage of light weight, simple operation, and it utilizes a power source that is compact and reliable. A further advantage is that if a failure of the actuation system that does not involve direct valve damage should occur, the EVA crew member would be no worse off than he is with the current generation of gloves. The control valves would return to their normal states, the actuators would evacuate and collapse, and the glove would no longer be effected by the actuation system. This points up another advantage of this technology, that this is a "piggy back" system that can take full advantage of any and all EVA glove improvements.

ACKNOWLEDGEMENTS

The authors wish to acknowledge the sponsorship of this project by the NASA Office of Aeronautics and Exploration Technology and additional support from the NASA National Space Grant College and Fellowship Program.

REFERENCES

1. Kosmo, Joseph J., Bassick, J. , and Porter, K., "Development of Higher Operating Pressure Extravehicular Space-Suit Glove Assemblies", SAE Technical Paper #881102, 18th ICES, July 1988.

2. Otto, Frei, Tensile Structures, M.I.T. Press, Cambridge MA, 1967, pp. 10-30.

3. O'Hara, J. and Briganti, M., "Extravehicular Activities Limitations Study, Vol. II, Establishment of Physiological and Performance Criteria for EVA Gloves", NASA Document N89-17393, p. 2-7.

4. Fisher, W. and Price, C., "Space Station Freedom External Maintenance Task Team, Final Report", NASA, Johnson Space Center, Houston, TX, July 1990.